**DOKUZ EYLÜL UNIVERSITY**
**GRADUATE SCHOOL OF NATURAL AND APPLIED SCIENCES**

# TREATMENT OF OLIVE MILL EFFLUENT BY IMMOBILIZED NANO-ZnO-MAGNETITE

**by**
**Merve BALABAN**

**September, 2015**
**İZMİR**

# TREATMENT OF OLIVE MILL EFFLUENT BY IMMOBILIZED NANO-ZnO-MAGNETITE

**A Thesis Submitted to the**
**Graduate School of Natural and Applied Sciences of Dokuz Eylül University**
**In Partial Fulfillment of the Requirements for the Degree of Master of Science in Environmental Engineering Program**

**by**
**Merve BALABAN**

**September, 2015**
**İZMİR**

## M. Sc THESIS EXAMINATION RESULT FORM

We have read the thesis entitled **"TREATMENT OF OLIVE MILL EFFLUENT BY IMMOBILIZED NANO-ZnO-MAGNETITE"** completed by **MERVE BALABAN** under supervision of **PROF. DR. DELIA TERESA SPONZA** and we certify that in our opinion it is fully adequate, in scope and in quality, as a thesis for the degree of Master of Science.

Prof.Dr. Delya T. SPONZA

Yönetici

Prof. Dr. Ayşegül PALA

Jüri Üyesi

Yard. Doç. Dr. Seray AKGAĞLAR

Jüri Üyesi

Prof.Dr. Ayşe OKUR

Müdür

Fen Bilimleri Enstitüsü

## ACKNOWLEDGMENTS

I would like to express my appreciation to my advisor Prof. Dr. Delia Terese SPONZA for his advice, guidance and encouragement during my Master Degree studies.

I wish to thank Çağlar ULUSOY, Pelin ALİCANOĞLU, Nefise ERDİNÇMER and Cansu DOĞAN for their contribution, guidance and support.

And also, I would like to express appreciation for the support of the sponsors; (TUBITAK PROJECT NUMBER: TOV 113O558).

Finally, my deepest gratitude to my lovely family, Kemal BALABAN and Türkan BALABAN.

Merve BALABAN

**TREATMENT OF OLIVE MILL EFFLUENT BY IMMOBILIZED NANO-ZnO-MAGNETITE**

## ABSTRACT

Olive mill wastewater (OMW) contains high concentration of organic matter, acidic pH values, suspended solids and high content of phenols and polyphenols which are toxic substances. The aim of this study is the removals of COD, total phenol, total solid (TS), total nitrogen, total phosphorus and polyphenos (caffeic acid, tyrosol and hydroxytyrosol) in the OMW by Nano-ZnO-Magnetite composite via adsorption and photocatalytic dagradation. The specific objectives of this study are to determine the optimum Nano-ZnO-Magnetite concentration, to evaluate effect of time and pH on the treatment of OMW pollutants for maximum removal of pollutants, and to investigate the recovery of composite.

For adsorption mechanism, the optimum concentration of Nano-ZnO-Magnetite, adsorption time and pH was determined as 3 gram per liter, 180 minute and 4, respectively. The maximum removal efficiencies of COD, total phenol, TS, total nitrogen and total phosphorus were found as 12, 9, 10, 7 and 10 percent, respectively. For photocatalytic degradation under UV, the optimum concentration of Nano-ZnO-Magnetite, irradiation time and pH was determined as 3 gram per liter, 30 minute and 4, respectively. The maximum removal efficiencies of COD, total phenol, TS, total nitrogen and total phosphorus were found as 80, 75, 70, 97 and 85 percent, respectively. And also, the maximum removal efficiencies of caffeic acid, tyrosol and hydroxytyrosol were found as 80, 80 and 51 percent, respectively Nano-ZnO-Magnetite concentration: 3 gram per liter, irradiation time: 30 minute, UV power: 300 W).

When we used the same Nano-ZnO-Magnetite for fifth times for treatment of OMW , the COD, phenol and TS removal efficiencies decreased from 80 to 52 percent, 75 to 48 percent and 70 to 56 percent, respectively. The cost to treat one liter of OMW is around 500 TL.

**Keywords:** Adsorption, nano- ZnO-Magnetite, photocatalytic degradation, UV and sunlight irradiation.

# İMMOBİLİZE EDİLMİŞ NANO-ZnO-MAGNETİT İLE KARASUYUNUN ARITILMASI

## ÖZ

Zeytin karasuyu, yüksek miktarlarda toksik madde olan fenol ve polifenoller, yüksek miktarlarda organik madde, asidik pH ve askıda katı madde içermektedir. Bu çalışmanın amacı, Nano-ZnO-Manyetit kompozitinin adsorpsiyonu ve fotokatalitik dagradasyonuyla, zeytin karasuyundan KOİ, toplam fenol, toplam katı madde, toplam azot, toplam fosfor ve ploifenollerin (kafeik asit, tyrosol ve hidroksityrosol) giderimidir. Spesifik amaç ise, maksimum kirletici giderimi için, optimum Nano-ZnO-Manyetit kompozitinin konsantrasyonuna karar vermek, zamanın ve pH ın zeytin karasyundaki kirleticilere etkisini değerlendirmek, ve kompositin yeniden geri kazanımını araştırmaktır.

Adsorpsiyon mekanizması için, optimum Nano-ZnO-Manyetit kompozitinin konsantrasyonu, adsorpsiyon süresi ve pH, sırasıyla 3 gram bölü litre, 180 dakika ve 4 olarak tespit edilmiştir. KOİ, toplam fenol, toplam katı madde, toplam azot ve toplam fosforun maksimum giderim verimleri sırasıyla yüzde 12, 9, 10, 7 ve 10 olarak bulunmuştur. UV altında fotokatalitik dagradasyon için, optimum Nano-ZnO-Manyetit kompozitinin konsantrasyonu, radyasyon süresi süresi ve pH, 3 gram bölü litre, 30 dakika ve 4 olarak tespit edilmiştir. KOİ, toplam fenol, toplam katı madde, toplam azot ve toplam fosforun maksimum giderim verimleri sırasıyla yüzde 80, 75, 70, 97 ve 85 olarak bulunmuştur. Ayrıca, maksimum kafeik asit, tyrosol ve hidroksityrosol giderim verimleri sırasıyla yüzde 80, 80 ve 51 olarak bulunmuştur (Nano-ZnO-Manyetit konsatrasyonu: 3 gram bölü litre, radyasyon süresi: 30 dakika, UV gücü: 300 W).

Biz zeytin karasuyunu arıtmak için aynı Nano-ZnO-Manyetit kompozitini beş kere kullandığımızda, KOİ, toplam fenol, toplam katı madde, toplam azot ve toplam fosforun giderim verimleri sırasıyla, yüzden 80'den 52'ye, 75'den 48'ye ve 70'den 56'a düşmektedir. Bir litre OMW arıtıma maliyeti yaklaşık 500 TL'dir.

**Anahtar kelimeler:** Adsorpsiyon, nano-ZnO-Magnetit, fotokatalitik degradasyon, UV ve güneş ışığı radyasyonu.

**CONTENTS**

**Page**

**LIST OF FIGURES**

**Page**

## LIST OF TABLES

**Page**

# CHAPTER ONE
# INTRODUCTION

## 1.1 Introduction

Olive mill wastewater (OMW) management and treatment has been a major issue of environmental concern in the Mediterranean. Olive oil factories, commonly known as olive mills, generate as by-product effluents an average daily amount of 1 $m^3$of wastewater derived from the washing of the olives, together with more than 10 $m^3$ of wastewater coming from the centrifugation process used for the extraction of the olive oil. OMW is an acidic, dark brown stream consisting of water, organic matter and minerals. In particular, OMW are strong, seasonally generated effluents with a highly diverse organic load that reaches values as high as 220 g/L COD and also contain large amounts of suspended solids up to about 190 g/L. Amongst other organic constituents, OMW contain high concentrations of phenolic compounds up to 10 g/L exhibiting hard non-biodegradable and quite phytotoxic properties (Mantzavinos & Kalogerakis, 2005; Komilis et al., 2005).OMW exhibits a series of characteristics that make their reclamation by conventional physicochemical treatments extremely difficult. The presence of phytotoxic refractory pollutants, such as phenolic compounds, organic acids, tannins, long chain fatty acids, an organo halogenated contaminants, makes these effluents recalcitrant to biological degradation and thus inhibits the efficiency of biological processes. Moreover, the physicochemical composition of OMW is extremely variable as it depends on several factors such as the extraction process, climatic, and cultivation parameters, as well as the type, quality, and maturity of the olives (Nieto et al., 2011; Niaounakisand & Halvadakis, 2006).Furthermore, OMW inhibits the microbial activity because of the biocidal activity of the aromatic compounds contained. Therefore, there has been an increasing effort for the development of processes capable of purifying OMW (Roig et al., 2006).

Conventional methods for the removal of phenolic pollutants in OMW can be divided into three main categories: physical, chemical and biological treatment.

Among them, physical adsorption method is generally considered to be the best, effective, low-cost and most frequently used method for the removal of phenolic pollutions. Therefore, the search for low cost and easily available adsorbents has led many researchers to search more economic and efficient techniques of using the natural and synthetic materials as adsorbent (Roostaei &Tezel, 2004).

Adsorption, as a simple and relatively economical method, is a widely used technique in the removal of pollutants. Although the adsorbents used may vary due to the change in adsorption conditions depending on the type of pollutants, the properties affecting the efficiency of an adsorbent are; a large surface area, the homogeneous pore size, well defined structural properties, selective adsorption ability, easy regeneration, and multiple use (Banat et al., 2000).

Advanced oxidation processes (AOPs) using UV/$H_2O_2$, UV/$O_3$ or UV/Fenton's reagent are alternative techniques for the destruction of phenolic compounds and many other organics in wastewater (Chen et al., 1999). Semiconductor mediated photocatalysis is a well-developed AOPs, which can be conveniently applied for the complete destruction of phenolic compounds into water and carbon dioxide (Lathasree et al., 2004). Metal oxide semiconductors such as $TiO_2$, ZnO, $SnO_2$, and $WO_3$, etc. have been attempted for the photocatalytic degradation of a wide variety of environmental contaminants (Oppenlander, 2003). While most of the researchers concentrated on $TiO_2$ as photocatalyst, plenitude of studies have also been focused to explore potential of other metal oxides for the degradation of environmental pollutants (Daneshvar et al., 2004; Abbruzzetti et al., 2001).

## 1.2 The Aim of this Master Thesis

The general purpose of the master thesis was

- to evaluate the performance of the adsorption proses of OMW pollutants such as COD, phenol, TS, total nitrogen, total phosphorous and polyphenols such as caffeic acid, tyrosol and hydroxytyrosol,
- to investigate the effect of Nano-ZnO-Magnetite concentrations (0.5 g/L, 1.5 g/L, 3 g/L, 7 g/L and 10 g/L), irradiation times (30 min, 60 min, 90 min, 180 min and 240 min) and pH (4, 7 and10).
- to evaluate the performance of photocatalytic proses generation of Nano-ZnO-Magnetite nanocomposite under laboratory conditions under UV and sun ligth powers,
- to compare the yields of adsorption and photooxidation,
- to choose the best treatment mechanism for the treatment of OMW,
- to make a cost analysis for both removal process and
- to detect the recovery of the catalyst.

The aim of this study is the removals of COD, total phenol, total suspended solid (TS), total nitrogen, total phosphorus and polyphenos (caffeic acid, tyrosol and hydroxytyrosol) in the OMW by Nano-ZnO-Magnetite composite via adsorption and photocatalytic processes.

The specific objectives of this study are to determine the optimum Nano-ZnO-Magnetite dose, to evaluate effect of time and pH on the treatment of OMW pollutants, and to determine the kinetic model for the removal of pollutants with adsorption and photocatalytic mechanisms.

## 1.3 Novelty of this Master Thesis

Many works were done on photocatalytic degradation using $TiO_2$. In this work, ZnO and magnetite nanoparticle were used as supporter material. Magnetite was immobilized to ZnO nanoparticles under laboratory conditions. The second component, zinc oxide (ZnO) is well-known as an important semiconducting and piezioelectric material promising for optoelectronic and piezoelectric devices, solarcells, sensor applications, or photocatalysis. Besides this, ZnO is bio safe and biocompatible (Wang et al., 2004). Among others, zinc oxide appears as promising photocatalyst, and the quantum efficiency of ZnO is significantly greater than that of $TiO_2$ powder and in some cases, ZnO has proven to be more effective than $TiO_2$ (Chen et al 2006; Kandavelu, 2004). OMW was treated using nano-ZnO-Magnetite by adsorption and photocatalytic degradation under UV and sunlight. All of these methods were comprised; the optimum dose and optimum retention time and optimum pH for maximum removals were detected. A cost analysis was performed, the reusability of the nano-ZnO-Magnetite, adsorption and photocatalytic kinetics were reserched. The most economic treatment technology was chosen for the treatment of OMW.

# CHAPTER TWO
# OLIVE MILL WASTEWATER

Olive oil is produced from olive trees, each olive tree yielding between 15 and 40 kg of olives per year. Worldwide olive oil production for the year 2002 was 2,546,306 t, produced from approximately 750 million productive olive trees, the majority of which are in the Mediterranean region (Niaounakis and Halyadakis, 2004). Mediterranean countries alone produce 97% of the total olive oil production, while European Union (EU) countries produce 80–84%.The biggest olive oil-producing country is Spain (890,100 t in 2002), then Italy (614,950 t), Greece (402,703 t) and Turkey (168,700 t), followed by Tunisia, Portugal, Morocco and Algeria (Niaounakis & Halyadakis, 2004).

In terms of pollution effect, 1 $m^3$ of OMW is equivalent to 100 - 200 $m^3$ of domestic sewage. Its uncontrolled disposal in water reservoirs leads to severe problems for the whole ecosystem and especially for the natural water bodies (ground water reservoirs, surface aquatic reservoirs, seashores, and sea). The most visible effect is discoloration, a result of oxidation and subsequent polymerization of tannins. OMW also has a considerable content of reduced sugars, high phosphorus content, and phenolic load that has a toxic action to some organisms. The high phosphorus content accelerates the growth of algae resulting in eutrophication (Fiorentino et al., 2004).

OMW dispersion on the ground and its subsequent metabolization (bymicroorganisms, insects, earthworms, etc.) to humic extracts or acids also could lead to soil enrichment with nutrients (i.e., organic matter, nitrogen, phosphorus and potassium) and a low-cost source of water. However, OMW with high concentration of potassium affects the cation exchange capacity of the soil, leading to change of environmental conditions for soil microorganisms and consequently to changes in the fertility of the soil. Soil porosity also could be affected. Other possible negative effects include the immobilization of available nitrogen and decreased available magnesium, perhaps because of the antagonistic effect on potassium. Finally, no land

disposal of OMW should be done without taking under consideration its severe phytotoxic and antimicrobial properties that may damage the existing crops (Cox et al., 1997; Paredes et al., 1999; Sierra et al., 2001).

The phytotoxic and antimicrobial properties of OMW have been mainly attributed to its phenolic content and some organic acids, such as acetic and formic acid, that are accumulated as microbial metabolites during storage. Its direct application on plants inhibits the germination of different seeds and early plant growth of different vegetable species and may cause leaf and fruit abscission as well. Different types of crops show different reactions to OMW spreading and some of them may tolerate a certain amount of OMW during early growing stages (Rinaldi et al., 2003).

Biotoxic properties of phenols in OMW constitute a significant inhibitor of the biological processes that take place in common wastewater treatment plants. Such plants do not present the desired performance with treatment of OMW. Thus, the treatment of straight OMW together with domestic sewage is not economically feasible, because of serious overload of the sewage treatment plant (Rinaldi et al., 2003). So, research is oriented toward more complex treatment methods that usually demand higher capital or operational costs.

The problems mentioned above make the technological design of an OMW treatment plant difficult. Factors that make the economic design of such a plant difficult are the intense and seasonal production of the waste (maximum 4 month each winter), the great variability both of synthesis and quantity, the high regional scattering of olive mills, and the small size of the majority of them in the olive oil producing regions (Rinaldi et al., 2003).

OMW characterization is summarized in the following Table 2.1.

Table 2.1 Characterization of OMW.

| **$COD_{inert}$ (mg/L)** | **Soluble $COD_{inert}$ (mg/L)** | **COD (mg/L)** | **Phenol (mg/L)** | **Total Solids (mg/L)** | **Total Nitrogen (mg/L)** | **Total Phosphorous (mg/L)** |
|---|---|---|---|---|---|---|
| 8765 ± 50 | 3674 ± 50 | 117.000 ± 800 | 660 ± 20 | 84.250±50 | 330 ± 20 | 890 ±20 |

## 2.1 Treatment of OMW

There have been done many works in literature to find efficient and cost-effective treatment alternatives for OMW treatment. Various alternatives including the chemical, physical and advanced methods are summarized for achieving this aim.

### *2.1.1 Conventional Treatment Methods of OMW*

Simple physical processes such as dilution, evaporation, sedimentation, filtration and centrifugation have been employed to treat OMW. Centrifugation and filtration increase the pH and conductivity of the effluents and remove organic matter through phase separation and exclusion respectively. Application of sedimentation followed by centrifugation and then filtration (Al-Malah et al.,2000), showed that, after centrifugation, COD was reduced by 21% and BOD by 15%. Additional filtration did not remove any COD, but a further 16% reduction in BOD was observed.

Coagulation and flocculation processes are an important part of water and wastewater treatment and have been practiced worldwide for almost a century. Generally, $FeCl_3$, $H_2SO_4$, HCl, $Ca(OH)_2$, $FeSO_4$, alum are used in these processes (Aktaş et al., 2001).

In coagulation-flocculation processes, various inorganic materials and organic poly-electrolytes were investigated by Ginos et al. (2006).Inorganic materials, such as lime, iron, magnesium and aluminium as well as four cationic and two anionic

commercial poly-electrolytes were added either alone or in various combinations and evaluated the removal efficiency of TSS, TP and COD. When lime or ferrous sulphate with cationic poly-electrolytes was used together, the removal efficiency of COD and total phenol were 10-40% and 30-80%, respectively. In another study, the effect of lime treatment on various OMW after a classic coagulation/flocculation/sedimentation/filtration process, (Aktaş et al., 2001) were determined using a range of lime doses from 10 to 40 $gL^{-1}$, revealed that lime dosing corresponding to a pH increase to 12 for optimal performance, resulting in 62–73% phenol removal depending on the process used for olive oil extraction. More than 40% COD removal and about 95% oil and grease removal were also observed with lime treatment process.

Meyssami & Kasaeian (2005), added coagulants, such as chitosan, starch, alum, and ferric chloride to olive oil-water emulsions and were then they transferred to an air flotation system. The objective of their experiment was the separation of coagulated oil droplets from suspension. It was shown that ferric chloride and starch were not effective coagulants, while alum as the main coagulant and chitosan as a coagulating aid were effective in reducing primary turbidity of the emulsions (90%). At optimized conditions of coagulation and flotation stages (100 ppm chitosan, air flow 3 L/min, aeration time 45 sec, 20 ◦C, pH 6 the COD reduction reached up to 95%.

### *2.1.2 Advanced Treatment Methods of OMW*

Advanced treatment methods have been extensively studied to treat OMW, and high removal efficiencies have been reported in literature. In recent years there has been growing interest in different advanced treatment methods for the treatment of industrial effluents and therefore for the treatment of OMW as well.

Ozone is a powerful oxidising agent that selectively attacks compounds containing aromatic rings and double bonds. Small COD reductions of 18–20% observed after 2 h of ozonation of OMW with an initial CODof 10 gL−1. Thus, can

be attributed to the breakdown of larger organic substances into smaller ones (Benitez et al., 1999).

Uğurlu and Kula (2007) removed the colour, lignin, total organic carbon and phenol efficiently from OMW by using $H_2O_2$/UV. Beltran et al. (1999) reported that 80-90% COD removal was achieved by using an $O_3$/ $H_2O_2$/UV process.

Fenton and Fenton-like processes was applied on OMW treatment and these processes showed high COD (>80%) and total-phenol (>85%) removal performance (Kiril et al., 2010).

COD, color and suspended solid (SS) from olive OMW was experimentally investigated by using electro-coagulation (EC) (İnal et al., 2004). Under 30-min retention time, 52% COD was removed by the aluminum anode and the 42% was removed by the iron anode. COD values in the range of 10-40 mA/cm$^2$ were tested after 10-min retention time each one. The color removal was 90-97% by this process.

Sonication was applied on OMW treatment by Oztekin and Sponza (2013) and the maximum COD, color, total phenol and total aromatic amines (TAAs) removal efficiencies were obtained 63, 82, 78 and 71%, respectively, at 60 $^0$C with sonication only.

Photocatalytic oxidation has been extensively used to treat olive-oil mill wastewater (Marques et al., 1996; Vigo & Cagliari, 1999). In a recent study, $TiO_2$ under UV irradiation was used for the treatment of diluted (1/100) olive mill wastewater. After 24h and in the presence of 1 g l-1 $TiO_2$, almost 22% and 94% of COD and phenols was removed (El Hajjouji et al., 2008).

Lucas and Peres (2009), indicate that the application of Fenton's reagent is a feasible method to partially treat olive mill wastewaters allowing achieve a significant decrease of COD. Fenton's reagent at initial pH 3.5, temperature = 30 ◦C,

molar ratio $H_2O_2$:$Fe^{2+}$ = 15 and weight ratio R=$H_2O_2$/COD= 1.75, leads to a COD reduction of 70%.

### *2.1.3 Treatment of OMW by Adsorption*

Adsorption is the attachment of dissolved compounds (adsorbate) from polluted waters to a solid substance (adsorbent) as a result of attractive interaction of the molecules of the adsorbate with micropores or macropores of the adsorbent having comparable dimensions to that of the molecules. In the case of OMW, adsorbates are polyphenols and tannins. The most widely used adsorbents for this purpose are activated carbon, activated clay, and superabsorbent polymers.

Activated carbon adsorption installations are associated with extremely high costs coming from both the high initial cost of the material and from subsequently high operational costs. A possible solution to this economic burden could be the use of activated carbons produced by olive stone and solvent-extracted live pulp, inexpensive by-products of the olive oil industry. In this way, the volume of solid waste also could be reduced (Galliatsatou et al., 2002). The use of activated clay is another cheap alternative with maximum removal of polyphenols about 81% and 71% for organic matter (Al-Malah et al., 2000).

Adsorption of the OMW onto activated clay reduced the COD by a further 71% and the phenol content by a maximum of 81% (Azzam et al., 2004). Adsorption/desorption equilibrium needs special care, as organic matter and phenols start to desorb after a certain contact time. WITH The combination of four treatment steps, namely settling, centrifugation, filtration and activated carbon adsorption (Azzam et al., 2004), achieved a maximum phenol removal of 94% and a maximum organic matter removal of 83%.

Adsorption on granular activated carbon (GAC) after coagulation / flocculation / sedimentation showed about 30% COD reduction with a requirement of 50 kg carbon $m^{-3}$ effluent (Kestioğlu et al., 2010).

# CHAPTER THREE
# ADSORPTION MECHANISM

Adsorption occurs at least partly as a result of and likewise influences and alters forces active within phase boundaries, or surface boundaries: these forces result in characteristic boundary energies (Weber, 1972). Classical chemistry defines a system by the properties of its mass: for surface phenomena with significant properties are those of the surface or boundary. A pure liquid reduces its free surface energy through the action of surface tension, which is quantitatively equal to the amount of work necessary to compensate the natural reduction in free surface energy. A large number of soluble materials can effectively alter the surface tension of a liquid. If a material which is active at surfaces is present in a liquid system, a decrease in the tension at the surface will occur upon movement of the solute to the surface (Weber, 1972). Migration of the substance to the surface or boundary results in a reduction of the work required to enlarge the surface area, the reduction being proportional to the concentration of adsorbate at the surface (Weber, 1972). The energy balance of the system thus favors adsorptive concentration of such surface-active substances at the phase interface. The tendency of an impurity to lower the surface tension of water is referred to as hydrophobicity; that is, the impurity 'dislikes' water (Weber, 1972).

The solubility of a substance in water is significant: solubility in the sense of the chemical compatibility between the water and the solute (Weber, 1972). The more hydrophilic substance the less likely it is to be adsorbed. Conversely, a hydrophobic substance will more likely be adsorbed (Weber, 1972).

In the context of solute affinity for the solid, it is common to distinguish between three types of adsorption (Weber, 1972). The affinity may be predominantly due to: (1) electrical attraction of the solute to the adsorbent (exchange adsorption): (2) van der Waals attraction (physical or ideal adsorption): or, (3) chemical reaction (chemisorption or chemical adsorption).

Adsorption results in the removal of solutes from solution and their concentration at a surface, until the amount of solute remaining in solution is in equilibrium with that at the surface (Weber, 1972). This equilibrium is described by expressing the amount of solute absorbed per unit weight of adsorbent q (mg/g), as a function of C (mg/L), the concentration of solute remaining in solution. An expression of this type is termed an adsorption isotherm.

The adsorption isotherm is useful for representing the capacity of an adsorbent for adsorbing organics from a waste, and in providing description of the functional dependence of capacity on the concentration of pollutant. The steeper the isotherm, that is, the sharper the rise of the isotherm to a given ultimate capacity as concentration increases, the higher will be the effective capacity at the concentration level desired for the treated water (Walter & Weber, 1972). Experimental determination of the isotherm is routine practice in evaluating the feasibility of adsorption for treatment and in estimating adsorbent dosage requirements. The Langmuir and Freundlich equations provide means for mathematical description of the experimentally observed dependence of capacity on concentration. The adsorption isotherm relates to an equilibrium condition, however, and practical detention times used in most treatment applications do not provide sufficient time for true equilibrium to obtain (Walter & Weber, 1972).

Extent of adsorption is generally proportional to specific surface area specific surface area being that portion of the total surface available for adsorption. If the mechanism of uptake is one of adsorption on external sites of a non-porous adsorbent, the rate should vary reciprocally with the first power of the diameter (Walter & Weber, 1972). This holds also for porous adsorbents when the rate is controlled by an external resistance, i.e. 'film transport'. Conversely, for cases in which intraparticle transport controls, the variation should be with the reciprocal of a higher power of the particle diameter (Walter & Weber, 1972).

Molecular size is of significance if the adsorption rate is controlled by intraparticle transport, in which case the reaction generally precedes more rapidly the

smaller the adsorbate molecule (Weber, 1972). It must be emphasized however, that rate dependence on molecular size can be generalized only within a particular chemical class or series of molecules. As shown by Weber and Morris (1963) large molecules of one chemical class may adsorb more rapidly than smaller ones of another if higher energies (driving forces) are involved. Many organic compounds exist, or have the potential of existing. As ionic species, fatty acids, phenolic species, amines, and many pesticides are a few materials which ionize under appropriate conditions of pH. Activated carbon commonly has a net negative surface charge: further many of the physical and chemical properties of certain compounds undergo changes upon ionization. Most observations point to the generalization that as long as compounds are structurally simple. Adsorption is at a minimum for neutral species. As compounds become more complex, the effect of ionization decreases. Studies of amphoteric compounds indicate an adsorption maximum at the isoelectric point; consistent with other observations that adsorption is at a maximum for neutral species (Walter & Weber, 1972).

# CHAPTER FOUR
# PHOTOCATALYSIS OVERVIEW

The use of titanium oxide in the photocatalytic splitting of water has been used in 1972 (Fujishima &Honda, 1972). Since that time several studies in this area have been conducted. A variety of semiconductors have been described as photolysis catalysts for many types of organic pollutants in water under light illumination (Hoffman et al., 1995; Peral et al., 1997). In the last twenty years scientists have developed many ways to understand the mechanism of photolysis (Chen, 2005). Good examples of photolysis catalysts are solid metal oxides, such zinc oxide and titaniumoxide. These substances have relatively high band gaps (Eg ~3.0 eV) and their conductive band edges are more positive potentials than the oxidation potentials needed for many organic contaminants. Once a photon with energy higher than Eg is absorbed by the photocatalyst, it excites the electron from Valence Band (VB) to the Conduction Band (CB).

The corresponding photocatalytic reaction at ZnO surface can be described by the following six steps:

(a) Adsorption of photons having an energy matches or greater than its band gap energy of ZnO.

(b) Promotion of an electron e- from the valence band to the conduction band generation a hole h+ in the valence band.

(c) e- and h+ diffuse and migrate to the surface where they can react.

(d) Recombination of the electron-hole pairs.

(e) Stabilization of e- and h+ at the surface to form a trapped electron and a trapped hole respectively.

(f) Reduction of a suitable electron accepter.

Among above reaction steps, the absorption of light (step (a)) and subsequent redox reaction at the surface (step (f)) are the key processes in photocatalysis. Steps (c) and (e) sometimes occur too fast to be observed in the reaction.

A well known mechanism for photocatalysis is shown in Figure 4.1.

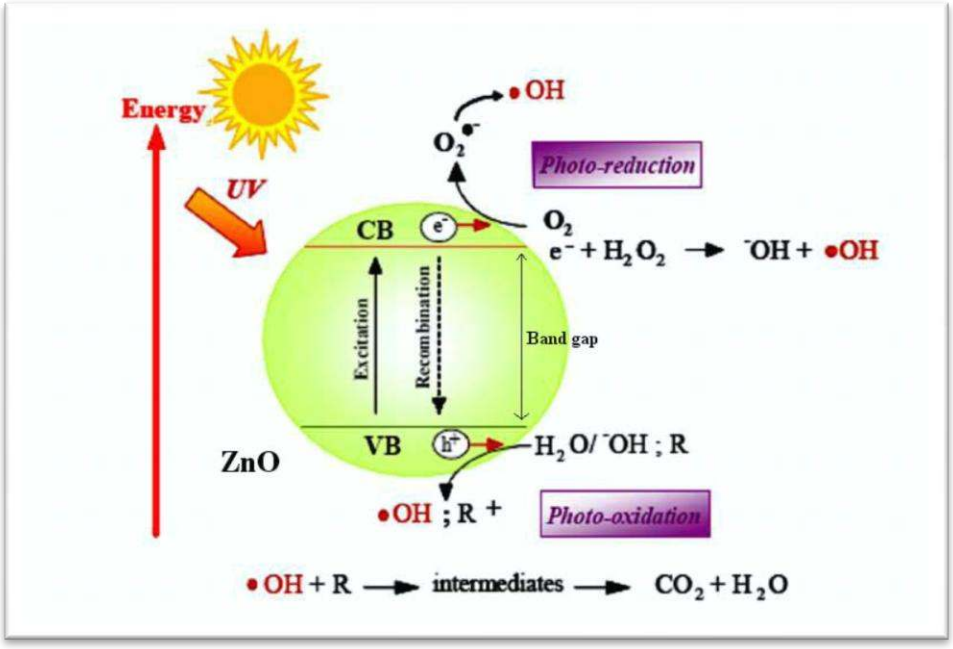


Figure 4.1 Mechanism of photo-catalysis .

The longest wavelength of the light source needed to excite the semiconductor depends on the value of the semiconductor band gap: For ZnO, the value for Eg is 3.2 eV, which is equivalent to wavelength of 387 nm.

## 4.1 Effect of Catalyst in the Contaminant Degradation via Photodegradation Under UV

In order to excite the photocatalyst, the photon must have energy higher than the band gap. To excite zinc oxide, the wavelength of incident light should be equal or shorter than 387nm (Turchi & Ollis, 1990). Thus degradation of pollutants occurs in the UV region only, with wavelengths equal or shorter than 387 nm (Turchi &Ollis, 1990). The absorbed photon energy is used in exciting the electron from the VB to the CB. Consequently, a positive hole (h+) is created in the VB. The electron and the hole may either recombine or separate away (Turchi & Ollis, 1990). Recombination may occur inside the catalyst particle or at the surface. To our advantage, we need electron-hole separation rather than recombination.

The photo excited electron-hole pairs move oppositely to the outer surface of the photocatalyst and start degradation of the adsorbed chemical specie by the reaction of one or more of the transfer reactions (Turchi &Ollis, 1990). The hole can oxidize a hydroxide ion to yield a hydroxyl radical Alternatively, the hole may react with water molecule to produce hydroxyl radical (•OH). The electron may react with oxygen to form super oxide radical anion ($\bullet O^{2-}$), which can further react to form hydrogenperoxide and other active oxygen radicals (Turchi &Ollis, 1990). Both resulting free radicals are able to degrade organic contaminants into water and carbondioxide and other minerals. The following equations explain the photo-degradation mechanism using Nano-ZnO (Lev, 2001; Ohko Et al., 2001; Turchi & Ollis, 1990):

$$ZnO \xrightarrow{h\nu} h^+ + e^- \quad (4.1)$$

$$h^+ + OH^- \longrightarrow \bullet OH \quad (4.2)$$

$$h^+ + H_2O \longrightarrow H^+ + \bullet OH \quad (4.3)$$

$$e^- + O_2 \longrightarrow \bullet O_2^- \quad (4.4)$$

$$O_2 + 2e^- + 2H^+ \longrightarrow H_2O_2 \quad (4.5)$$

$$H_2O_2 + \bullet O_2 \longrightarrow OH\bullet + OH^- + O_2 \quad (4.6)$$

$$OH\bullet + MO \longrightarrow \text{degradation products} \quad (4.7)$$

The hydroxide radical reacts with organic compounds (RH) at the catalystsurface by removing the hydrogen atom on the carbon atom, and converts itto free radical (R•) and water by the chemical equation as follows (Ohko Et al., 2001; Turchi & Ollis., 1990):

$$\bullet OH + RH \longrightarrow R\bullet + H_2O \quad (4.8)$$

Then, the resulting radical (R•) reacts with the reactive oxygen radicals(•OH) to form hydroxy-substituted species (ROH),

$$\bullet OH + R\bullet \longrightarrow ROH \quad (4.9)$$

Or can form tetra oxide species, which are highly unstable (Lev D., 2001; Ohko Et al., 2001; Turchi & Ollis 1990):

$$R\bullet + O_2 + HO_2\bullet \longrightarrow [ROOOOH] \rightarrow CO_2 + H_2O \qquad (4.10)$$

The resulting species releases carbon dioxide.Finally all organic compounds can be degraded by the oxidation reactionusing ZnO under solar light to carbon dioxide and water see Figure 4.2.

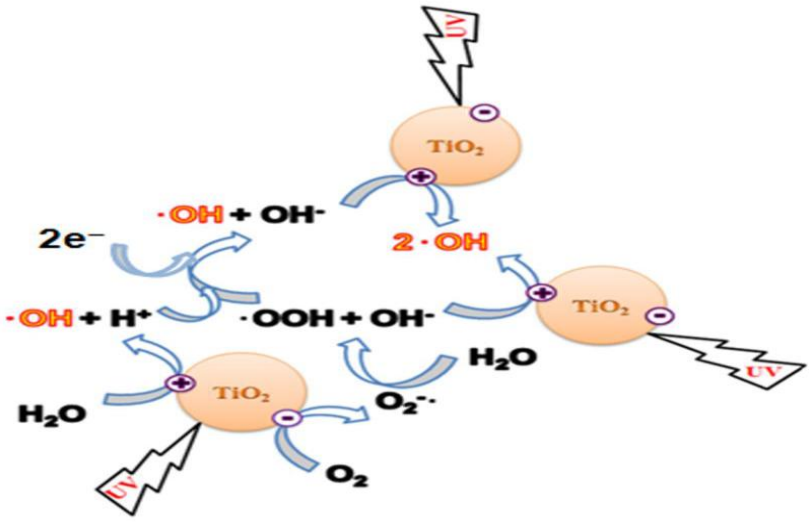


Figure 4.2 Photocatalyticgeneration of hydroxylradicals.

## 4.2 Why ZnO Rather Than $TiO_2$?

In recent years, ZnO has been used as semiconductor photocatalysts. An ideal photocatalyst should be stable, inexpensive, non-toxic and, of course, highly photoactive. Another primary criteria for the degradation of organic compounds is that the redox potential of the $H_2O/\bullet OH$ couple ($OH^-\bullet OH + e^-$; $E^0 = -2.8V$) lies within the band gap of the semiconductor (Hoffman et al., 1995). Several semiconductors have band gap energies sufficient for catalysing a wide range of chemical reactions. These include $TiO_2$, $WO_3$, $SrTiO_3$, -$Fe_2O_3$, ZnO and ZnS.

Titanium oxide ($TiO_2$) and zinc oxide (ZnO) have been extensively investigated as heterogeneous semiconductor photocatalysts (Dhananjeyan et al., 2000). This is because they offer several advantages such as, the use of oxygen as the only required

oxidant and their ability to simultaneously catalyze oxidative and reductive reactions. They also offer low cost, use of sunlight, mild reaction conditions, high photochemical reactivity, low environmental toxicity and stability to photocorrosion (Kamat, 1993).

However, ZnO is better because it absorbs large fraction of the solar spectrum and more light quanta than $TiO_2$ (Sakthivel et al., 2003). Researchers have highlighted the performance of ZnO on degradation of some organic compounds (Gouvea et al., 2000; Lizama et al., 2002).In addition, ZnO has more functions than $TiO_2$ (Kamat et al., 2002).Recently, researchers have pointed out that ZnO can also be used in theacidic or alkaline conditions through proper treatment (Comparelli et al., 2005; Fouad et al., 2006). Furthermorethe optimum pH reported for ZnO process is close to neutral value, whereasthe optimum pH for $TiO_2$ mostly lies in acidic region. Hence the ZnO process is more economical for the treatment of industrial effluents.

ZnO has been reported to be more efficient than $TiO_2$ in some processes such as the advanced oxidation of pulp mill bleaching wastewater (Yeber et al., 1999), the photooxidation of phenol (Khodja et al.,2001) and photocatalysed oxidation 2-phenyl phenol (Serpone et al., 2001). In particular, ZnO has attracted much attention with respect to the degradation of various pollutants due to its high photosensitivity, stability and wide band gap. While $TiO_2$ is widely employed as a photocatalyst, ZnO is a suitable alternative to $TiO_2$ as it has a similar band gap energy (3.2 eV) (Sakthivel et al., 2003), with larger quantum efficiency. Higher photocatalytic degradation efficiencies of contaminant dyes have been reported (Sharma et al., 1995; Dindar and Icli , 2001). Therefore, more study on ZnO catalyst system is necessary.

### 4.3 ZnO Nanoparticles

The rate of photocatalytic degradation of organic pollutant dependson the size of the catalyst, crystanility, surface morphology and the preparation methods. Nano-particles of catalyst show distinguished changes in their optical properties compared

to those of bulk materials as macro size. So particle size and surface area are the effective parameters of photocatalytic activity of nano-materials. Higher reduction activity and smaller band gap energy occur for two reasons, firstly there is more radiation intensity and secondly shorter wavelengths are needed to excite electrons in nano-materials.

Nano-size particles absorb more radiation, due to their higher surface areas. Effect of size on the photo-degradation efficiency can be ascribed to following reasons: when the size of ZnO crystals decreases, the amount of the dispersion particles per volume in the solution will increase, resulting the enhancement of the photon absorbance, at the same time, the surface area of ZnO photocatalyst will increase, which will promote the adsorption of more pollutants on the surface (Daneshvar et al., 2008). Nano-particles also exhibit blue shift (shorter wavelengths) as the particle size is reduced (Poole Jr & Owens, 2003). Nano-sized catalysts exhibited higher reaction rates due to low mass-transfer limitations (Yuan & Keane, 2003). Therefore, the increased surface area of nano-sized particles and high absorptivity may prove beneficial for the decomposition of dyes in aqueous media.

## 4.4 Magnetite Nanoparticles

Magnetite is a ferri magnetic mineral belonging to the family of inverse spinels with chemical formula $[Fe^{3+}]_A[Fe^{2+}Fe^{3+}]_BO_4$, A and B being the tetrahedral and octahedral sites, respectively (Özgür et al., 2005). $Fe_3O_4$ has a cubic inverse spinel structure which consists of a cubic close packed array of oxide ions where all of the $Fe^{2+}$ ions occupy half of the octahedral sites and the $Fe^{3+}$ are split evenly across the remaining octahedral sites and the tetrahedral sites (Özgür et al., 2005). Both FeO and $\gamma$-$Fe_2O_3$ have a similar cubic close packed array of oxide ions and this accounts for the ready interchangeability between the three compounds on oxidation and reduction as these reactions entail a relatively small change to the overall structure. $Fe_3O_4$ samples can be non-stoichiometric. The ferri-magnetism of $Fe_3O_4$ arises because the electron spins of the FeII and FeIII ions in the octahedral sites are coupled and the spins of the FeIII ions in the tetrahedral sites are coupled but anti-

parallel to the former. The net effect is that the magnetic contributions of both sets are not balanced and there is a permanent magnetism (Greenwood & Earnshaw, 1997).

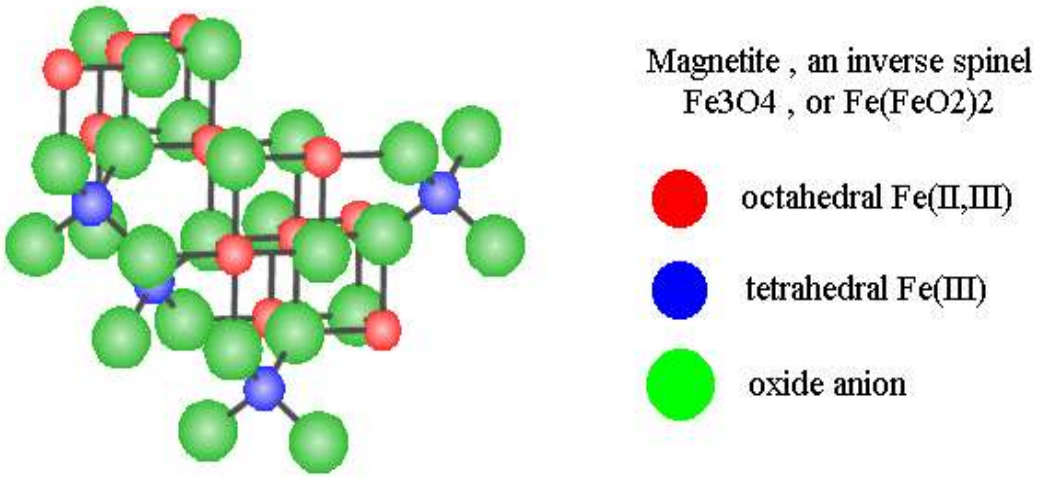


Figure 4.3 Chemical structure of Magnetite.

Magnetite ($Fe_3O_4$) is a representative of large family of ferrites with spinel structure. A some of the most important magnetic materials, it has been considered to have great potential in various fields, such as targeted drug delivery, hyperthermia treatment of cancer, magnetic resonance imaging, and catalysis because of its unique magnetic properties, together with low toxicity and biocompatibility (Pankhurst et al., 2009; Hua et al., 2011).

## 4.5 Immobilization

In this study, we are used immobilization process for produced Nano-ZnO-Magnetite. In recent years, considerable attention has been paid to the size and shape-controllable synthesis of the mono-disperse in organic nanocrystals, owing to their unique size and shape dependent properties, as well as their potential applications in technique areas (Mikulec et al., 2000).

However, for these nanocrystals, many of them merely supply one single function commonly. For example, inorganic semiconductor nanoparticles are widely used as

fluorescence probes for visualizing biological processes in vitro as well as in vivo; magnetic nanoparticles are important for magnetic resonance imaging (MRI), drug delivery, cell labeling, and tracking (Guin et al., 2007). As a practical example of the technology, multifunctional nanoparticles can be used as reusable catalysts. It has been shown that it is more convenient to separate catalysts if silicon nano wires and carbon nanotubes are utilized as carriers (Hu et al., 2007).

However, ineffective separation method could result in the loss of the catalysts. Now, immobilizing catalytic parts onto the surface of the magnetic nanoparticles is an effective way to solve the above problem, as they can be separated easily from the solution with the help of an external magnet (Liu et al, 2009).

Immobilization and the support material influence the photocatalyst activity. The surface area of the catalyst is minimized since the coating layer has a lower porosity (Balasubramanian et al., 2004). The type of support material influences the adsorption characteristics and consequently the decomposition rate of pollutants (Sakthivel et al., 2002).

Furthermore, immobilized catalyst showed flow rate dependence of the reaction (Bideau et al., 1995; Kobayakawa et al., 1998).Thus, the support should have the following characteristics (Pozzo et al., 1997):

(a) transparent to irradiation;

(b) strong surface bonding with the ZnO catalyst without negatively affecting the reactivity;

(c) high specific surface area;

(d) good absorption capability for organic compounds;

(e) separability;

(f) facilitating mass transfer processes and

(g )chemical inert.

Hereby, synthesis of $Fe_3O_4$/ZnO nanocomposites is interesting, because these nanostructures can be served as effective recoverable photocatalysts in not only

various organic syntheses but also photodegradation reactions. It is well known that both the surface defects and the interface properties of the metal oxides play important role in the photocatalytic activities. The reason is that, doping of metal oxide with other metals cans restraint the recombination of photo-induced hole–electron pairs (Wang et al., 2004).

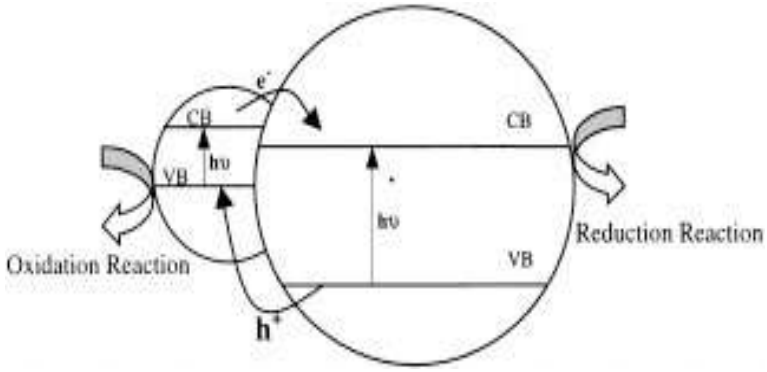


Figure 4.4 Charge transfer in a coupled semiconductor system.

Thus, ZnO which has photocatalyst effect had small size after it was composited by $Fe_3O_4$. Larger specific surface area led nanocomposites to have much more space to be available for the absorption. Therefore, the improvement of photocatalytic degradation percentage was inevitable. On the other hand, in the formation processes of ZnO crystals, partial $Fe^{3+}$ on the $Fe_3O_4$ surface entered into the ZnO lattice and the defects was formed in the lattice. These defects would be shallow potential wells of electrons or holes. Thus, the chance of recombination of electrons and holes would decrease and the life span of photo-electrons and holes would extend. Then more surface oxygen vacancies came in to being and the energy belt of pure ZnOreduced (Wang et al., 2003).

Subsequently, the rate of photos production increased. All of these would-be favor to photocatalyst degradation. Nevertheless, with increasing content of $Fe_3O_4$, the percentage of pure catalysts (ZnO) became smaller, which could decrease the photocatalytic activity of the composites. Moreover, when increased the content of $Fe_3O_4$, excessive $Fe^{3+}$ would capture a large quantity electrons and holes (Wang et al., 2003; Chen et al., 2008), then the performance of semiconductor became weak.

# CHAPTER FIVE
# MATERIALS AND METHODS

## 5.1 Wastewater Origin

Raw OMW was taken from an olive mill industry located in Aydın and used without any pre-treatment, in November 2013.

## 5.2 Reagents and Chemicals

Nano- ZnO and Magnetite were bought externally. Zinc acetate monohydrate (99.9%, Merk, India) and N,N-dimethylformamide (DMF) (99.9%, Thomas Baker) are used as supplied without further purification. Natural magnetite and Nano-ZnO were purchased from Synergy Laboratory Products Ltd., Turkey. Demineralized water was used for preparation of reagents solutions. 0.1 M HCl and 0.1 M NaOH are used to adjust pH vales of olive mill wastewater.

## 5.3 Experimental Procedures

### *5.3.1 Batch Reactors for Adsorption Process*

The investigations were carried out in batch mode at different conditions of pH, Nano-ZnO-Magnetite concentrations, and time, to check the propensity of adsorption process. The adsorption experiments were carried out isothermally in static BATCH mode at room temperature. The experiments were conducted by adding Nano-ZnO-Magnetite composite concentrations increasing from 0.5 g/L, 1.5 g/L, 3 g/L, 7 g/L up to 10 g/L in the OMW in conical Teflon coated glass reactors with a volume of 250 mL. These reactors were placed on a rotating shaker. The pH of the OMW were adjusted between 4, 7 and 10 during the contact periods of 30, 60, 90, 180 and 220 min. Samples were withdrawn at suitable intervals and were separated from the Nano-ZnO-Magnetite composite by centrifugation at 9000 rpm for 15 min. The analyses were carried out in supernatants.

The amount of maximum adsorption capacity of Nano-ZnO-Magnetite composite for the pollutant parameters was calculated according to Eq. (5.1):

$$qe = \frac{(C0-Ce).V}{W} \quad (5.1)$$

where qe is the capacity of adsorbent ( mg/g), Co and Ce are the initial and equilibrium liquid concentrations (mg/L), respectively; V is the volume of solution (L); and W is the weight of adsorbent (g).

### *5.3.2 Quartz Glass Reactors for Photocatalytic Processes*

Photocatalytic degradation experiments were carried out in self-designed quartz glass reactors. The dimensions of the reactors were 38 and 3.5 cm and the costant power of the UV lamps was 300 W. The experiments were performed at room temperature and the pH of the reaction mixture was adjusted from 4 to 7 and 10 using 1 mol/L of $H_2SO_4$ and NaOH solution. Photocatalytic experiments were carried out with a known quantity of Nano-ZnO-Magnetite composite varying between 0.5 g/L, 1.5 g/L, 3 g/L, 7 g/L up to 10 g/L AT different irradiations times (30 min, 60 min, 90 min, 180 min and 240 min). Then, they were irradiated in a closed isolated device with steinlesss cover using UV lamps with constant power of 300 W. Figure 5.1 shows the device used for UV irradiation in an open condition.

Figure 5.1 The device used for UV irradiation.

And also, photocatalytic degradation experiments were carried out under sunlight in same quartz glass reactors which have the same dimensions. Experiments were carried out at different retention times of the day (3 h, 8 h, 15 h and 24 h) and the reactors were placed at an angle of 90 degrees to the sun. The pH of the reaction mixture was adjusted from 4 to 7 and 10 using 1 mol/L of $H_2SO_4$ and NaOH solution. Experiments were carried out at the same Nano-ZnO-Magnetite composite concentrations varying between 0.5 g/L, 1.5 g/L, 3 g/L, 7 g/L and 10 g/L. During the experimentation, the samples were taken out from the reactors after a definite time intervals (3 h, 8 h, 15 h and 24 h), then they were centrifuged for 15 min and the supernatants were analyzed. The sunligth power was measures as 80 W with a light-meter.

## 5.4 Synthesis of Nano-ZnO-Magnetite Composite under Laboratory Conditions

Nanoparticle is produced under laboratory conditions and immobilization method is used for this purpose. The magnetite sample was ground and sieved to 200-mesh size, then is washed with demineralized water for 3–4 times. The slurry of magnetite was prepared in water and it was stirred for 1 h, kept overnight, filtered under vacuum and the resultant solid cake was exposed to slow evaporation till the completely dry material was obtained. 10 g of magnetite was added to a solution

containing 2 g zinc acetate dihydrate dissolved in 250 ml of N,N-dimethyl formamide and the mixture was sonicated for about 3 h in order to obtain homogeneous suspension. To this solution, 100 ml of 0.1 M $NaOH/H_2O$ solution was added with constant stirring for 1 h. The nanocomposite powder was obtained after successive centrifugation and dispersions in alcohol and the solid mass was dried at 75 ◦C under vacuum incubator for 4 h. Then it is calcinated at 200 ºC for 2–3 h in a Muffle furnace. The dried Nano-ZnO-Magnetite nanocomposite was then used for adsorption and photocatalytic experimentations.

## 5.5 Analytical Methods

### *5.5.1 Chemical Oxygen Demand (COD) Measurements*

COD was determined with Close Reflux Method following the Standard Methods 5220-D (APHA-AWWA-WEF, 2005) using an Aqua mate thermo electron corporation UV visible spectrophotometer. First, the samples were centrifuged for 10 min at 9000 rpm. Secondly, 2.50 ml volume wastewater samples were treated with 1.50 ml 10216 mg/L $K_2Cr_2O_7$ with 33.30 g/L $HgSO_4$ and 3.50 $H_2SO_4$ which contains 0.55% (w/w) $Ag_2SO_4$.thirdly, the closed sample tubes were stored in a 148 $^0$C heater (thermo reactor, CR 4200 WTW, 2008) for 2 h. Finally, after cooling, the samples were measured at 610 nm with an Aqua mate thermo electron corporation UV visible spectrophotometer.

#### *5.5.1.1 COD Calibration Curves*

KPH was used to prepare the standard solution of 17 gKPH/L, which is equivalent to 20 gCOD/L (Table 5.1 and Figure 5.2).

Table 5.1 Absorbance data for COD calibration.

| Concentration of COD (mg/L) | Absorbance (Wavelenght at 610 nm) |
|---|---|
| 100 | 0.111 |
| 300 | 0.148 |
| 500 | 0.234 |
| 700 | 0.274 |
| 900 | 0,326 |

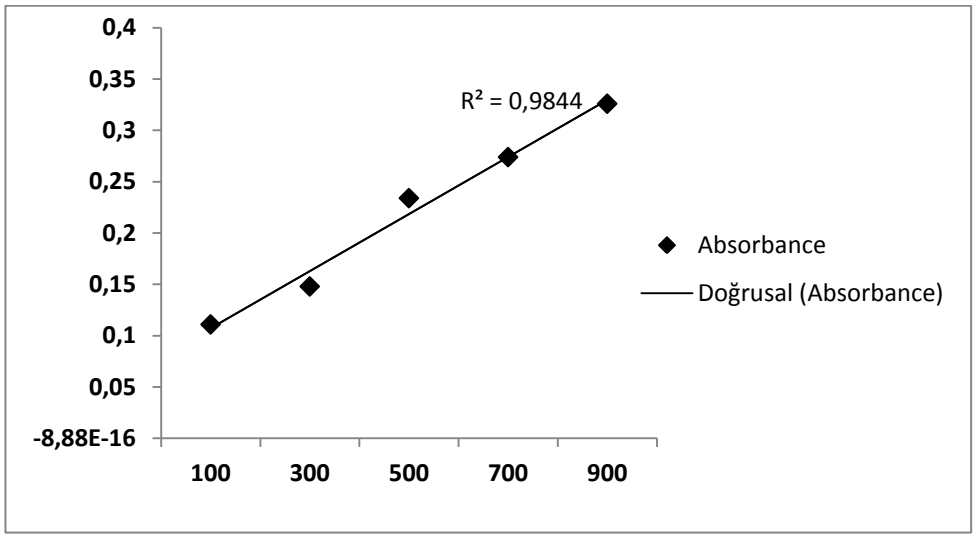


Figure 5.2 Calibration curve of the COD.

### *5.5.1.2 COD Subcategories*

The inert COD and soluble inert COD were measured following the methods proposed by Ekama et al., (1986). The soluble inert COD was measured using the glucose comparison method. This method involves running three batch reactors, two with the wastewater to be studied and the third with glucose. One of the wastewater reactors has the total COD, the second has the total soluble COD, whereas the initial COD in the glucose reactor is adjusted to equal COD value. The experimental studies are performed until all the biodegradable COD is depleted, where the COD profiles reach a plateau and stay unchanged. The difference between glucose COD and wastewater COD gives the inert COD.

### *5.5.2 Phenol Measurements*

The total phenol was determined by using analytical kits (Specturoquant N 1.14551.0001, Merck Chemical Company, Germany) and a NOVA-60 spectrophotometer (Merck).

### *5.5.3 Polyphenol Measurements*

*HPLC Equipment Specifications:* A HPLC Degasser (Agilent 1100), a HPLC Pump (Agilent 1100), a HPLC Auto-Sampler (Agilent 1100), a HPLC Column Oven (Agilent 1100) and a HPLC Diode-Array-Detector (DAD) (Agilent 1100) were used. Figure 8 shows the molecular structure of 3 polypenol namely caffeic acid, tyrosol and hydroxytyrosol determined in the OMW.


Figure 5.3 The structures of 3 polyphenol detected in the OMW.

*Standard Solutions and Calibration Curves:* For quantization, an external standard method was utilized. Peak areas from the HPLC chromatogram were plotted against the known concentrations of stock solutions at varying concentrations. Equations generated by linear regression were used to establish concentrations for OMW and standard solutions.

About 10 mg of a standard of phenolic acids (caffeic acid, tyrosol and hydroxytyrosol) was weighed accurately and they were dissolved into volumetric flasks containing 10 mL 1:1 MeOH/distilled water to obtain stock solutions. For calibration curves, the stock solution was diluted with 1:4 MeOH/distilled water to obtain the concentration sequence. The linear range and the equations of linear regression were obtained through such a sequence of 50 mg/L, 20 mg/L, 10 and 5

mg/L. Mean areas generated from the standard solutions were plotted against concentration to establish calibration equations.

### *5.5.3.1 Caffeic Acid*

*Reagent and Materials:* Caffeic acid was purchased from Fluka (Buchs, Switzerland). Trifluoroacetic acid (TFA), purchased from Merck (Hohenbrunn, Germany), was of analytical grade. Methanol of HPLC grade was purchased from Fisher (Fairlawn, NJ). Deionized water ($10^{-18}$ohm) was re-purified by using an ELGA Purelab UHQ.

*HPLC Analysis:* A C-18 (5 µm, 4.6 mm 150 mm, Agela, Newark, DE) was utilized for succeeding optimization. The flow rate of the mobile phase was kept at 0.5 mL/min. Mobile phase A was water containing 0.02% TFA, and phase B was methanol containing 0.02% TFA. The gradient conditions were as follows: (0-5min, 25% B ; 5-10 min, 25-30% B; 10-16 min, 30-45% B; 16-18min, 45% B; 18-25 min, 45-80% B; 25-30 min, 80% B; 30-40min, 80-25% B. The temperature of column was controlled at 25 °C. Injection volume was 10 µL. The detection wavelengths of diode-array detector (DAD) were set at 320 nm. Prior to each run, the HPLC-DAD system was allowed to warm, and the baseline was monitored until it was stable before sample analysis.

$R^2$ values of calibration graphs of caffeic acid, was found as 0.99 (Figure 5.4).

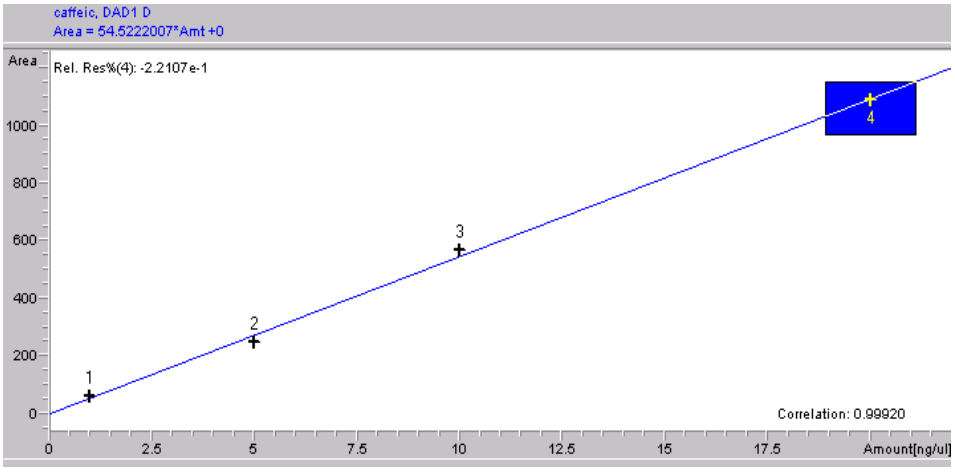


Figure 5.4 Calibration graph of caffeic acid.

### *5.5.3.2 Tyrosol and hydroxytyrosol*

*Reagent and Materials:* Tyrosol were purchased from Fluka (Buchs, Switzerland). Hydroxytyrosol were purchased from Applichem. Panreac. Phosphoric acid and acetonitrile (DharmadrugGmbH, Germany) were purchased from Merck (Hohenbrunn, Germany), was of analytical grade. Deionized water ($10^{-18}$ohm) was repurified by using an ELGA Purelab UHQ.

*HPLC Analysis:* A C-18 (5 µm, 4.6 mm 150 mm, Agela, Newark, DE) was utilized for analyzing polyphenols. Elutes were detected at 280 nm. The temperature was maintained at 40 $^{0}$C. FOR the mobile phase used was 0.1% phosphoric acid in water (A) versus 70% acetonitrile water (B) for a total running time of 50 min, and the following proportions of solvent B were used for the elution: 0–30 min, 20–50%; 30–35 min, 50%; and 35–50 min, 50–20%. The flow rate was 0.5 mL/min, and the injection volume was 20 µL.

$R^2$ values of calibration graphs of tyrosol and hydorxytyrosol were found as 0.99 and 0.99, respectively (Figure 5.5 and Figure 5.6).

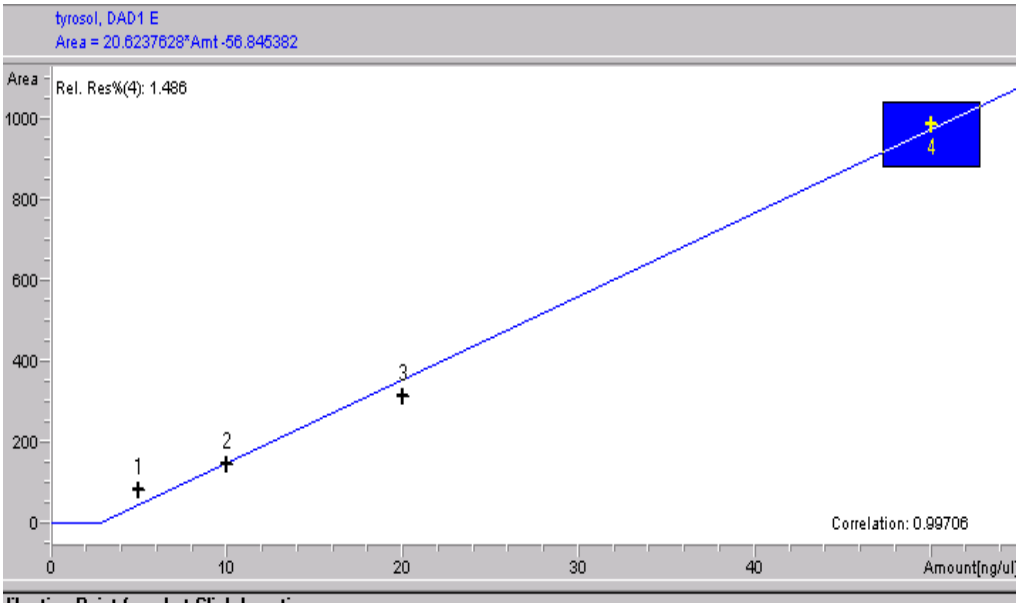


Figure 5.5 Calibration graph of tyrosol.

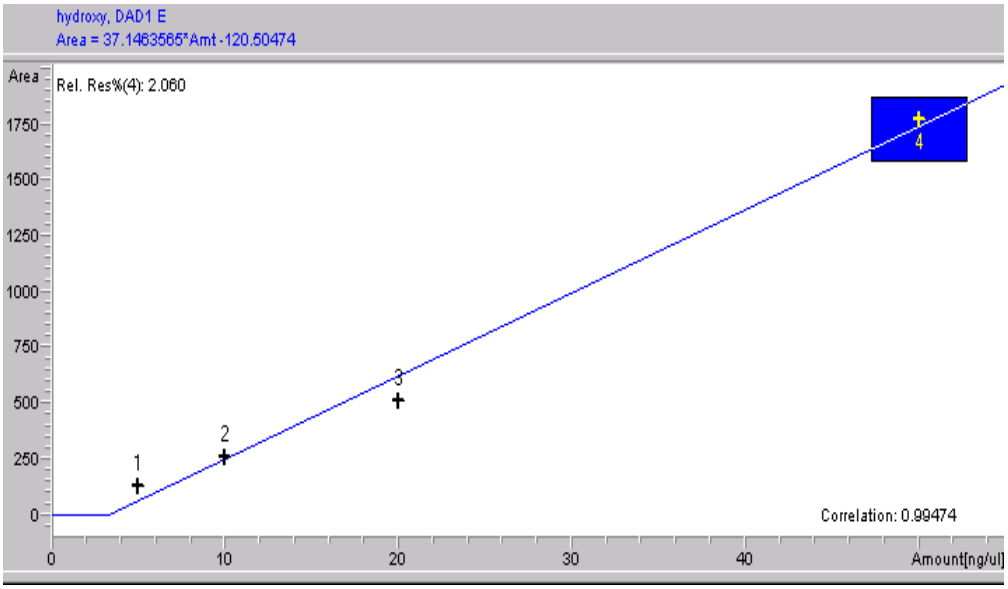


Figure 5.6 Calibration graph of hydroxytyrosol.

### *5.5.4 Total Solid Measurements*

‘‘Total solids’’ is the term applied to the material residue left in the vessel after evaporation of a sample and its subsequent drying in an oven at a defined temperature. TS was determined with following the Standard Methods 2540-B (APHA-AWWA-WEF, 2005) using an incubator with a temperature of 105 $^{0}$C. A well-mixed sample is evaporated in a weighed dish and dried to constant weight (g/L) in an oven at 103 to 105°C. The differences in weight over that of the empty dish represent the total solids

### *5.5.5 Total Nitrogen and Total Phosphorous Measurements*

The total nitrogen and total phosphorous were determined by using analytical kits (Specturoquant N 1.14537.0001 and Specturoquant $PO_4$-P1.14729.0001, Merck Chemical Company, Germany) and a NOVA-60 spectrophotometer (Merck).

## 5.6 Instrumental Characterization

### *5.6.1 X-ray Diffraction (XRD)*

XRD measurements were carried out with the RIGAKU D-Max 2200 PC. X-ray diffraction has been in use in two main areas, for the fingerprint characterization of crystalline materials and the determination of their structure. Each crystalline solid has its unique characteristic X-ray powder pattern which may be used as a "fingerprint" for its identification. Once the material has been identified, X-ray crystallography may be used to determine its structure, i.e. how the atoms pack together in the crystalline state and what the interatomic distance and angle are etc (Loye, 2013).

### *5.6.2 Fourier Transform Infrared (FT-IR)*

FTIR spectra were obtained using the Perkin Elmer FTIR System Spectrum BX. Fourier transform infrared spectroscopy (FTIR) is a technique which is used to obtain an infrared spectrum of absorption, emission, photoconductivity or Raman scattering of a solid, liquid or gas. An FTIR spectrometer simultaneously collects high spectral resolution data over a wide spectral range. This confers a significant advantage over a dispersive spectrometer which measures intensity over a narrow range of wavelengths at a time (Griffiths & Hasseth, 2007).

### *5.6.3 Scanning Electron Microscope (SEM)*

The morphological and structural observation was made on a scanning electron microscope VegaII/LMU (Tescan, CzechRepublic). SEM is a type of microscope that uses a beam of high-energy electrons to image a sample. The examined area is irradiated with a finely focus ion beam, which can scan the sample in a raster scan pattern. Information about the sample's surface topography, composition, and other properties such as electrical conductivity is obtained from the signals produced through the interaction between the electrons and atoms. The types of signals

produced contain backscattered electrons, secondary electrons, characteristic xrays, specimen current, transmitted electrons and photons of various energies (Bedard and Krause, 2007).

## 5.7 Kinetic Studies

Adsorption is widely used in the removal of contaminants from wastewaters. Innumerable physical, chemical and biological processes take place at the boundary between two phases, while others are initiated at that interface. The change in concentration of a given substance at the interface as compared with the neighboring phases is referred as "adsorption". The fundamental concept in adsorption science is that named as the adsorption isotherm. It is the equilibrium relation between the quantity of the adsorbed material and the concentration in the bulk fluid phase at constant temperature. The design and efficient operation of adsorption processes require equilibrium adsorption data for use in kinetic and mass transfer models. These models can then be used to predict the performance of the adsorption contact processes under a range of operating conditions (Banat et al., 2000). In this study, Langmuir isotherm (Eq. 5.2) and Lagergren's equation isoterm (Eq. 5.3) were used for the adsorption of phenol and COD to Nano-Zno-Magnetite composites.

### *5.7.1 Langmuir Isotherm*

The Langmuir adsorption isotherm is often expressed as equation (5.2);

$$qe = \frac{qm.KL.Ce}{1+KL.Ce} \tag{5.2}$$

The Langmuir constants, $K_L$ and $q_m$ were calculated by the linearization of Eq. (5.2): This gives the Eq.(5.3)

$$\frac{C_e}{q_e} = \frac{1}{b.q_m} + \frac{C_e}{q_m} \tag{5.3}$$

Where $q_e$ is the capacity of adsorbent (mg/g), $C_e$ is the initial and equilibrium liquid concentrations (mg/L), $q_m$ is the maximum capacity of adsorbent, respectively; $K_L$ is the Langmuir isotherm constant.

### *5.7.2 Lagergren's Equation for Pseudo-First-Order Reaction*

The integrated form of Lagergren's equation for pseudo-first-order reaction can be expressed as Eq.(5.4):

$$\log(q_e - q_t) = \log(q_e) - (k_1/2.303).t \qquad (5.4)$$

where $q_e$, $q_t$ are the amount of OMW adsorbed (mg) per unit dry weight (g) of the adsorbent at equilibrium and at any time t (min), respectively and $k_1$ is the rate constant of pseudo-first-order adsorption ($min^{-1}$). The value of $k_1$ and qe can be calculated from the plot of log ($q_e - q_t$) versus t.

### *5.7.3 Recovery of Nano-ZnO-Magnetite Photocatalyst*

After first use the Nano-ZnO-Magnetite nanoparticles were filtered after photocatalytic degradation, washed three times by water and ethanol and dried at 75 $^0$C.

Five sequential treatment steps were investigated in order to detect the effect of recovery of Nnano-ZnO-Magnetite based on significant removal yields of COD, phenol and TS under UV irradiation.

### *5.7.4 Analysis of Variance*

Analysis of variance (ANOVA) is a collection of statistical models used to analyze the differences among group means and their associated procedures (such as "variation" among and between groups). This method is often used in scientific

experiments when treatments, processes, materials or products are being compared. (Rosie Cornish, 2006). In this study, the ANOVA test is used all of the experiments. α (Alpha) value of ANOVA is taken as 0.05.

# CHAPTER SIX
# RESULT AND DISCUSSION

## 6.1 Characterization of OMW

The average total inert COD, soluble inert COD, COD, phenol, total solids, total nitrogen and total phosphorous contents of the raw olive mill effluent were 8765 mg/L, 3674 mg/L, 117000 mg/L, 660 mg/L, 84250 mg/L, 330 mg/L and 890 mg/L, respectively, while its average pH value was 3.5- 4.5. The samples were stored at room temperature and shaken well before all the experiments.

Table 6.1 Characterization of OMW

| **$COD_{inert}$ (mg/L)** | **Soluble $COD_{inert}$ (mg/L)** | **COD (mg/L)** | **Phenol (mg/L)** | **Total Solids (mg/L)** | **Total Nitrogen (mg/L)** | **Total Phosphorous (mg/L)** |
|---|---|---|---|---|---|---|
| 8765 ± 50 | 3674 ± 50 | 117.000 ± 800 | 660 ± 20 | 84.250±50 | 330 20 | 890 ± 20 |

## 6.2 Physicochemical Properties of Nano-Zno-Magnetite

### *6.2.1 X-ray diffraction (XRD) Analysis Results*

XRD was used to verify the chemical composition and the crystal structure of $Fe_3O_4$ and ZnO nanoparticles and Nano-ZnO-Magnetite nanocomposite (Hasanpour et al., 2012). Figure 6.1 shows x-ray diffraction (XRD) patterns of the $Fe_3O_4$, ZnO, Nano-ZnO-Magnetite and Nano-ZnO-Magnetite after treatment. As it is shown in Figure a, b and c the XRD peaks can match well with peaks of $Fe_3O_4$, ZnO and Nano-ZnO-Magnetite. Figure 9c represents the XRD pattern of Nano-ZnO-Magnetite core/shell. Considering this figure, it is shown that after coating, we have enhancement in peak intensity which is caused by overlapping of $Fe_3O_4$ peaks (Nikazar et al., 2014). No peaks corresponding to the impurities are detected, indicating that $Fe_3O_4$–ZnO heterostructure were formed during the photodegradation

process (Wan et al., 2009). After UV irradiation, $Fe_3O_4$/ZnO nanocomposites have an amorphous structure as illustrated in Figure d. An amorphous or non-crystalline solid is a solid that lacks the long-range order characteristic of a crystal (Zarzycki, 1982).

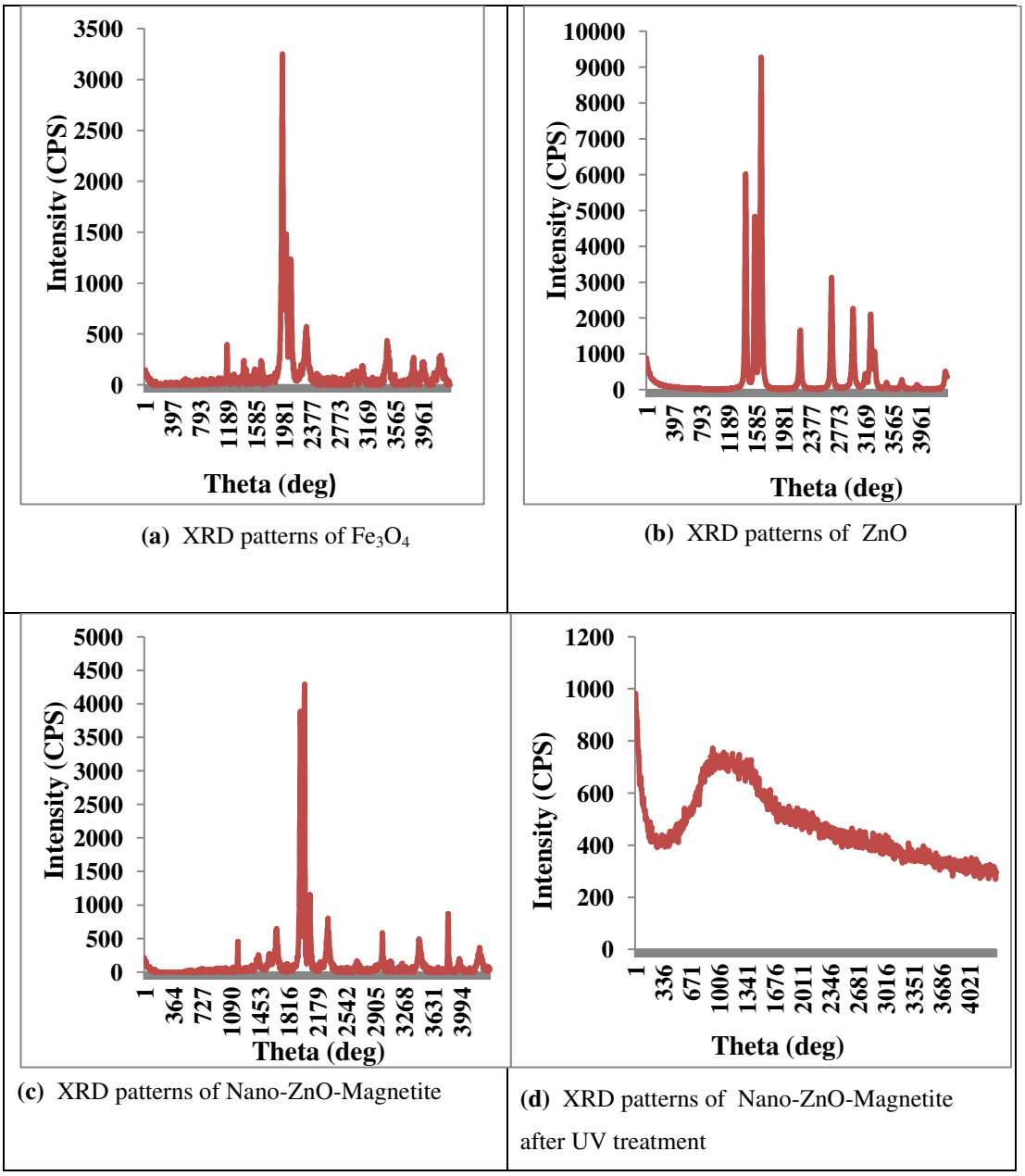


Figure 6.1 XRD patterns of Fe3O4, ZnO, Nano-ZnO-Magnetite and Nano-ZnO-Magnetite after UV treatment.

### *6.2.2 Fourier Transform Infrared (FTIR) Analyses Results*

Figure 6.2 shows the FT-IR spectra of $Fe_3O_4$, ZnO, Nano-ZnO-Magnetite and Nano-ZnO-Magnetite after UV treatment. It can be seen that the characteristic absorption of Fe-O bond is at 582.78/cm and 620.21/cm, while that of -OH bond is at 3449.26/cm. The absorptions at 1395.25/cm and 1591.29/cm are characteristic peaks of the COO-Fe bond, which may be due to the reaction of hydroxide radical groups on the surface of $Fe_3O_4$ (Nikazar et al., 2014). These peaks reveal that magnetite ($Fe_3O_4$) has been successfully immobilized onto the surface of ZnO. Combining the XRD results, it can be concluded that ZnO had been coated on the $Fe_3O_4$, successfully. From figure 10d, it can be seen that the pollutants in wastewater binds to the surface of Nano-ZnO-Magnetit composite after UV irradiation Therefore, crystal form of Nano-ZnO-Magnetit composite converts the amorphous shape. As a result, the peak number in the Nano-ZnO-Magnetit composite decreases in the amorphous shape.

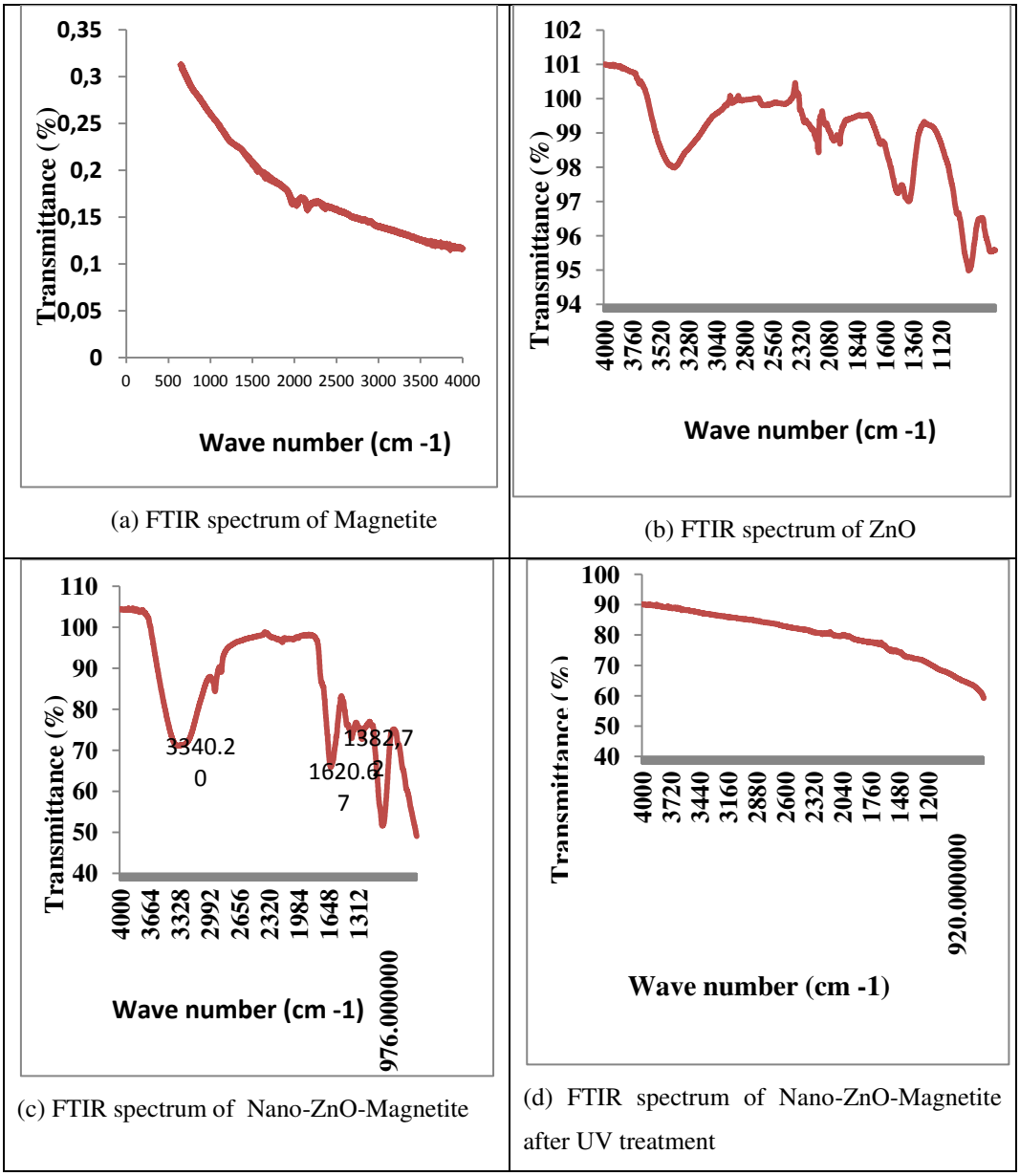


(a) FTIR spectrum of Magnetite

(b) FTIR spectrum of ZnO

(c) FTIR spectrum of Nano-ZnO-Magnetite

(d) FTIR spectrum of Nano-ZnO-Magnetite after UV treatment

Figure 6.2 FTIR spectrum of $Fe_3O_4$, ZnO, Nano-ZnO-Magnetite and Nano-ZnO-Magnetite after UV treatment.

### *6.2.3 Scanning Electron Microscopy (SEM)*

SEM images of Nano-ZnO-Magnetite and Nano-ZnO-Magnetite after UV treatment are presented in Figure a and b before and after treatment, respectively. It is shown that the dispersion of Nano-ZnO-Magnetite is better than modified Nano-ZnO-Magnetite after UV treatment. The average particle size was obtained about 500

nm and 1μm, in Figures a and b for Nano-ZnO-Magnetite and Nano-ZnO-Magnetite after UV treatment, respectively.

**(a)** SEM images of Nano-ZnO-Magnetite

**(b)**SEM images of Nano-ZnO Magnetite after UV treatment

Figure 6.3 SEM images of Nano-ZnO-Magnetite.

## 6.3 Batch Adsorption Studies

### *6.3.1 Determination of Optimum Nano-ZnO-Magnetite Concentration*

Effect of Nano-ZnO-Magnetite concentrations on the removals of COD, phenol, total solids, total nitrogen and total phosphorous was investigated in the OMW with constant adsorption time (180 min.) for the Nano-ZnO-Magnetite nanocomposite concentrations of 0.5 g/L, 1.5 g/L, 3 g/L, 7 g/L and 10 g/L at a original pH of OMW (pH: 4.60) at a temperature of ±20 $^0$C (Figure 6.4, 6.5, 6.6, 6.7 and 6.8)

From Figure 6.4., as the Nano-ZnO-Magnetite nanocomposite concentrations were increased from 0.5 g/L to 1.5 g/L, from 1.5 g/L to 3 g/L, from 3 g/L to 7 g/L, from 7 g/L to 10 g/L, the COD removal efficiency increased from 5% to 8%, from

8% to 10%, from 10% to 12%, and stabilized to 12%, respectively, at a pH of 4.60 at a temperature of ±20 $^{0}$C after 180 min adsorption time. This trend can be explained by the increased active sites for the removal of contaminants along with the increase of Nano-ZnO-Magnetite nanocomposite concentrations. The rapid adsorption at initial reaction time may be attributed to the abundance of free active sites on the surface of Nano-ZnO-Magnetite and easy availability of them for COD in the OMW although the COD yields were not so high. The maximum COD removal was obtained as 12 % at 7 g/L Nano-ZnO-Magnetite composite concentration. In economical point of view the optimum Nano-ZnO-Magnetite composite concentration was found to be 3 g/L corresponding to a COD removal efficiency of 10%. At this 3 g/L Nano-ZnO-Magnetite composite level, the initial COD concentration decreased from 117000 mg/L to 102950 mg/L in the effluent. The increase in Nano-ZnO-Magnetite composite concentration over 3 g/L has not allowed any additional improvement in COD adsorption. This behavior can be explained by the saturation of adsorption sites of increasing Nano-ZnO-Magnetite composite (at 7 and 10 mg/L) through the adsorption process (Han et al., 2006).

A linear relationship between Nano-ZnO-Magnetite composite concentrations and COD adsorption efficiencies was obtained up to a Nano-ZnO-Magnetite composite concentration of 7 g/L (R =0.88) while this regression is not significant (ANOVA, $p=0.15 > \alpha=0.05$ and F=10.36).

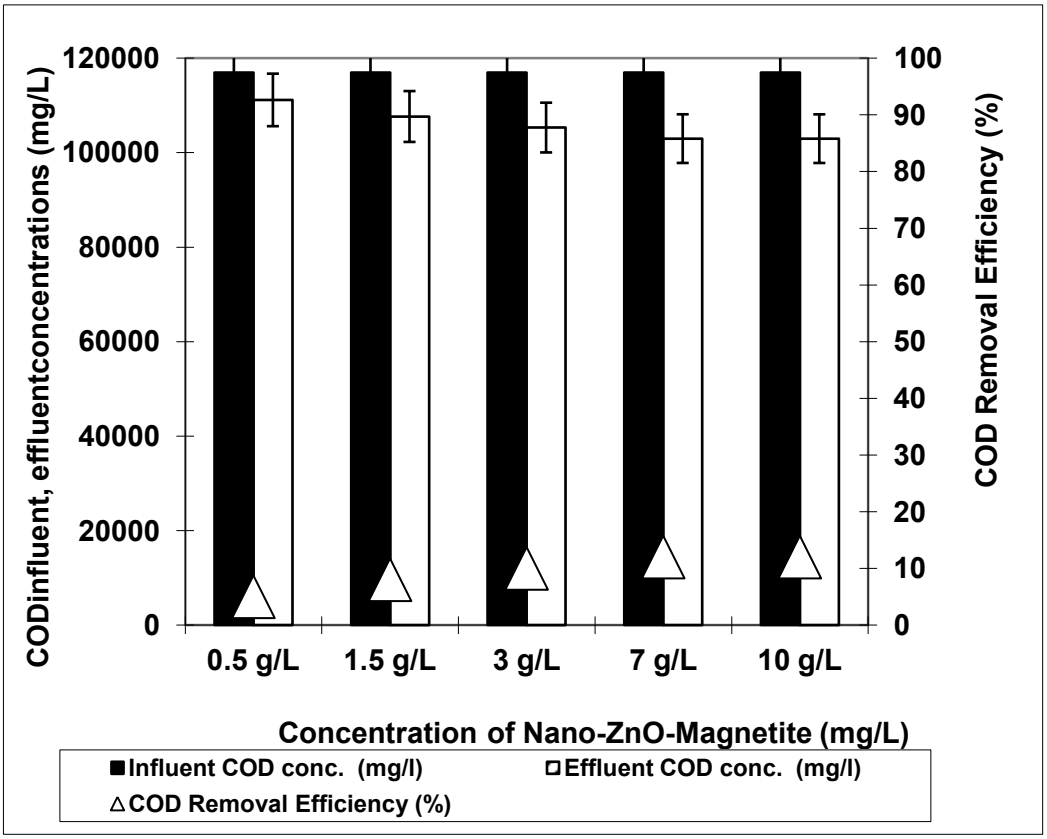


Figure 6.4 The effect of Nano-ZnO-Magnetite concentration on COD yield (Influent Conc.: 117000 mg/L, T: ±20 $^0$C, pH: 4.60, Adsorption time 180 min).

When the concentration of Nano-ZnO-Magnetite increased from 0.5 g/L to 1.5 g/L, from 1.5 g/L to 3 g/L, from 3 g/L to 7 g/L and from 7 g/L up to 10 g/L, the removal efficiency of phenol increased from 3% to 5%, from 5% to 6%, from 6% to 7% and stabilized to 7%, respectively, at a pH of 4.60 at a temperature of ±20 $^0$C after 180 min adsorption time (Figure 6.5). The maximum phenol removal by adsorption was obtained as 7% at 7 g/L Nano-ZnO-Magnetite composite concentration. Low phenol removals at low Nano-ZnO-Magnetite composite concentrations can be attributed to the ratio of surface active sites in the surface of Nano-ZnO-Magnetite composite are not enough to adsorbe the total phenol components in the OMW as reported by Juan-Ding et al., (2013).

A linear relationship between Nano-ZnO-Magnetite composite concentrations and phenol adsorption efficiencies was obtained up to 10 g/l Nano-ZnO-Magnetite

composite cencentration (R =0.85) while this regression is not significant (ANOVA p=0.19 > α=0.05 and F=8.05).

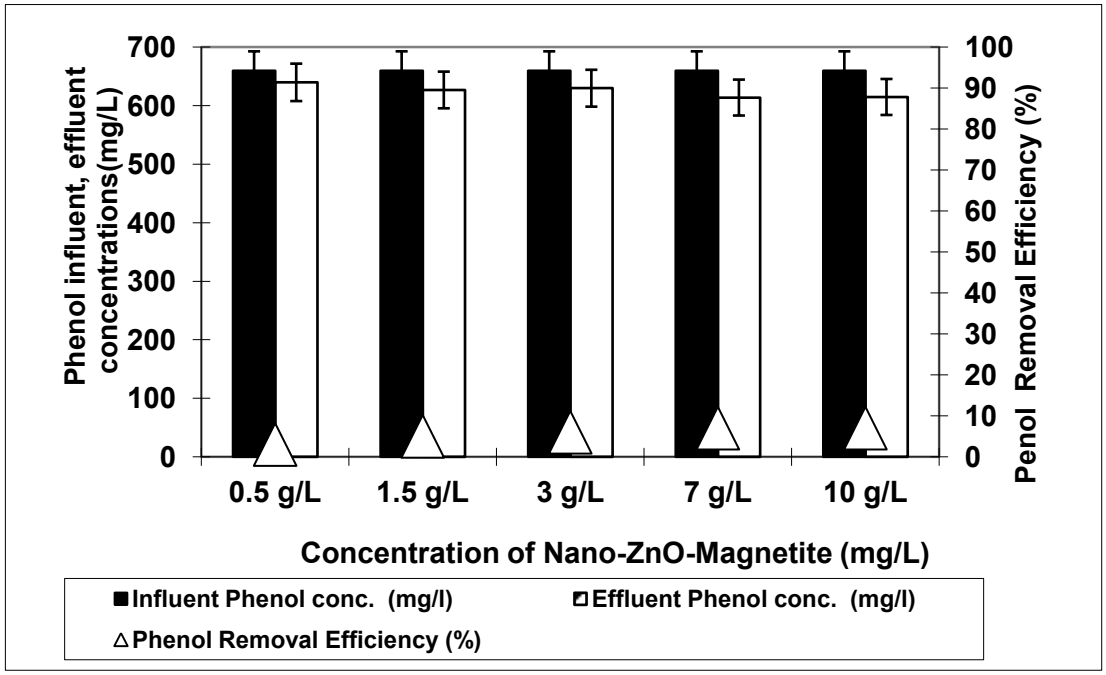


Figure 6.5 The effect of Nano-ZnO-Magnetite concentration on Phenol yield (Influent Conc.: 660 mg/L, T: ±20$^0$C, pH: 4.60, Adsorption time 180 min).

TS removal efficiencies were found as 12 %, 10%, 9%, 7% and 5% for 0.5 g/L, 1.5 g/L, 3 g/L, 7 g/L and 10 g/L Nano-ZnO-Magnetite nanocomposite, respectively, at a pH of 4.60 at a temperature of ±20 $^0$C after 180 min adsorption time (Figure 6.6). For maximum removal efficiency of TS, the optimum Nano-ZnO-Magnetite composite concentration was found to be 0.5 g/L. After 3 g/L Nano-ZnO-Magnetite composite, increasing the Nano-ZnO-Magnetite composite concentration from 0.5 g/L to 10 g/L affect negatively the removal efficiency of TS. When the Nano-ZnO-Magnetite composite concentrations increased above the optimum value, the adsorption efficiency decreased due to an increase in turbidity of the OMW. Therefore the active sites are occupied by TS, and adsorption yields decreased due to having little available active sites on the Nano-ZnO-Magnetite composite surface (Ip et al., 2010).

A linear relationship between Nano-ZnO-Magnetite composite concentrations and TS adsorption efficiencies was obtained (R =0.98) and this regression is significant (ANOVA p=0.001 < α=0.05 and F=80.83)

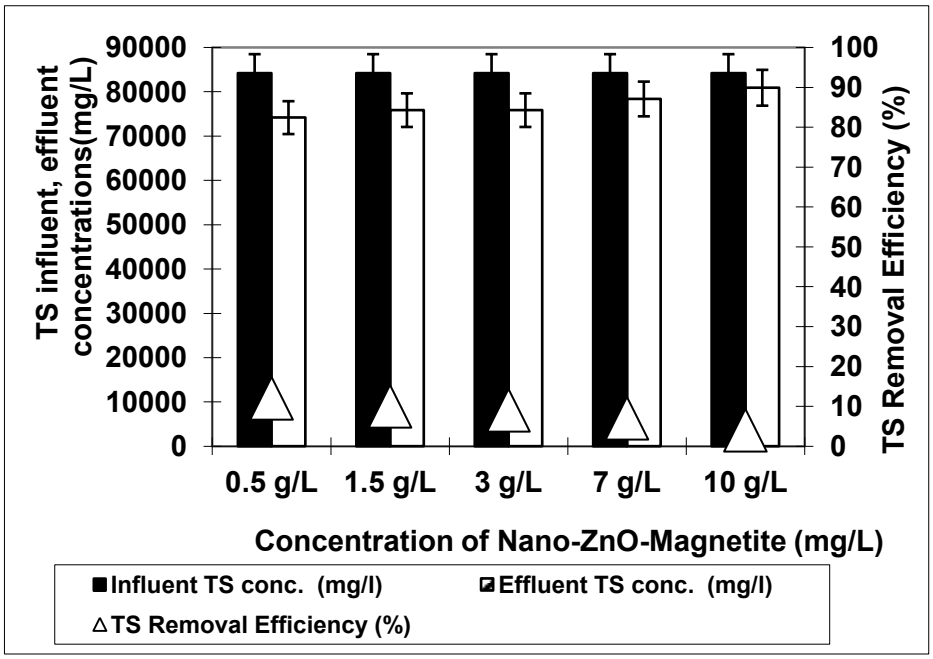


Figure 6.6 The effect of Nano-ZnO-Magnetite concentration on TS yield (Influent Conc.: 84250 mg/L, T: ±20$^0$C, pH: 4.60, Adsorption time 180 min).

Figure 6.7 shows the nitrogen removal rate with different Nano-ZnO-Magnetite composite concentrations at a pH of 4.60 at a temperature of ±20 $^0$C after 180 min adsorption time. At 0.5 g/L and 1.5 g/L Nano-ZnO-Magnetite composite concentrations, no removal efficiency of total nitrogen was achieved (0%, Figure 6.7). The total nitrogen removal efficiency was increased to 3% at 3 g/L Nano-ZnO-Magnetite composite. When the Nano-ZnO-Magnetite composite concentration increased to 7 g/L, the maximum removal efficiency of total nitrogen was established (5%) and maintained stable at 10 g/L Nano-ZnO-Magnetite composite concentration. Increasing of Nano-ZnO-Magnetite composite concentrations to 20 g/L or 30 g/L, did not significantly rise the nitrogen yields (2%) (data not shown). On the other hand, the high Nano-ZnO-Magnetite concentrations are not economically suitable. Nano-ZnO-Magnetite composite concentrations had little effect on the removal of total nitrogen. For the total nitrogen removal, the optimum Nano-ZnO-Magnetite

composite concentration is 7 g/L with a yield of 5%. $Fe_3O_4$ nanoparticles have hydrophilic surface, thus, have oxygen functional groups (Ma P, et al., 2008). Murti et al. (2003), suggested that oxygen functional groups that release $CO_2$, such as carboxylic functional groups, inhibit the adsorption of nitrogen compounds.

A linear relationship between Nano-ZnO-Magnetite composite concentrations and total nitrogen adsorption efficiencies was not obtained (R =0.62) and this regression is not significant (ANOVA p=0.66 > α=0.05 and F=16.18).

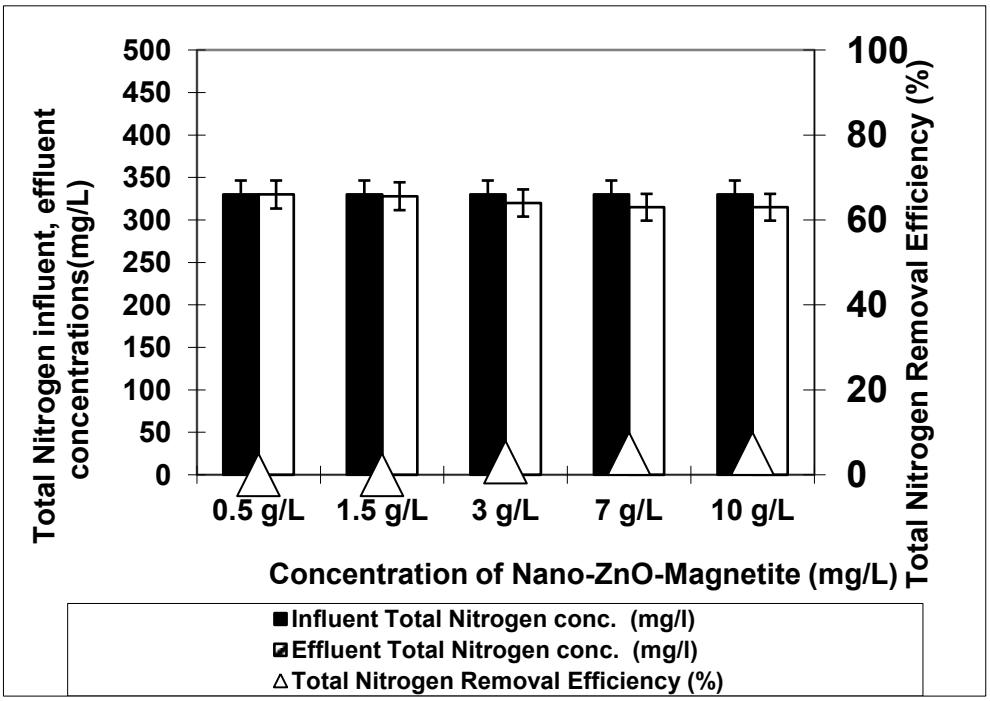


Figure 6.7 The effect of Nano-ZnO-Magnetite concentration on Total Nitrogen yield (Influent Conc.: 330 mg/L, T: ±20 $^0$C, pH: 4.60, Adsorption time 180 min).

Figure 6.8 presents the effects of Nano-ZnO-Magnetite composite concentrations on total phosphorous removal efficiency. The total phosphorous yield decreased from 20% to 18%, from 18% to 15%, from 15% to 8% and from 8% to 2%, with increasing of Nano-ZnO-Magnetite composite concentration from 0.5 g/L to 1.5 g/L, from 1.5 g/L to 3 g/L, from 3 g/L to 7 g/L and from 7 g/L to 10 g/L, respectively, at a pH of 4.60 at a temperature of ±20 $^0$C after 180 min adsorption time (Figure 6.8). A significant drop was observed in total phosphorous efficiency after 3 g/L Nano-ZnO-Magnetite composite (%8). When Nano-ZnO-Magnetite composite concentration

was 0.5 g/L, the total phosphorous removal efficiency reached the maximum (20%). Thus, the best Nano-ZnO-Magnetite composite concentration in this study was 0.5 g/L for the maximum total phosphorous removal. Higher Nano-ZnO-Magnetite composite concentration than 3 g/L caused a decrease in total phosphorous removal efficiency.

A linear relationship between Nano-ZnO-Magnetite composite concentrations and total phosphorous adsorption efficiencies was obtained (R =0.99) and this regression is significant (ANOVA p= 2,2407E-06 < α=0.05 and F=4633.2).

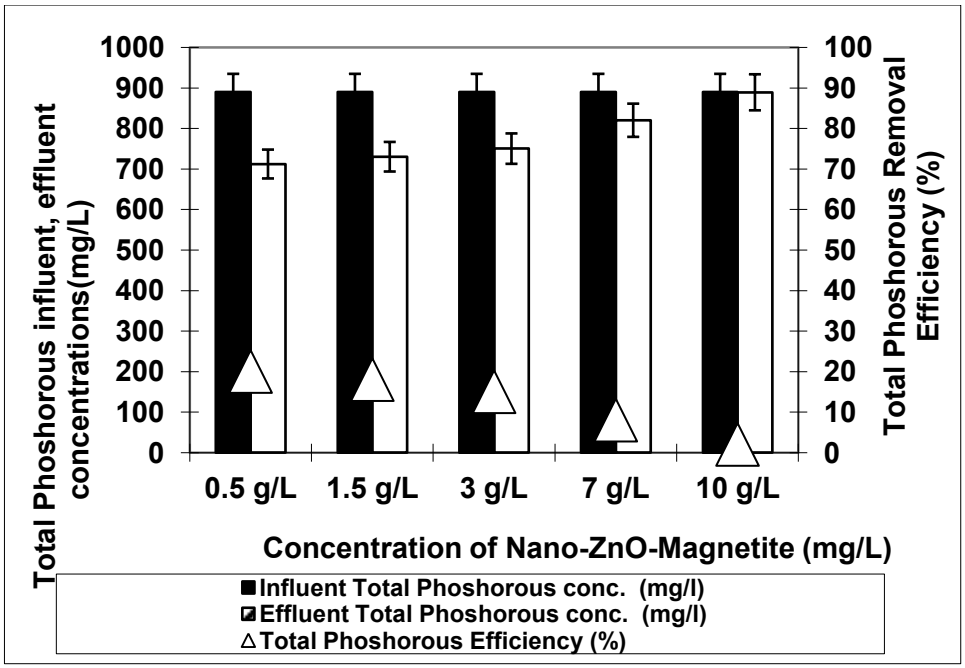


Figure 6.8 The effect of Nano-ZnO-Magnetite concentration on Total Phosphorous yield (Influent Conc.: 890 mg/L, T: ±20 $^0$C, pH: 4.60, Adsorption time 180 min).

Considering all the removal efficiencies for studied parameters in the OMW, an optimum nanocomposite concentration was chosen for maximum yields. The optimum Nano-ZnO-Magnetite composite concentration was selected as 3 g/L for the maximum removals of all pollutant parameters.

### *6.3.2 Determination of Optimum Adsorption Time*

Figures 6.9, 6.10, 6.11, 6.12 and 6.13 illustrate the effect of the adsorption time on the removal of COD, phenol, TS, total nitrogen and total phosphorous, respectively. As aforementioned in the upper section, the optimum Nano-ZnO-Magnetite composite concentration was found as 3 g/L. Therefore, the effects of adsorption times on the COD, phenol, TS, total nitrogen and total phosphorous removal efficiencies were investigated at five different adsorption times (30 min., 60 min., 90 min., 180 min. and 240 min) at a pH of 4.60 at a temperature of ±20 $^0$C at constant 3 g/L Nano-ZnO-Magnetite composite concentration.

The adsorption of COD on Nano-ZnO-Magnetite composite was also studied as a function of contact time in order to find out the equilibrium time for maximum adsorption. The results from Figure 6.9 shows that the time required for the adsorption of COD on 3 g/L Nano-ZnO-Magnetite composite was 180 min for OMW with an initial COD concentration of 117000 mg/L. From figure 6.9, it can be seen that as the adsorption time were increased from 30 min, to 60 min, to 90 min, and to 180 min, the COD yield increased from 2%, to 6%, to 10%, to 15%, and stabilized to 15%. Further increase of adsorption time to 240 min did not increase the COD yield. At this adsorption time the COD yield remained constant as 15% as is at 180 min adsorption time. The maximum removal efficiency of COD occurred at 180 min, so this adsorption time was chosen as optimum contact time.

A linear relationship between adsorption times up to 240 min and COD adsorption efficiencies was obtained ($R = 0.94$) and this regression is significant (ANOVA $p = 0.63 > \alpha = 0.05$ and $F = 21.01$)

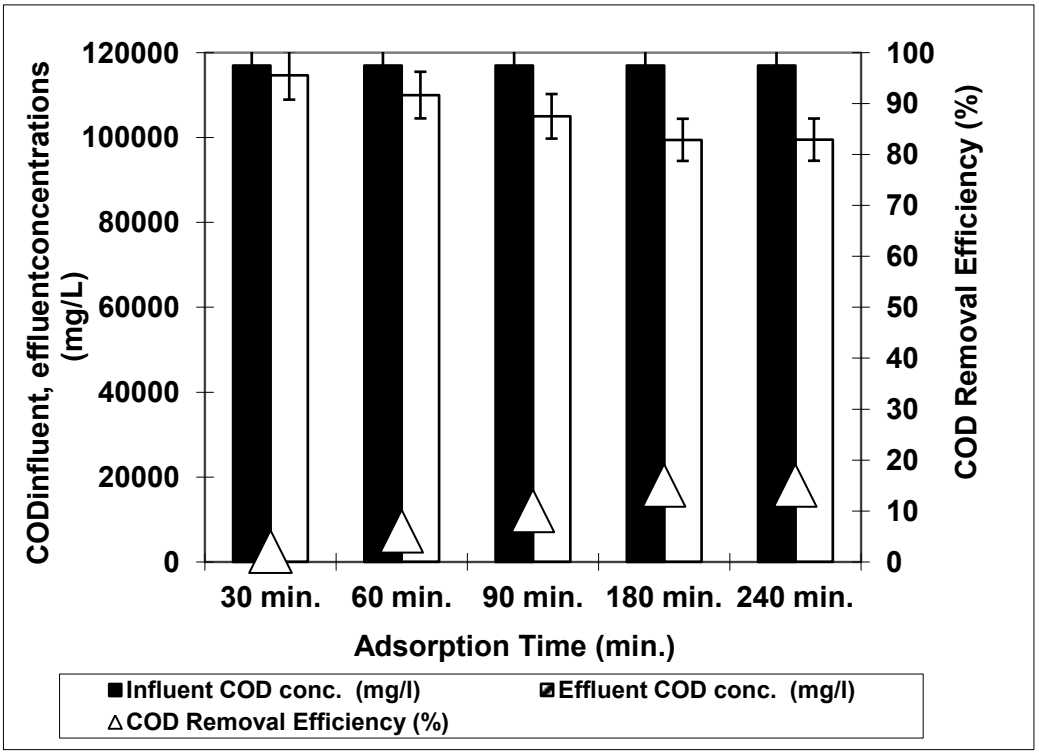


Figure 6.9 The effect of adsorption time on COD yield (Influent Conc.: 117000 mg/L, T: ±20 $^0$C, pH: 4.60, Nano-ZnO-Magnetite conc.: 3g/L).

From Figure 6.10, it can be seen that the phenol yield was 3% after 30 minutes, while the yield increased up to 5% after 90 th minutes. The phenol yield continued to rise up to 9% after 180 minute at the original pH of OMW (pH: 4.60) at 3g/L nano-ZnO-Magnetite and at a temperature of ±20 $^0$C. The maximum phenol removal was obtained as 9 % after 180 min adsorption time. Further increase of time (240 min) did not affect the phenol removal. Phenols are considered to be one of the important organic pollutants discharged by OMW into the environment causing significant damage and threat to the ecosystem in water bodies and human health. Feng et al., (2014) found that no phenol adsorption capacity for both the $Fe_3O_4$ and $Fe_3O_4$/ZnO hybrid nanoparticles in the first 150 min. In the comparison of the results, in our study higher phenol adsorption yields were obtained.

A linear relationship between adsorption times up to 240 min and phenol adsorption efficiencies was not obtained (R =0.96) and this regression is not significant (ANOVA p=0.25 > α=0.05 and F=36.42)

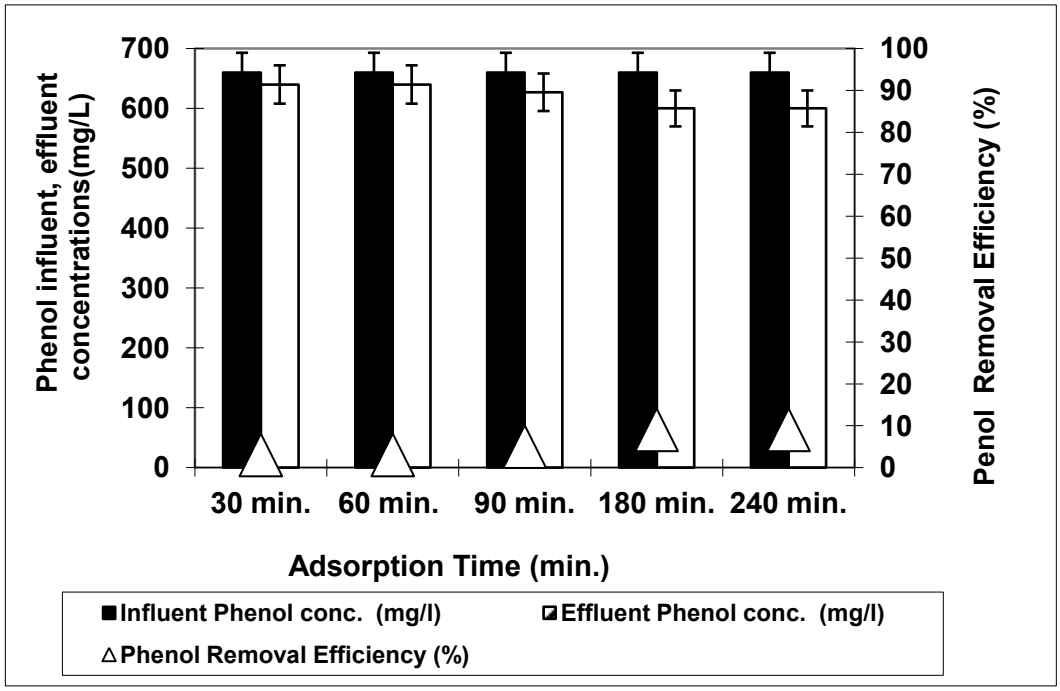


Figure 6.10 The effect of adsorption time on Phenol yield (Influent Conc.: 660 mg/L, T: ±20 $^0$C, pH: 4.60, Nano-ZnO-Magnetite conc.: 3g/L).

Low TS removal efficiency (12%) was observed with adsorption at an original pH of OMW (pH: 4.60) at 3g/L Nano-ZnO-Magnetite and at a temperature of ±20 $^0$C as shown in Figure 6.11. After 30 minutes adsorption times the TS yield reached 12% with the initial TS concentration of 84250 mg/ at an original pH of OMW (pH: 4.60) at 3g/L nano-ZnO-Magnetite and at a temperature of ±20 $^0$C . This TS concentration decreased to 74140 mg/L. Long adsorption times affect negatively the removal efficiency of TS. The removal efficiency of TS decreased from 12% to 10%, to 9% and to 7% with the increasing the adsorption time from 30 min to 60 min, to 90 min, to 180 min and 240 min, respectively. The optimum adsorption time was found to be 30 min for 12% TS efficiency. At low adsorption time the adsorption efficiencies decreased as the active sites of Nano-ZnO-Magnetite composite are not contacted enough time with TS and the activated sites on the composite are low as reported by Ip et al. (2010).

A linear relationship between adsorption times and TS adsorption efficiencies was obtained (R =0.94) and this regression is significant (ANOVA $p=0.008 < \alpha=0.05$ and F=24.59)

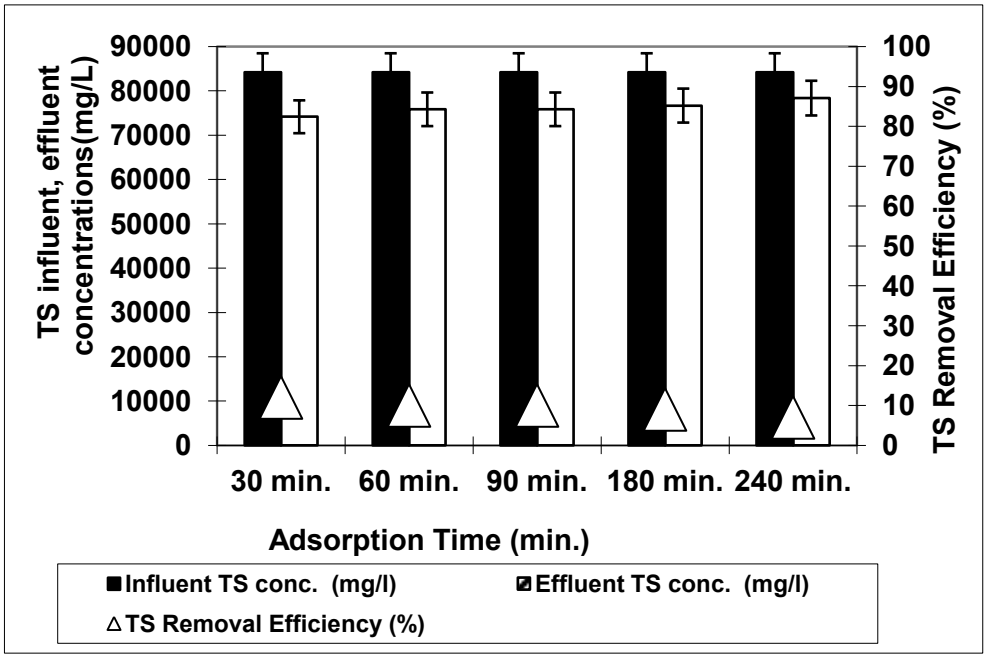


Figure 6.11 The effect of adsorption time on TS yield (Influent Conc.: 84250 mg/L, T: ±20 $^0$C, pH: 4.60, Nano-ZnO-Magnetite conc.: 3g/L).

Figure 6.12 shows the nitrogen removal efficiency with different adsorption times at a pH of 4.60, at 3g/L nano-ZnO-Magnetite and at a temperature of ±20 $^0$C. After 30 min adsorption time, no removal efficiency of total nitrogen was obtained. Increasing the adsorption time from 30 min to 60 min, to 90 min, to 180 min increased the total nitrogen efficiencies to 1%, to 3%, to 5%. The increasing of time to 240 min did not affect the total nitrogen yield. For maximum yield of total nitrogen, the optimum adsorption time was found to be 180 min.

A linear relationship between adsorption times and total nitrogen adsorption efficiencies was not obtained (R =0.94) and this regression is not significant (ANOVA p=0.51 > $\alpha$=0.05 and F=22.81)

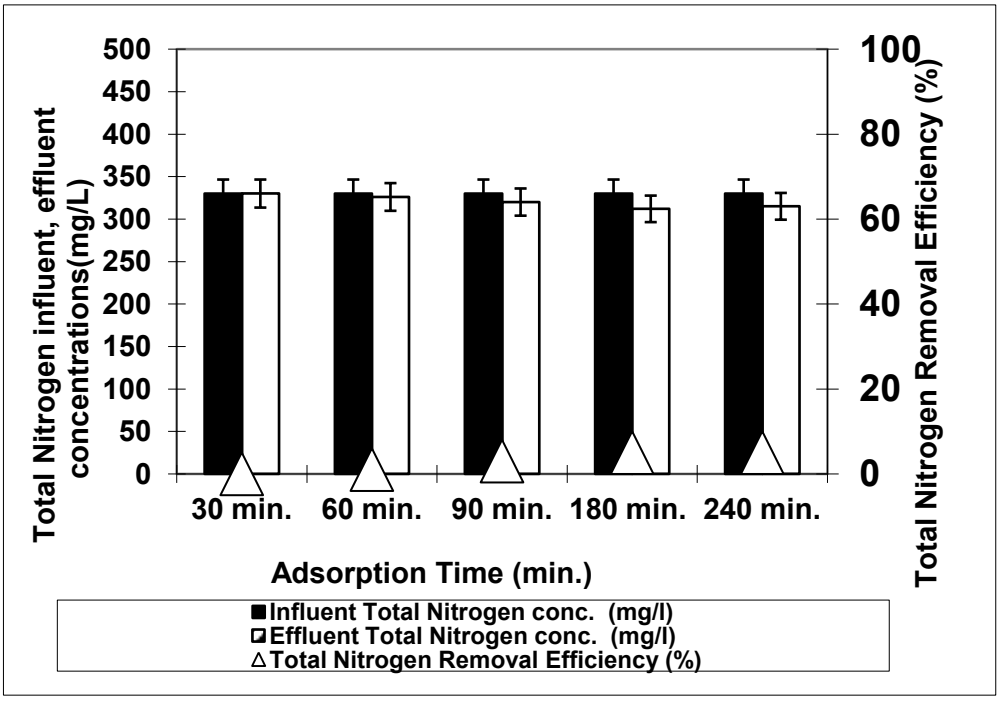


Figure 6.12 The effect of adsorption time on Total Nitrogen yield (Influent Conc.: 330 mg/L, T: ±20 $^0$C, pH: 4.60, Nano-ZnO-Magnetite conc.: 3g/L).

Figure 6.13 shows the removal efficiency of total phosphorous. It was found that total phosphorous efficiency decreased with increasing adsorption time. The total phosphorous yield decreased from 20% to 19%, to 15%, to 12%, and to 10% with increasing of adsorption times from 30 min to 60 min, to 90 min, to 180 min and to 240 min at a pH of 4.60, at 3g/L nano-ZnO-Magnetite and at a temperature of ±20 $^0$C (Figure 6.13). The optimum adsorption time can be considered as 180 min for the maximum removal efficiency of total phosphorus (20%). The maximum total phosphorus removal efficiency is 20% for 30 min adsorption time. After that the yield decreased.

A linear relationship between adsorption times and total phosphorous adsorption efficiencies was obtained (R =0.97) and this regression is significant (ANOVA $p=0.002 < \alpha=0.05$ and F=50.65)

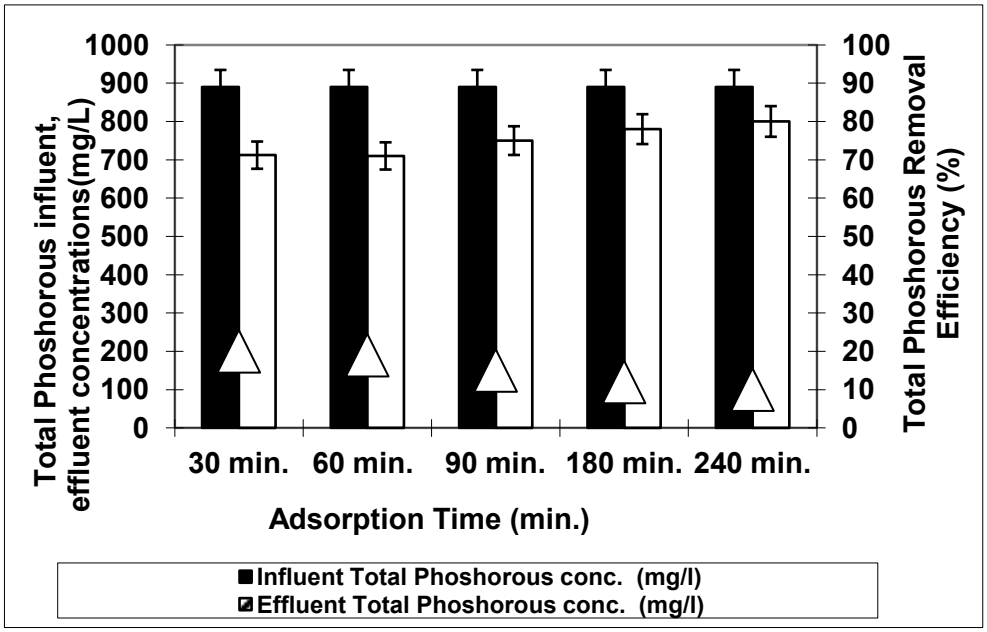


Figure 6.13 The effect of adsorption time on Total Phosphorous yield (Influent Conc.: 890 mg/L, T: ±20 $^0$C, pH: 4.60, Nano-ZnO-Magnetite conc.: 3g/L).

Optimum adsorption time was selected as 180 min because the adsorption equilibrium was reached within 180 min for maximum yields in all pollutant parameters studied in the OMW.

### *6.3.3 Effects of pH on the of Removal OMW throughout Adsorption*

The variations in removals of COD, phenol, TS, total nitrogen and total phosphorous using 3 g/L Nano-ZnO-Magnetite concentrations under acidic (pH 4), neutral (pH 7) and alkaline (pH 10) pH's at a temperature of ±20 $^0$C after 180 min adsorption time were given in Figures 6.14, 6.15, 6.16, 6.17 and 6.18.

From Figure 6.14, it is evident that the maximum removal of COD by adsorption was observed at a temperature of 20 $^0$C after 180 min adsorption time at a 3 g/L concentration of nano-ZnO-Magnetite concentration. The solution pH is recognized as one of the important parameters that governs the adsorption process. Generally, surface charge of the adsorbents and speciation of ionic contaminants is variable with variation of solution pH. When the initial pH was increased from 4 to 7 and 10, the COD removal efficiencies decreased from 12% to 3% and 2%. The maximum

removal of COD was 12% at a temperature of 20 $^0$C after 180 min adsorption time at a 3 g/L nano-ZnO-Magnetite concentration.

A strong influence of pH on adsorption kinetics of some pollutants in the OMW is caused by two reasons: pH affects state of pollutant molecules in solution and surface chemistry of adsorbents. Because pollutants are often weak electrolytes, they have ionizable functional groups that depend on pH. Besides, depending on nature of surface functional groups, adsorbent may be neutral, positively or negatively charged due to protonation or dissociation of the functional groups (Dolinina and Parfenyuk, 2014). The reason for the better adsorption capacity observed at pH 4.0 may be attributed to the larger number of H+ ions present, which in turn neutralize the negatively charged adsorbent surface. At higher pH, the capacity of the adsorbent recessed. The reduction in adsorption at high pH may be possible due to the abundance of $OH^-$ ions, causing increased hinder to diffusion of organics (contributing to COD) ions (Aluyor et al., 2008).

A linear relationship between pH variations and COD adsorption efficiencies was obtained (R =0.98) and this regression is not significant (ANOVA p=0.09 > α=0.05 and F=27).

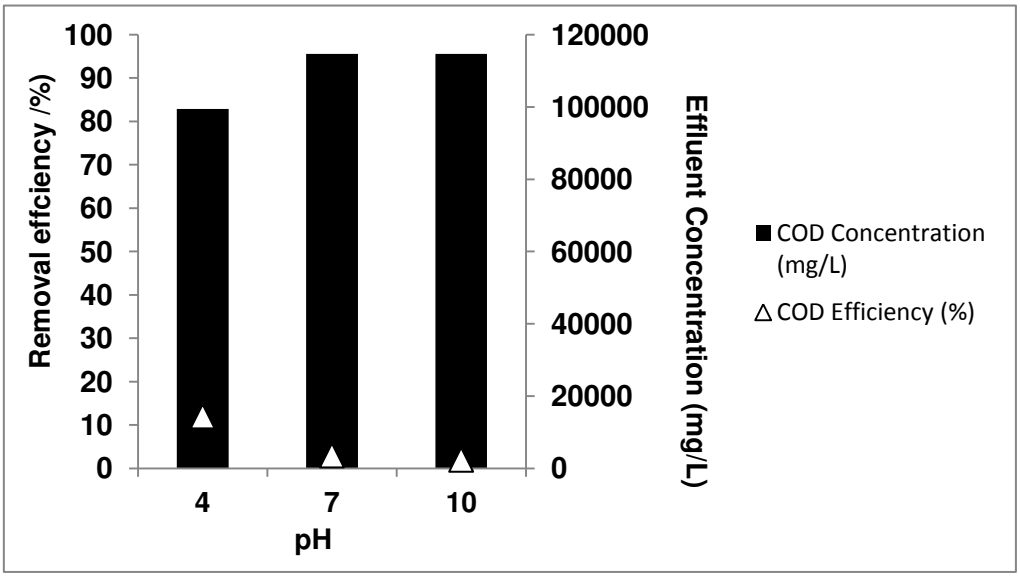


Figure 6.14 The effect of pH on COD yield (Influent Conc.:117000 mg/L, T: ±20 $^0$C, Nano-ZnO-Magnetite conc.: 3g/L, Adsorption time: 180 min).

From Figure 6.15, it can be clearly seen that the removal of phenol was not affected from the pH changes significantly. The yields of phenol decreased from 9% to 3% and 1% with increasing of pH from 4 to 7 and 10, respectively, at a temperature of 20 $^0$C after 180 min adsorption time at a 3 g/L concentration of nano-ZnO-Magnetite concentration. The maximum phenol yields by adsorption was 9% at pH=4.0. At a pH higher than $pH_{zero}$, the Nano-ZnO-Magnetite composite surface is negatively charged attracting cations, whereas at a lower pH, the surface is positively charged attracting anions. Phenol is a water-soluble weak acid. In aqueous solution, the phenol molecule dissociates negative anion as illustrated in reaction (6.1). As per (6.2), hydrogen atom leaves the molecule to form $H_3O^+$ and resulted in a negatively charged phenoxide ion. Hence, at low pH value, acidic media, an electrostatic attraction exists between the positively charged surface of the nanoparticles and the phenoxide molecules (Clifford & Luis, 1979).

$$C_6H_5OH + H_2O \Leftrightarrow C_6H_5O^- + H_3O^+ \quad (6.1)$$

On the other hand, in an alkaline environment, at high values of pH, phenol reacts with NaOH as per reaction (6.2) to form a positively charged sodium phenoxide, which prefers adsorption onto a negatively charged surface (Clifford & Luis, 1979).

$$C_6H_5OH + NaOH \Leftrightarrow C_6H_5ONa^+ + H_2O \quad (6.2)$$

For the case of OMW, the pollutant amount adsorbed was partly dependent of pH in region of 4–10. In fact, this result is expected and not far away from the results of model molecule, phenol. However, adsorption decreased with further increase in solution pH. This could be probably due to the increase of solubility of the pollutant at high pH values.

A linear relationship between pH variations and phenol adsorption efficiencies was obtained (R =1) and this regression is significant (ANOVA p= 2,37035E-17 < $\alpha$=0.05 and F= 2,74E+32)

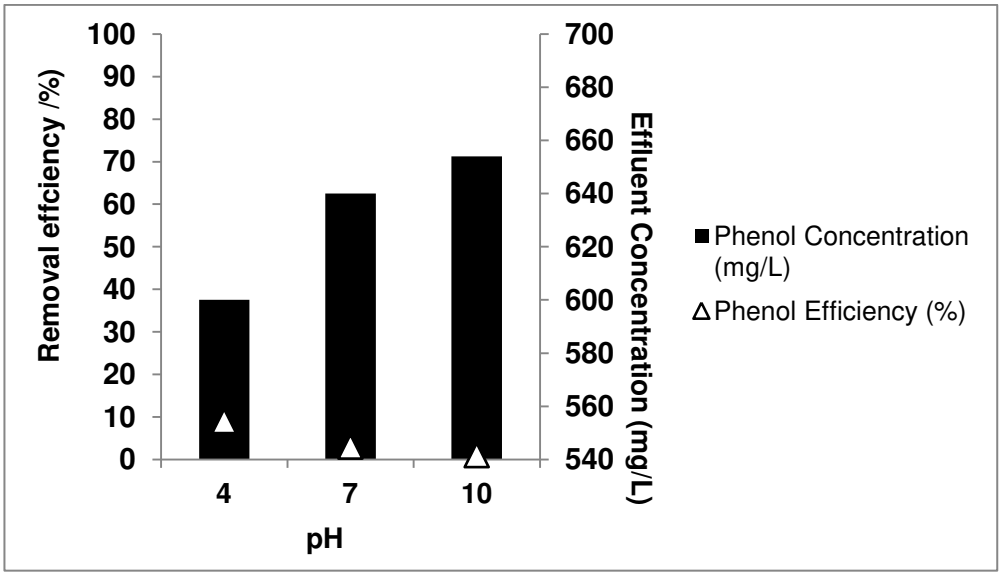


Figure 6.15 The effect of pH on phenol yield (Influent Conc.:660 mg/L, T: ±20 $^0$C, , Nano-ZnO-Magnetite conc.: 3g/L, Adsorption time: 180 min).

Figure 6.16 illustrates the removal of TS with different pH (4, 7 and 10) at a temperature of 20 $^0$C after 180 min adsorption time at a 3 g/L concentration of nano-ZnO-Magnetite concentration. The maximum removal of TS was observed at pH 4 with a yield of 10 %. When the pH of OMW was increased from 4 to 7 and 10, the removal efficiency of TS decreased from 10% to 4% and 2%, respectively. Pinotti and Zaritzky, (2001) reported that when the pH value was more than 5.0 it leads to precipitate the pollutants in the OMW. This shows that the de-stabilization of suspended solid in alkaline conditions while stabilization of suspended solids under acidic conditions.

A linear relationship between pH variations and TS adsorption efficiencies was obtained (R =0.96) and this regression is not significant (ANOVA p=0.11 > α=0.05 and F=12)

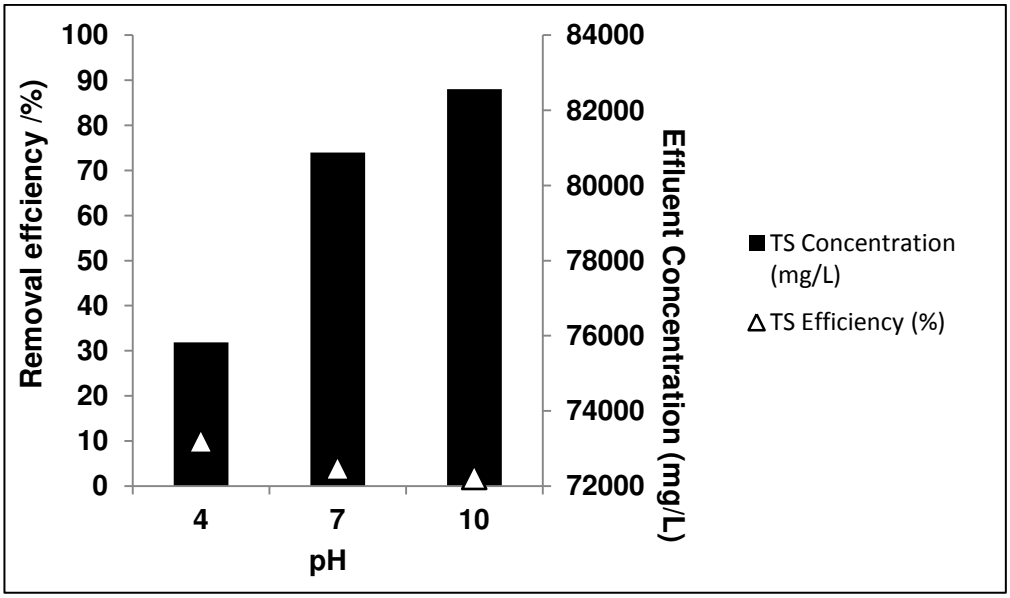


Figure 6.16 The effect of pH on TS yield (Influent Conc.:84250 mg/L, T: ±20 $^0$C, Nano-ZnO-Magnetite conc.: 3g/L, Adsorption time: 180 min).

The maximum removal of total nitrogen is observed at pH 10 as % 7 at a temperature of 20 $^0$C after 180 min adsorption time at a 3 g/L concentration of nano-ZnO-Magnetite concentration (Figure 6.17). Opposite to the previous sections when the removals of COD, phenol and TS decreased with increasing of pH, the yields of total nitrogen increased from 2% to 5% and 7, with increasing of pH from 4 to 7 and 10, respectively. Change of pH value in adsorption rector system could lead to the transformation of the chemical characteristics on the surface of Nano-ZnO-Magnetite composite. Acidic or alkaline species may change the surface chemistry of the adsorbent by reacting with the surface groups. The functional groups exhibit pH-dependent interactions with OMW, which result in the transformation of the active sites (Contescu et al., 1998; Radovic, 1999).

A linear relationship between pH variations and total nitrogen adsorption efficiencies was obtained (R =0.99) and this regression is not significant (ANOVA $p=0.35 > \alpha=0.05$ and F=75)

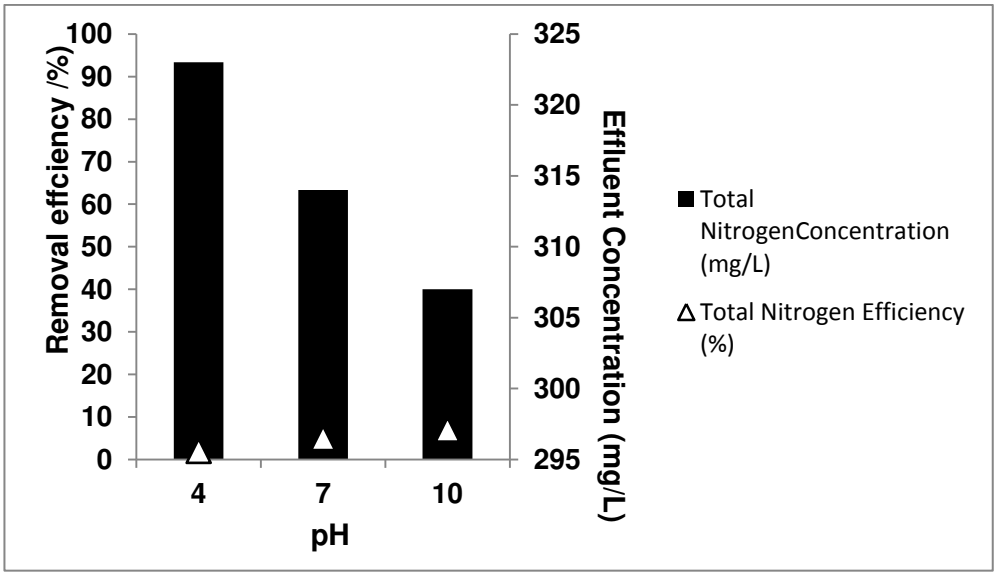


Figure 6.17 The effect of pH on total nitrogen yield (Influent Conc.:330 mg/L, T: ±20 $^0$C, Nano-ZnO-Magnetite conc.: 3g/L, Adsorption time: 180 min).

Figure 6.18 shows the total phosphorous removal efficiency with increasing pH values of 4, 7 and 10. As is observed in COD, phenol and TS removals, the removal of total phosphorous decreased from 10% to 3% and 1% with increasing of pH from 4 to 7 and 10, respectively, at a temperature of 20 $^0$C after 180 min adsorption time at a 3 g/L Nano-ZnO-Magnetite concentration. Phosphorus removal capacity of Nano-ZnO-Magnetite has reduced under pH>4. The pH-dependency of the Nano-ZnO-Magnetite was more significant under acidic conditions. The observed partial pH-dependency of Nano-ZnO-Magnetite is due to the hindering of pollutant adsorption on high pH as reported by Yang et al., (2010).

A linear relationship between pH variations and total phosphorous adsorption efficiencies was obtained (R =0.99) while this regression is significant (ANOVA $p=0.02 < \alpha=0.05$ and F=243)

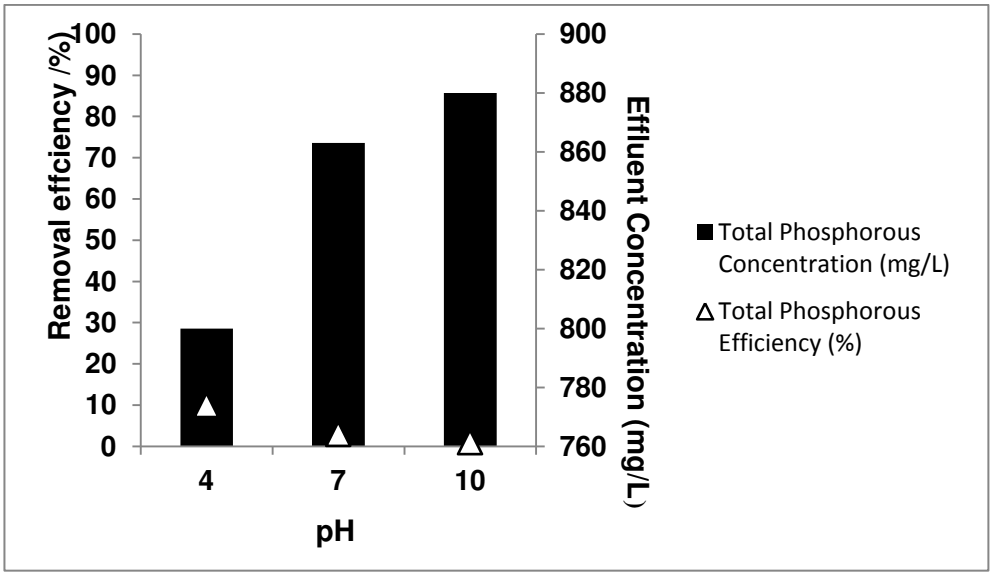


Figure 6.18 The effect of pH on total phosphorous yield (Influent Conc.:890 mg/L, T: ±20 0C, Nano-ZnO-Magnetite conc.: 3g/L, Adsorption time: 180 min).

Optimum pH was selected as 4 because adsorption equilibrium was reached at the original pH of OMW for maximum yields in all pollutant parameters investigated in the OMW.

### *6.3.4 Adsorption Capacity of Nano-ZnO-Magnetite*

The amount of adsorption capacity of Nano-ZnO-Magnetite for the COD was calculated according to Eq. (6.3):

$$qe = \frac{(Co - Ce).V}{W} \tag{6.3}$$

where $q_e$ is the capacity of adsorbent ( mg/g), $C_0$ and Ce are the initial and equilibrium liquid concentrations (mg/L), respectively; V is the volume of solution (L); and W is the weight of adsorbent (g).

Table 6.2. Adsorption capacity of Nano-ZnO-Magnetite for COD

| **Nano-ZnO-Magnetite Conc. (g/L)** | 0.5 | 1.5 | 3 | 7 | 10 |
|---|---|---|---|---|---|
| **Influent COD conc.(mg/L)** | 117000 | 117000 | 117000 | 117000 | 117000 |
| **Effluent COD conc.(mg/L)** | 111150 | 107640 | 105300 | 102960 | 102950 |
| **$q_e$ (mg/g)** | 11700 | 6240 | 3900 | 2006 | 1405 |

Table 6.3 Adsorption capacity of Nano-ZnO-Magnetite for phenol

| **Nano-ZnO-Magnetite Conc. (g/L)** | 0.5 | 1.5 | 3 | 7 | 10 |
|---|---|---|---|---|---|
| **Influent phenol conc.(mg/L)** | 660 | 660 | 660 | 660 | 660 |
| **Effluent phenol conc.(mg/L)** | 640 | 630 | 627 | 615 | 615 |
| **$q_e$ (mg/g)** | 40 | 20 | 11 | 6.42 | 4.5 |

When the concentration of Nano-ZnO-Magnetite nanocomposite increased from 0.5 g/L to 1.5 g/L, to 3 g/L, to 7 g/L and to 10 g/L, the adsorption capacity of Nano-ZnO-Magnetite nanocomposite decreased from 11700 mg/g to 6240 mg/g , to 3900 mg/g, to 2006 mg/g and to 1405 mg/g for COD, respectively. Similarly, When the concentration of Nano-ZnO-Magnetite nanocomposite increased from 0.5 g/L to 1.5 g/L, to 3 g/L, to 7 g/L and to 10 g/L, the adsorption capacity of Nano-ZnO-Magnetite nanocomposite decreased from 40 mg/g to 20 mg/g , to 11 mg/g, to 6.42 mg/g and to 4.5 mg/g for phenol, respectively. This may be attributed to many factors such as availability of solute, interference between binding sites, electrostatic

interactions, and reduced mixing due to high Nano-ZnO-Magnetite concentration in the OMW. Many of the adsorption sites, therefore, remain unsaturated due to the limited availability of the sorbate, which in turn lowers the uptake and the adsorption efficiency (Abu Al-Rub, et al., 2006).

### *6.3.5 Adsorption Isotherms of COD on Nano-Zno-Magnetite Nanocomposite*

The fundamental concept in adsorption science is named as the adsorption isotherm. It is the equilibrium relation between the quantity of the adsorbed material and the concentration in the bulk fluid phase at constant temperature. The design and efficient operation of adsorption processes require equilibrium adsorption data for use in kinetic and mass transfer models. These models can then be used to predict the performance of the adsorption contact processes under a range of operating conditions (Banat et al., 2000).

In this study, Langmuir isotherm and Lagergren's Equation For Pseudo-First-Order reaction were investigated for detect the adsorption kinetic of pollutants (based on COD and phenol) on the surface of Nano-Zno-Magnetite nanocomposite. The Kinetics of COD and phenol adsorption were investigated with Lagergren's equation ( Eq. 6.5) which is a pseudo-first-order reaction.

#### *6.3.5.1 Langmuir Isotherm*

The Langmuir isotherm theory assumes monolayer coverage of adsorbate over a homogenous adsorbent surface (Langmuir, 1918). Therefore, at equilibrium, a saturation point is reached where no further adsorption can occur. The Langmuir isotherm, expressed in its linearized form by the Eq. (6.4):

$$\frac{C_e}{q_e} = \frac{1}{b.q_m} + \frac{C_e}{q_m} \qquad (6.4)$$

is applicable if the monolayer coverage of adsorbent with adsorbate takes place on a homogeneous adsorbent surface. The Langmuir coefficients b and qm representing

the adsorption equilibrium constant and maximum adsorption capacity respectively, which were obtained from the intercepts and slopes of the plots Ce/qe versus which are linear (Eba et al. 2010).

Ce : Effluent COD concentration (mg/L)

qe: COD amount adsorbed on unit adsorbent (mg/g)

qm: Maximum adsorption capacity (mg/g)

b: Adsorption equilibrium constant

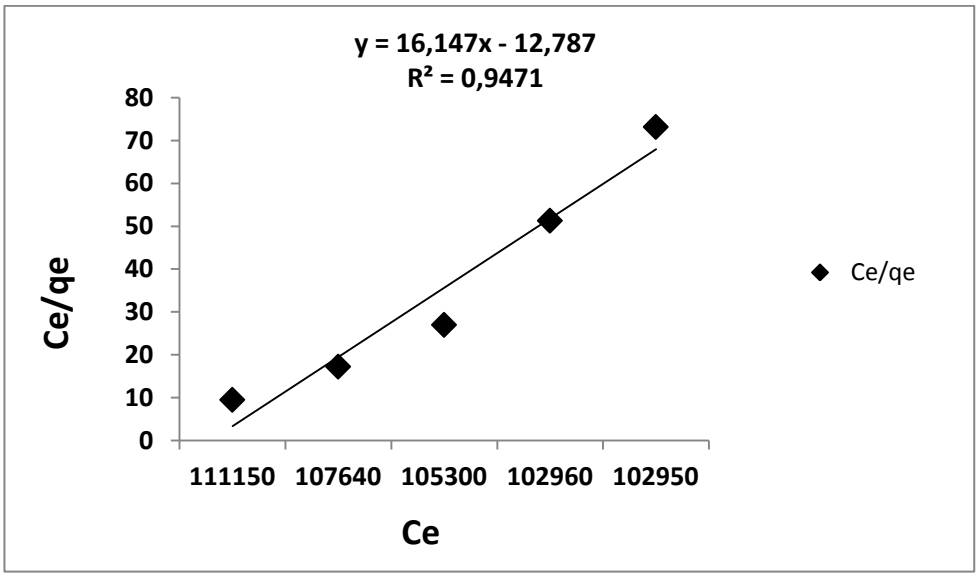


Figure 6.19 Langmuir isotherm for COD adsorption.

From Figure 6.19, the $R^2$ value for linear lines between Ce and Ce/qe showed a value of 0.9471 for COD adsorbing on the surface of Nano-ZnO-Magnetite. Langmuir isotherm constant (b) and the maximum capacity of adsorbent (qm) values were 12.787 unitless and 16.147 mg/g for COD adsorbed on Nano-Zno-Magnetite. The kinetic constants were meaningfull for Langmuir isotherm. This showed that the adsorptions of COD to the Nano-ZnO-Magnetite can be explained with Langmuir isotherm.

### *6.3.5.2 Lagergren's Equation For Pseudo-First-Order Reaction*

The integrated form of Lagergren's equation for pseudo-first-order reaction can be expressed as Eq.(6.5):

$$\log(q_e - q_t) = \log(q_e) - (k_1/2.303).t \qquad (6.5)$$

where qe, qt are the amount of OMW adsorbed (mg) per unit dry weight (g) of the adsorbent at equilibrium and at any time t (min), respectively and $k_1$ is the rate constant of pseudo-first-order adsorption ($min^{-1}$). The value of $k_1$ and qe can be calculated from the plot of $\log(q_e - q_t)$ versus t.

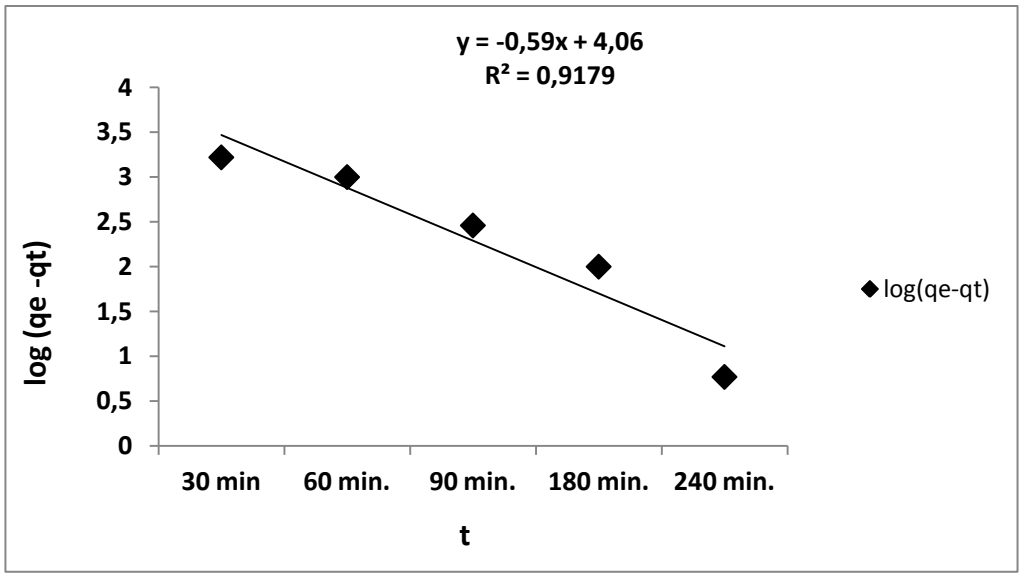


Figure 6.20 Lagergren Isotherm for COD adsorption.

The $R^2$ values for Lagergren Isotherm was found to be 0.9179 for COD performed with Nano-ZnO-Magnetite. The graph between log(qe −qt) and t gives Lagergren's the first order rate kinetic constant ($k_1$). The k1 values evaluated from Lagergren plots were found to be 0.59 $min^{-1}$ for Nano-Zno-Magnetite.

Table 6.4 Isotherm correlation coefficients of Langmuir isotherm and Lagergren's equation for COD adsorption.

| **Isotherms** | **$R^2$ Value** | **Constants** |
|---|---|---|
| Langmuir isotherm | 0.9471 | b= 12.787 unitless<br>qm= 16.147 mg/g |
| Lagergren's equation | 0.9179 | k1=0.59 $min^{-1}$ |

Among the adsorption isoterm used it was found that Langmuir adsorption isotherm with isotherm constant (b: 12.787 unitless ) and the maximum capacity of adsorbent (qm: 16.147 mg/g) values are suitable for the removal of COD from the OMW.

### *6.3.6 Adsorption Isotherms of Phenol on Nano-Zno-Magnetite Nanocomposite*

#### *6.3.6.1 Langmuir isotherm*

From Figure 6.21, the $R^2$ value for linear lines between Ce and Ce/qe showed a value of 0.9687 for phenol adsorbing on the surface of Nano-ZnO-Magnetite. Langmuir isotherm constant (b) and the maximum capacity of adsorbent (qm) values were 24.26 unitless and 30.54 mg/g for phenol adsorbed on Nano-Zno-Magnetite. The kinetic constants were meaningfull for Langmuir isotherm. This showed that the adsorptions of phenol to the Nano-ZnO-Magnetite can be explained with Langmuir isotherm.

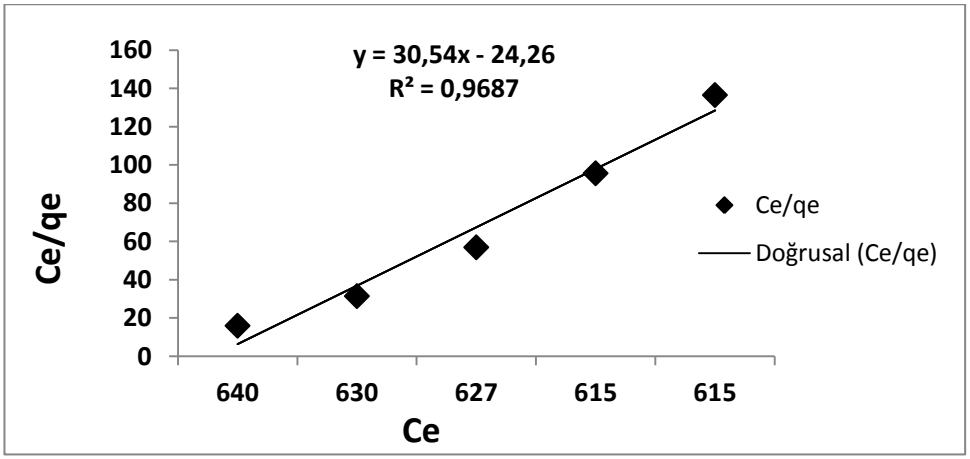


Figure 6.21 Langmuir isotherm for COD adsorption.

### *6.3.6.2 Lagergren's Equation For Pseudo-First-Order Reaction*

The $R^2$ values for Lagergren Isotherm was found to be 0.8836 for phenol performed with Nano-ZnO-Magnetite. The graph between log(qe −qt) and t gives Lagergren's the first order rate kinetic constant (k1). The k1 values evaluated from Lagergren plots were found to be 0.276 min-1 for Nano-Zno-Magnetite.

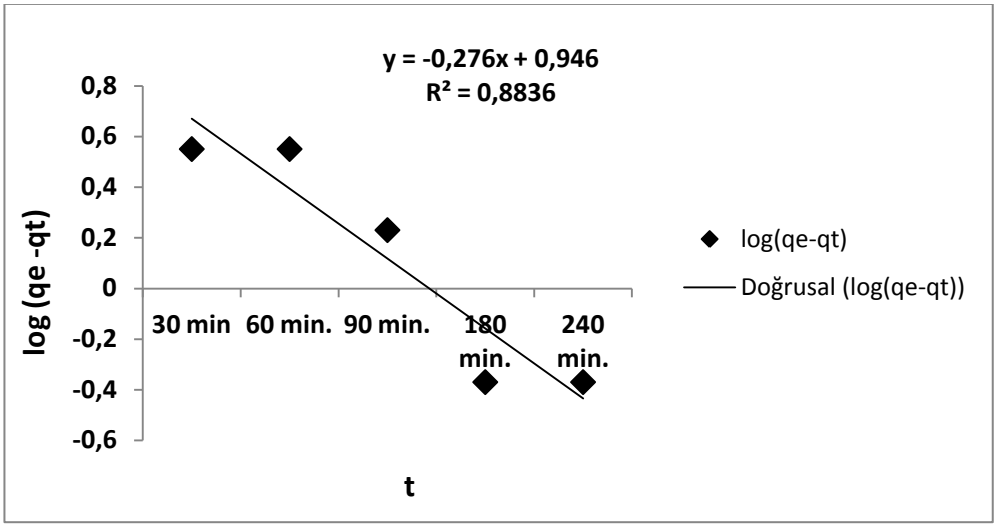


Figure 6.22 Lagergren Isotherm for phenol adsorption.

Table 6.5 Isotherm correlation coefficients of Langmuir isotherm and Lagergren's equation for COD adsorption.

| **Isotherms** | **$R^2$ Value** | **Constants** |
|---|---|---|
| Langmuir isotherm | 0.9687 | b= 24.26 unitless<br>qm= 30.54 mg/g |
| Lagergren's equation | 0.8836 | k1= 0.276 $min^{-1}$ |

Among the adsorption isoterm used it was found that Langmuir adsorption isotherm with isotherm constant (b: 24.26 unitless) and the maximum capacity of adsorbent ($q_m$: 30.54 mg/g) values are suitable for the removal of phenol from the OMW.

## 6.4 Photocatalytic Treatment Process of OMW under UV Light

### *6.4.1 Determination of Optimum Nano-ZnO-Magnetite Concentration under UV Light*

In this step of this study the pollutants in the OMW were treated via photodegradation under UV light power in the presence of a nano composite (Nano-ZnO-Magnetite*)* generated under laboratory conditions. In the photocatalytic treatment when Nano-ZnO-Magnetite is illuminated with the light of UV, electrons are promoted from the valence band to the conduction band of the semiconducting oxide to give electron–hole pairs. The valence band ($h_{VB}^{+}$) potential is positive enough to generate hydroxyl radicals at the surface and the conduction band ($e_{CB}^{-}$) potential is negative enough to reduce molecular oxygen. The hydroxyl radical is a powerful oxidizing agent and attacks organic pollutants present at or near the surface of Nano-ZnO-Magnetite. This phenomenon causes photooxidation of pollutants such as COD, phenol, total solids, total nitrogen and total phosphorous in the OMW resulting in destructing of them (Galindo et al., 2000).

The mechanism of photodegradation of COD, phenol, total solids, total nitrogen and total phosphorous on Nano-ZnO-Magnetite nanocomposite surface was as follows: The excitation of Nano-ZnO-Magnetite nanocomposite by UV energy leads to the formation of an electron-hole pair. The hole combines with water ($H_2O$) to form hydroxyl radicals ($OH\cdot$) while electron converts oxygen ($O_2$) to superoxide radical ($O_2\cdot^{-}$), a strong oxidizing species as shown in the following (Sponza and Öztekin, 2015):

$$\text{Nano-ZnO-Magnetite} + hv \leftrightarrow \text{Nano-ZnO-Magnetite nanocomposite} + h_{VB}^{+} + e_{CB}^{-} \quad (6.6)$$

$$\text{Nano-ZnO-Magnetite} + hv \leftrightarrow \text{Nano-ZnO-Magnetite}\ (h_{VB}^{+} + e_{CB}^{-}) \quad (6.7)$$

$$\text{Nano-ZnO-Magnetite} \mid OH^{-} + h_{VB}^{+} \rightarrow \text{Nano-ZnO-Magnetite} \mid OH\cdot \quad (6.8)$$

$$\text{Nano-ZnO-Magnetite} \mid OH_2 + h_{VB}^{+} \rightarrow \text{Nano-ZnO-Magnetite} \mid OH\cdot + H^{+} \quad (6.9)$$

$$\text{Nano-ZnO-Magnetite} \mid OH\cdot + Red_{org} \rightarrow Ox_{org} \rightarrow \text{photodegradation of OMW pollutants} \quad (6.10)$$

$$h_{VB}^{+} + Red_{org} \rightarrow Ox_{org} \rightarrow \text{photodegradation of OMW pollutants} \quad (6.11)$$

$$OH\cdot + OH\cdot \rightarrow H_2O_2 \quad (6.12)$$

$$H_2O_2 \text{ (or } 2OH\cdot) \rightarrow 2H^{+} + O_2 \quad (6.13)$$

Effects of 0.5 g/L, 1.5 g/L, 3 g/L, 7 g/L and 10 g/L Nano-ZnO-Magnetite concentrations on the removals of COD, phenol, total solids, total nitrogen and total phosphorous in the OMW were studied with constant irradiation time (30 min) at an original pH of OMW (pH: 4.60) at a temperature of ±20 $^{0}$C with UV lamps with powers of 300 W (Figures, 6.23, 6.24, 6.25, 6.26 and 6.27).

The effect of the concentration of Nano-ZnO-Magnetite nanocomposite on the COD removal was studied as shown in Figure 6.23. The photodegradation efficiency increases with an increase in the amount of Nano-ZnO-Magnetite photocatalyst from 0.5 g/L up to 7 g/L. COD photodegradation efficiencies were found as 62 %, 65%, 72% and 80% for 0.5 g/L, 1.5 g/L, 3 g/L and 7 g/L Nano-ZnO-Magnetite nanocomposite concentrations, respectively, at a pH of 4.60 at a temperature of ±20 $^{0}$C after 30 min irradiation time with an UV lamp having a power of 300 W. Further increase of Nano-ZnO-Magnetite photocatalyst concentration to 10 g/L did not affect the COD yield. On the other word, the addition of higher quantities of Nano-ZnO-Magnetite photocatalyst would have no effect on the photodegradation efficiency of the polutants in the OMW. Probably the structural decomposition of photocatalysts and the pore surfaces of photocatalysts might have been covered completely with the particles of pollutant parameters (COD, phenol) or other radical species (e.g. carbon based radicals). Low photocatalyst quantity decreases the number of active sites on the Nano-ZnO-Magnetite surface, which in turn decreases the numbers of hydroxyl (OH·) radicals (Sponza and Öztekin, 2015).

A linear relationship between Nano-ZnO-Magnetite composite concentrations and COD photodegradation efficiencies was obtained up to a Nano-ZnO-Magnetite

composite concentration of 10 g/L (R =0.94) and this regression is significant (ANOVA p=0.02 < α=0.05 and F=23.02).

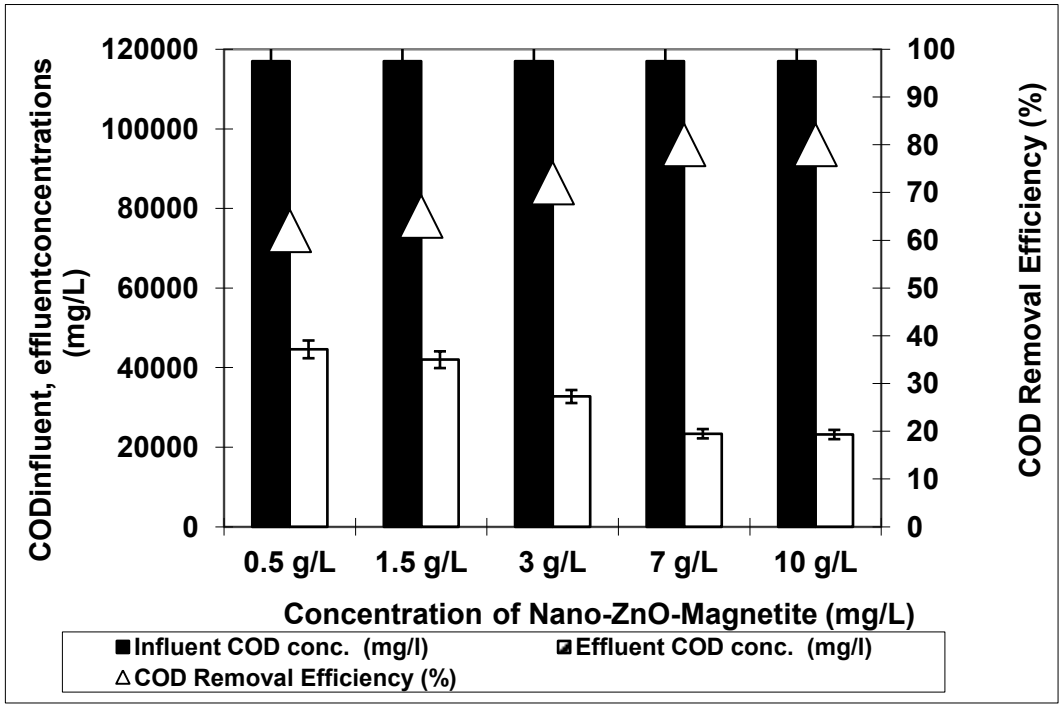


Figure 6.23 The effect of Nano-ZnO-Magnetite concentration on COD yield (Influent Conc.: 117000 mg/L, T: ±20 $^0$C, pH: 4.60, Irradiation time 30 min, UV power: 300 W).

Figure 6.24 shows the degradation efficiency of phenol with increasing of Nano-ZnO-Magnetite photocatalyst concentrations from 0.5 g/L, to 1.5 g/L, 3 g/L, 7 g/L and to 10 g/L at a pH of 4.60 at a temperature of ±20 $^0$C after 30 min irradiation time with an UV lamp with a power of 300 W. When the concentration of Nano-ZnO-Magnetite increased from 0.5 g/L to 1.5 g/L, 1.5 g/L to 3 g/L from 3 g/L to 7 g/L, the removal efficiency of phenol increased from 57% to 60%, from 60% to 67%, from 67% to 77%, respectively. When Nano-ZnO-Magnetite photocatalyst concentration further increased up to 10 g/L, the phenol yield sligtly decreased to 75%. The maximum phenol removal was obtained as 77% at 7 g/L Nano-ZnO-Magnetite composite concentration. The enhanced photocatalytic activity of Nano-ZnO-Magnetite ($Fe_3O_4$) possibly can be attributed to the retardation of recombination of electron–hole pair as reported by Hong et al. (2008) at 7 g/L Nano-ZnO-Magnetite composite concentration. Khodja et al. (2001) found that the photoemission intensity

of the Nano-ZnO-Magnetite composite is lower than that of ZnO, indicating a slower electron–hole recombination in the Nano-ZnO-Magnetite composite. This is probably due to the presence of $Fe^{3+}$ ions in Nano-ZnO-Magnetite composite. It has been reported that $Fe^{3+}$ ions in $Fe_3O_4$ can act as a photo-excited electron-trapping site to prevent the fast recombination of photoinduced charge carriers and prolonged life-times (Ambrus et al., 2008). In this study, the photo-generated electron in the conduction band of ZnO might be captured by the $Fe^{3+}$ ions. This would lead to the formation of reduced iron ions, $Fe^{2+}$, which are relatively unstable in comparison with $Fe^{3+}$. The $Fe^{2+}$ ions further react with the oxygen dissolved in the reaction mixture of OMW to generate $Fe^{3+}$ ions. A similar phenomenon has been observed in Fe-doped $TiO_2$ and ZnO by various researchers (Yu et al., 2009 and Ba-Abbad et al., 2013). The presence of $Fe^{3+}$ also has been suggested as a trigger for the enhanced photocatalytic activity.

A linear relationship between Nano-ZnO-Magnetite composite concentrations and phenol photodegradation efficiencies was obtained up to a Nano-ZnO-Magnetite composite concentration of 7 g/L ($R = 0.92$) and this regression is significant (ANOVA $p=0.04 < \alpha=0.05$ and $F=16.92$).

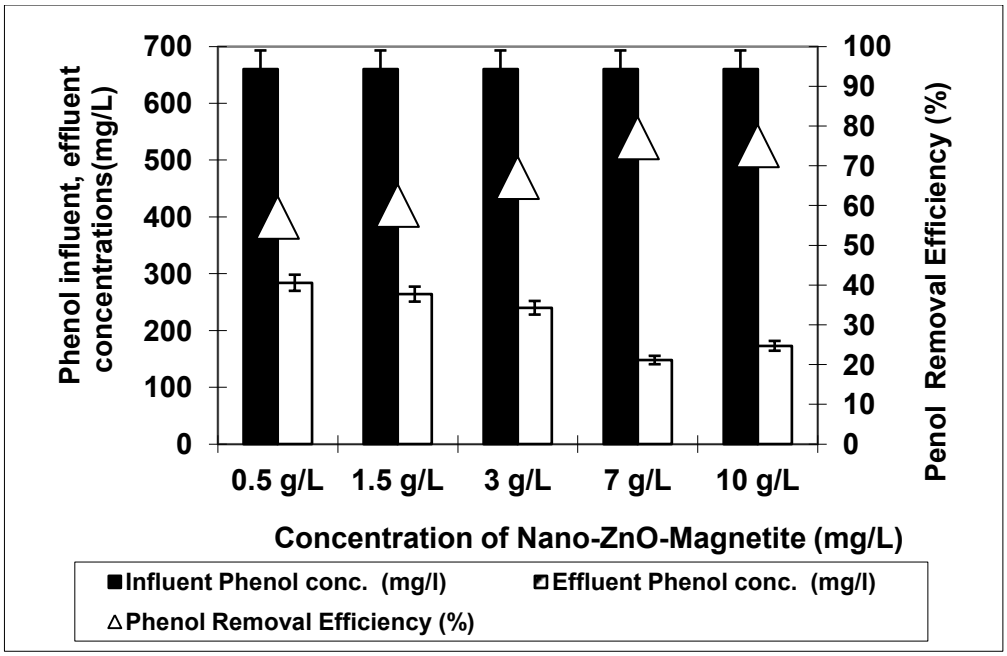


Figure 6.24 The effect of Nano-ZnO-Magnetite concentration on phenol yield (Influent Conc.: 660 mg/L, T: $\pm 20^0$C , pH: 4.60, Irradiation time 30 min, UV power: 300 W).

Figure 6.25 shows the photodagradation efficiencies of TS at increasing Nano-ZnO-Magnetite photocatalyst concentrations of 0.5 g/L, 1.5 g/L, 3 g/L, 7 g/L and 10 g/L. The photocatalytic yields were found as 70 %, 66%, 63%, 57% and 50%, respectively, at a pH of 4.60 at a temperature of ±20 $^0$C after 30 min irradiation time with an UV lamp with a power of 300 W. It was found that the percentage photodegradation efficiency decreased with increase in initial concentration of the Nano-ZnO-Magnetite composite from 0.5 g/L to 10 g/L. Thus could be attributed to the increase of concentration gradient and saturation of adsorption and photocatalytic points in the presence of high Nano-ZnO-Magnetite composite. The maximum TS removal efficiency is 70% at 0.5 g/L Nano-ZnO-Magnetite photocatalyst concentration. Magnetite ($Fe_3O_4$) nanoparticles are easily subject to aggregation in aqueous system. $Fe_3O_4$ nanoparticles exhibit the hydrophilic surface due to presence of hydroxyl groups. There is hydrophilic interaction between particles and these particles form the agglomerate and resulted in large clusters (Teja and Koh, 2009). The agglomerates may cause to increase TS removal efficiency.

A linear relationship between Nano-ZnO-Magnetite composite concentrations and TS photodegradation efficiencies was obtained ($R = 0.98$) and this regression is significant (ANOVA $p=0.001 < \alpha=0.05$ and $F=91.54$).

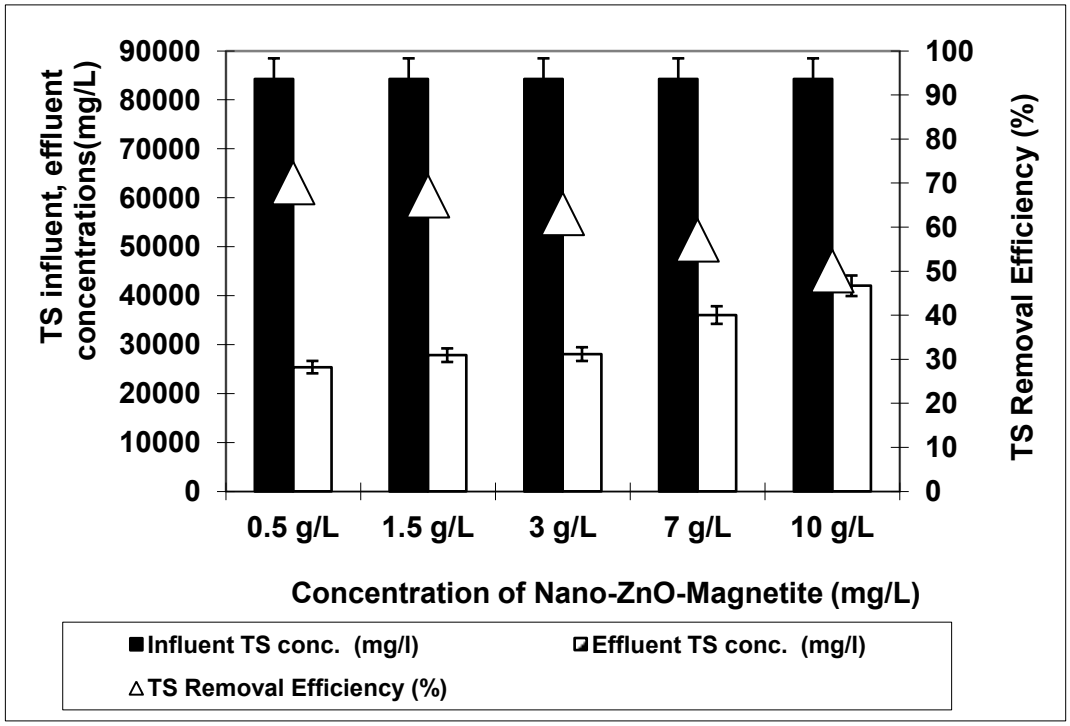


Figure 6.25 The effect of Nano-ZnO-Magnetite concentration on TS yield (Influent Conc.: 84250 mg/L, T: $\pm 20^0$C, pH: 4.60, Irradiation time 30 min, UV power: 300 W).

Figure 6.26 summarizes the effects of increasing Nano-ZnO-Magnetite photocatalyst concentrations (0.5 g/L, 1.5 g/L, 3 g/L, 7 g/L and 10 g/L) on total nitrogen photodegradation yields at a pH of 4.60 at a temperature of $\pm 20\ ^0$C after 30 min irradiation time with an UV lamp with a power of 300 W. According to the aforementioned Nano-ZnO-Magnetite photocatalyst concentrations the photodegradation yields of total nitrogen were 79%, 75%, 70%, 66% and 54%, respectively. As the Nano-ZnO-Magnetite photocatalyst concentrations were increased, the photodegradation yields of total nitrogen decreased as TS parameter in the OMW. Further increase in catalyst concentration from 0.5 g/L up to 10 g/L reduces the specific activity of the catalyst because of agglomeration of catalyst particles and light scattering and screening effect, thus leading to the decreased photocatalytic degradation efficiency. On the other hand, at high catalyst concentration, it is difficult to maintain the homogeneous suspension due to particle agglomeration, which may also reduce the photocatalytic activity. So the photodegradation efficiency of total nitrogen decreases gradually as reported by Ma et al., (2015). This could be attributed to the increasing of turbidity of the OMW

suspension. This resulting in decreasing of UV ligth and power a result of excess of Nano-ZnO-Magnetite particles (Goncalves et al, 1999).

A linear relationship between Nano-ZnO-Magnetite composite to concentrations and total nitrogen photodegradation efficiencies was obtained (R =0.96) and this regression is significant (ANOVA $p=0.003 < \alpha=0.05$ and F=45.06).

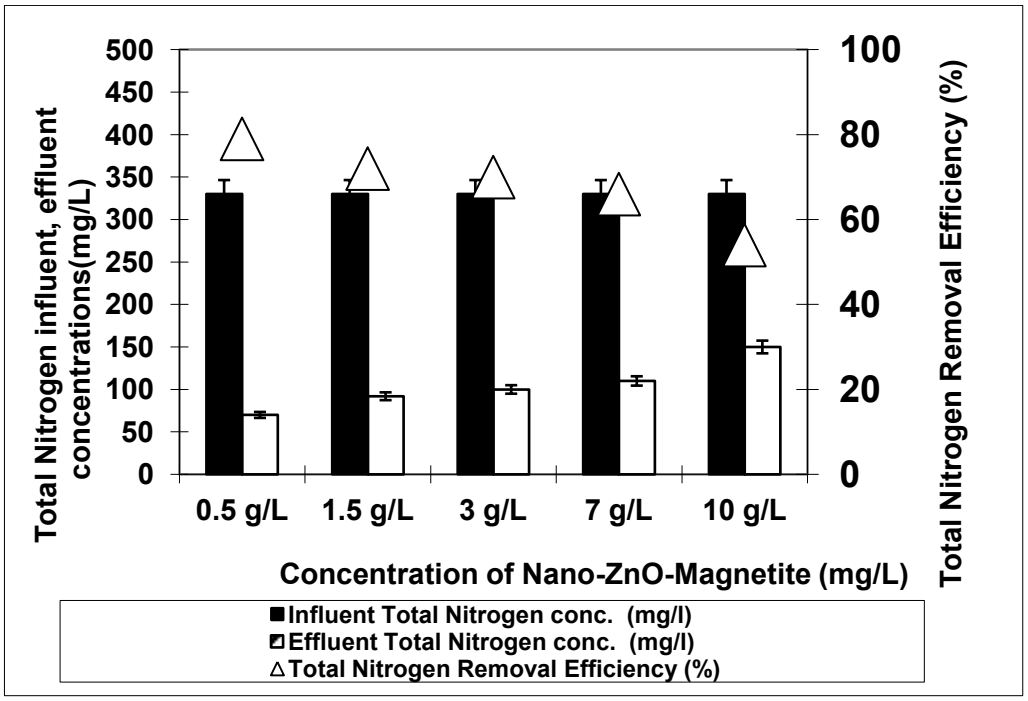


Figure 6.26 The effect of Nano-ZnO-Magnetite concentration on total nitrogen yield (Influent Conc.: 330 mg/L, T: ±20 $^0$C, pH: 4.60, Irradiation time 30 min, UV power: 300 W).

From Figure 6.27, it can be seen that when the concentration of Nano-ZnO-Magnetite increased from 0.5 g/L to 1.5 g/L, 1.5 g/L to 3 g/L from 3 g/L to 7 g/L, from 7 g/L to 10 g/L, the removal efficiency of total phosphorous increased from 37% to 45%, from 45% to 52%, from 52% to 66% and from 66% to 85%, respectively, at a pH of 4.60 at a temperature of ±20 $^0$C after 30 min irradiation time with an UV lamp with a power of 300 W. The maximum total phosphorous removal was obtained as 85% at 10 g/L Nano-ZnO-Magnetite composite concentration. This high yield can be attributed to the irradiation of an aqueous Nano-ZnO-Magnetite suspension with light energy greater than the band gap energy of the semiconductor (hv>Eg=3.2 eV) conduction band electrons (e-) and valence band holes (h+) are

generated as reported by Pelizzetti and Minero, (1993). After this primary event, part of the photogenerated carriers recombine in the bulk of the semiconductor with heat emission, while the rest reach the surface where the holes as well as the electrons act as powerful oxidants and reductants respectively. The photogenerated electrons react with the adsorbed molecular $O_2$ on the Nano-ZnO-Magnetite reducing it to superoxide radical anion $O^{-2}$, while the photogenerated holes can oxidize either the nitrogen directly or the $OH^-$ ions and the $H_2O$ molecules adsorbed at the Nano-ZnO-Magnetite surface to produce $OH^{\cdot}$ Radicals (Pelizzetti and Minero, 1993). Given above based on the explainations $OH^{\cdot}$ radicals degraded total phosphorus pollutants from olive mill wastewater. With increasing Nano-ZnO-Magnetite composite concentration, more surface area of Nano-ZnO-Magnetite is generated and the more $OH^{\cdot}$ radicals are formed, phosphorus removal efficiency increases.

A linear relationship between Nano-ZnO-Magnetite composite concentrations and total phosphorous photodegradation efficiencies was obtained (R =0.99) and this regression is significant (ANOVA $p=0.003 < \alpha=0.05$ and F=200.62).

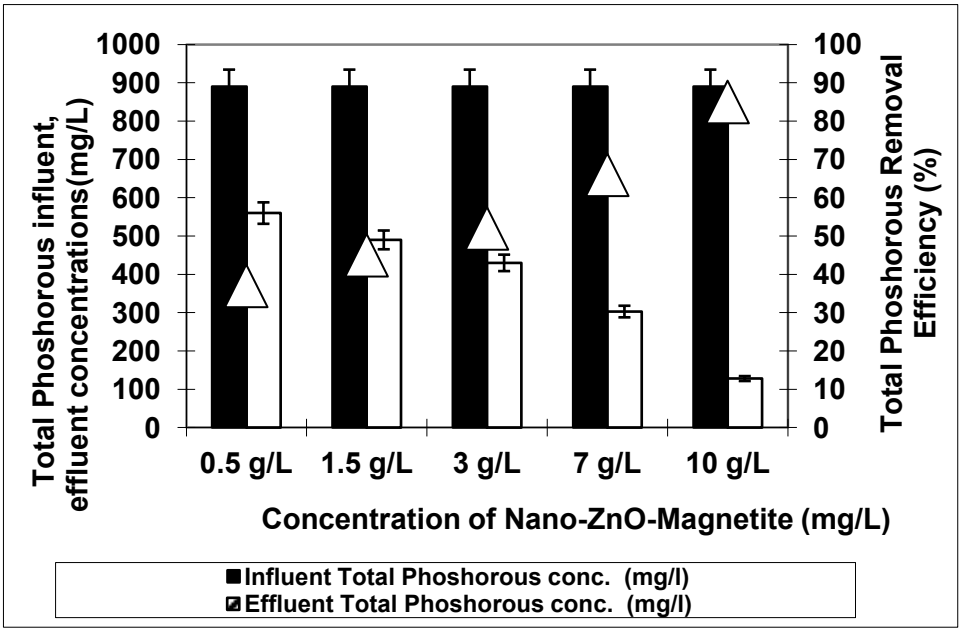


Figure 6.27 The effect of Nano-ZnO-Magnetite concentration on total phosphorous yield (Influent Conc.: 890 mg/L, T: ±20 $^0$C, pH: 4.60, Irradiation time 30 min, UV power: 300 W).

Considering all the removal efficiencies for studied parameters in the OMW, a significant nanocomposite concentration was obtained for maximum yields throughout photoxidation of pollutant parameters in the OMW. The optimum Nano-ZnO-Magnetite composite concentration was selected as 3 g/L for the maximum removals of all pollutant parameters in the OMW via photocatalysis.

### *6.4.2 Determination of Optimum Irradiation Time of UV Light*

Figures 6.28, 6.29, 6.30, 6.31 and 6.32 illustrate the effect of the irradiation time on the removal of COD, phenol, TS, total nitrogen and total phosphorous in the OMW throghout photocatalysis, respectively at a pH of 4.60 at a temperature of ±20 $^0$C at constant 3 g/L Nano-ZnO-Magnetite composite concentration with an UV lamp with a power of 300 W. As aforementioned in the upper section, the optimum Nano-ZnO-Magnetite composite concentration was found as 3 g/L. Therefore, the effects of irradiation times on the COD, phenol, TS, total nitrogen and total phosphorous removal efficiencies were investigated at five different adsorption times (30 min., 60 min., 90 min., 180 min. and 240 min) at a pH of 4.60 at a temperature of ±20 $^0$C at constant 3 g/L Nano-ZnO-Magnetite composite concentration with an UV lamp with a power of 300 W.

Figure 6.38 illustrates the removal of COD with different irradiation times (30 min., 60 min., 90 min., 180 min. and 240 min) at a pH of 4.60 at a temperature of 20 $^0$C after at a 3 g/L concentration of Nano-ZnO-Magnetite nanocomposite. The maximum removal of COD was observed at 30 min irradiation time with a maximum yield of 80 %. COD removal efficiencies were found as 80 %, 80%, 69%, 65% and 62% for 30 min., 60 min., 90 min., 180 min. and 240 min irradiation time, respectively. The removal efficiencies decreased as the irradiation time was increased from 30 min to 240 min in the OMW, under UV light. The reduction of yield could be due to the formation of small colourless metabolite organic molecules which, at least temporarily, remain in the solution, for instance ethanol, glycerol and simple sugars which can be considered as degradation intermediates (Hajjouj et al., 2008).) Hajjouji et al., (2008), was investigated the UV/$TiO_2$ treatment of olive mill

wastewater and reported only 22% removal efficiency of COD after 24 h UV irradiation.

The reduction of COD can be summarized as follows (Lucas & Peres, 2009):

Step 1: COD + UV → partially oxidized species

Step 2: partially oxidized species + UV→ $CO_2$ + $H_2O$ + inorganic salts

A linear relationship between irradiation times and COD photodegradation efficiencies was not obtained from 30 min up to 60 min irradiation times (R =0.92) and this regression is not significant. However, a linear relationship between irradiation times and COD photodegradation efficiencies (R= 0.92) was obtained from 90 min to 240 min irradiation times and this regression is significant (ANOVA $p=0.01 < \alpha=0.05$ and F=18.62).

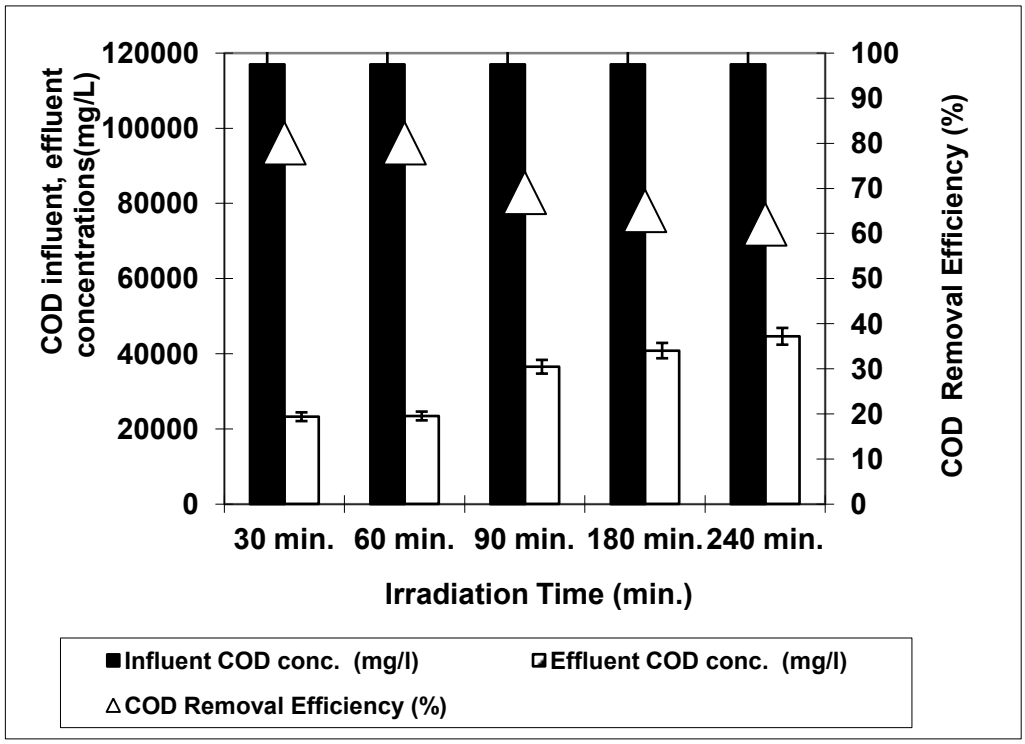


Figure 6.28 The effect of Irradiation time on COD yield (Influent Conc.: 117000 mg/L, T: ±20 $^0$C, pH: 4.60, Nano-ZnO-Magnetite concentration: 3g/L, UV power: 300 W).

Figure 6.29 shows the effect of different UV irradiation times (30 min., 60 min., 90 min., 180 min. and 240 min) on photodegradation of phenol at a pH of 4.60 at a

temperature of 20 $^{0}$C after at a 3 g/L concentration of Nano-ZnO-Magnetite nanocomposite with an UV lamp with a power of 300 W. From Figure 6.29 it can be seen that as the irradiation time were increased from 30 min, to 60 min, to 90 min, and to 180 min, the phenol yield increased from 57%, to 63%, to 65%, to 77%, and stabilized to 77%. Further increase of adsorption time to 240 min did not increase the phenol yield. The optimum irradiation time can be considered as 180 min for the maximum removal efficiency of phenol (77%). Similar results were found by Feng et al. (2014) in the presence of $Fe_3O_4$-ZnO. The percentage of degradation of phenol was 65.5% under UV light after 150 min irradiation time. The phenol degradation was only 52% when pure ZnO was used, which is lower than that in the presence of either $Fe_3O_4$-ZnO.

Semiconductors like Nano-ZnO-Magnetite absorb a photon taking a certain amount of energy and then are transferred from electron band to conductive band. Meanwhile, an electron vacancy forms and joins the redox reaction with the absorbed substance, by transmigrating to the electron and vacancy catalyst surface. Mechanism in the photocatalyst realized through the usage of Nano-ZnO-Magnetite and reactions arising in this process are outlined as follows reported by Ugurlu and Karaoglu, (2011).

$$\text{Nano-ZnO-Magnetite} + hv \rightarrow e^-_{cb} + h^+_{vb} \quad (6.14)$$

$$O_2 + e^-_{cb} \rightarrow O_2^{\bullet -} \quad (6.15)$$

$$O_2^{\bullet -} + H_2O \rightarrow O_{\bullet} + OH^- + O_2 + HO^-_2 \quad (6.16)$$

$$H_2O + h^+vb \rightarrow HO^{\bullet} + H^+ \quad (6.17)$$

Due to the high concentration of $HO_{\bullet}$ and $O_2{}_{\bullet}^{-}$ absorbed in the particle surface, organic substances could be broken down through oxidative decomposition as indicated in Eq. (6.18):

$$\text{Organic composite} + O_2^{\bullet -} + HO \rightarrow CO_2 + H_2O + \text{sub composite} \quad (6.18)$$

A linear relationship between irradiation times and phenol photodegradation efficiencies was obtained up to a irradiaition time of 180 min (R =0.92) while this regression is not significant (ANOVA p=0.04 < α=0.05 and F=16.92).

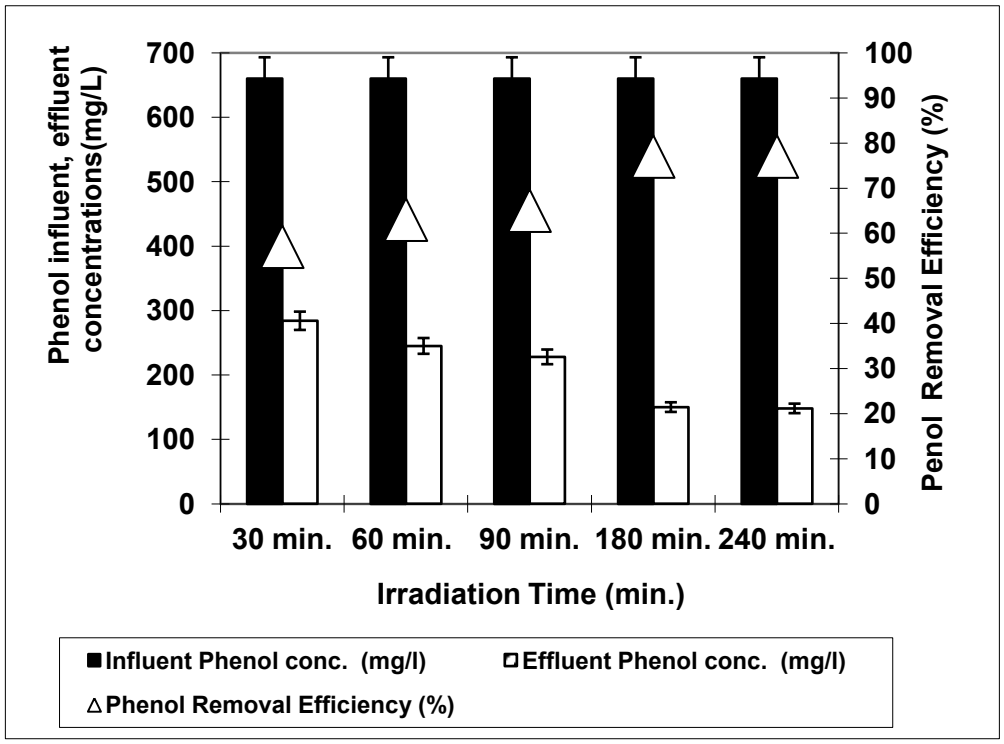


Figure 6.29 The effect of Irradiation time on phenol yield (Influent Conc.: 660 mg/L, T: ±20 $^0$C, pH: 4.60, Nano-ZnO-Magnetite concentration: 3g/L, UV power: 300 W ).

TS removal efficiencies were observed versus UV irradiation times such as 30 min., 60 min., 90 min., 180 min. and 240 min at an original pH of OMW (pH: 4.60) at 3g/L Nano-ZnO-Magnetite and at a temperature of ±20 $^0$C with an UV lamp with a power of 300 W as shown from Figure 6.30. After 30 minutes irradiation times the TS yield reached 67%. The removal efficiency of TS decreased from 67% to 66%, to 65% and to 62% with the increasing the irradiation time from 30 min to 60 min, to 90 min, to 180 min and 240 min, respectively. This TS yield decreased sligthly to 62% after 240 min irradiation times. Long irradiation times affect negatively the removal efficiency of TS. The optimum irradiation time was found to be 30 min for 67% TS efficiency. These results showed that the photocatalysis of TS in the OMW was not dependent to irradiation time. Badawy et al. (2009), found that the TS removal efficiency for UV/$TiO_2$ was 48.9% after 80 min irradiation time.

A linear relationship between irradiation times and TS photodegradation efficiencies was not obtained (R =0.95) and this regression is significant (ANOVA $p=0.01 < \alpha=0.05$ and F=28.44).

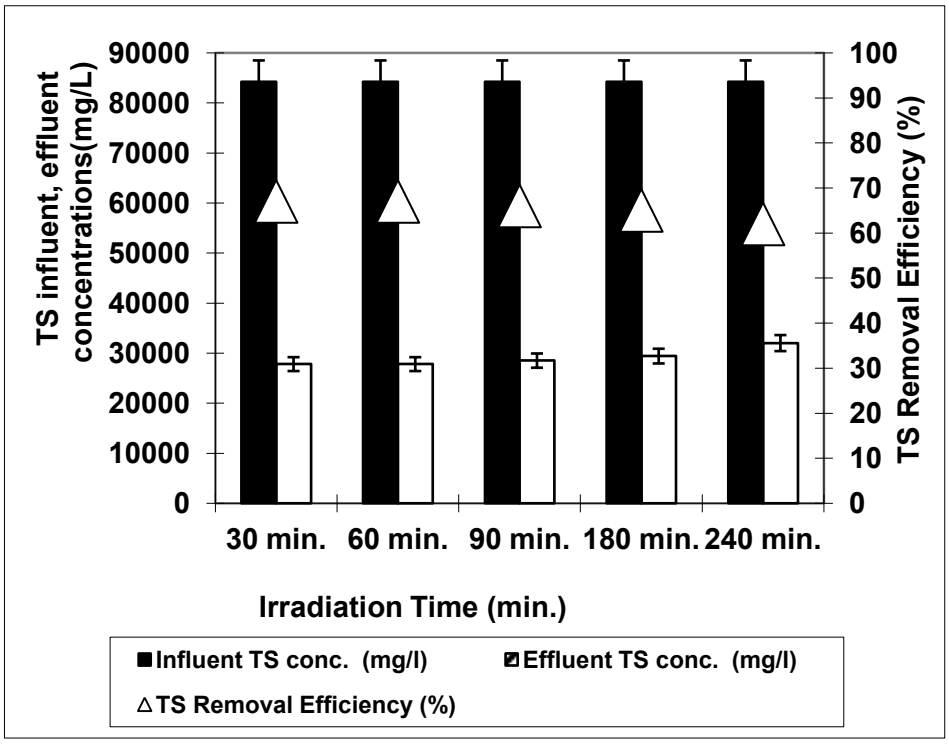


Figure 6.30 The effect of Irradiation time on TS yield (Influent Conc.: 84250 mg/L, T: ±20 $^0$C, pH: 4.60, Nano-ZnO-Magnetite concentration: 3g/L , UV power: 300 W).

Figure 6.31 shows the photodegradation efficiency of total nitrogen with increasing of irradiation times 30 min., 60 min., 90 min., 180 min. and 240 min at an original pH of OMW (pH: 4.60) at 3g/L Nano-ZnO-Magnetite and at a temperature of ±20 $^0$C with an UV lamp with a power of 300 W. When the irradiation time increased from 30 min to 60 min, from 60 min to 90 min, from 90 min to 180 min, from 180 min to 240 min, the removal efficiency of total nitrogen decreased from 79% to 75%, from 75% to 70%, from 70% to 68% and decreased from 68% to 65%, respectively. For maximum yield of total nitrogen, the optimum irradiation time was found to be 30 min. Uğurlu and Karaoğlu (2009) observed that 25.0 mg/L of $TiO_2$ was enough for the 65% removal of the total nitrogen after a irradiation time of 50 min.

A linear relationship between irradiation times and total nitrogen photodegradation efficiencies was obtained (R =0.93) and this regression is significant (ANOVA p=0.01 < α=0.05 and F=20.83).

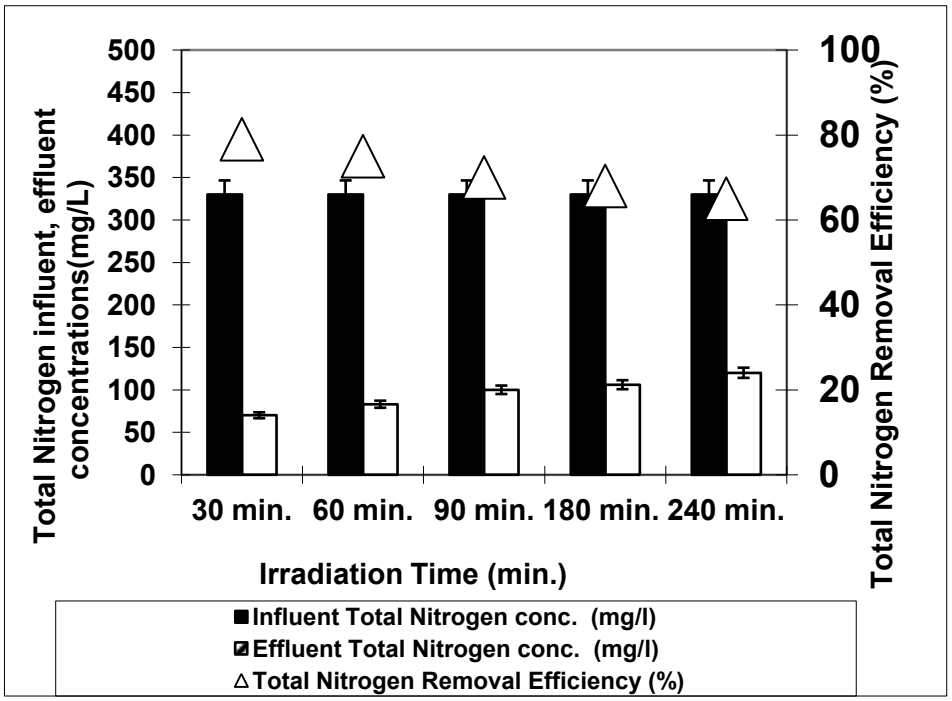


Figure 6.31 The effect of Irradiation time on total nitrogen yield (Influent Conc.: 330 mg/L, T: ±20 $^0$C, pH: 4.60, Nano-ZnO-Magnetite concentration: 3g/L, UV power: 300 W).

As shown in Figure 6.32, the photodegradation of total phosphorous decreases from 66% to 64%, to 55%, to 52%, to 50% along increasing of irradiation times from 30 min. to 60 min., to 90 min., to 180 min. and to 240 min at an original pH of OMW (pH: 4.60) at 3g/L Nano-ZnO-Magnetite and at a temperature of ±20 $^0$C with an UV lamp with a power of 300 W. Experiments on the photodegradation have shown that high irradiation time has negatively affected the total phosphorous removal efficiency. The maximum efficiency is 66% for 30 min irradiation time. After that the total phosphorus yields decreased.

A linear relationship between irradiation times and total phosphorous photodegradation efficiencies was not obtained (R =0.52) and this regression is significant (ANOVA p=0.02 < α=0.05 and F=15.94).

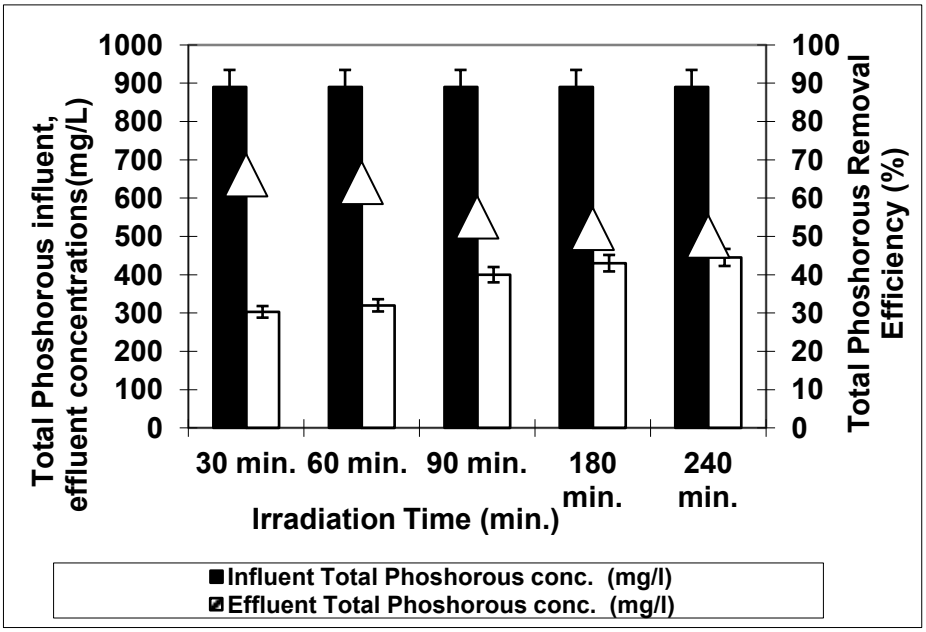


Figure 6.32 The effect of Irradiation time on total phosphorous yield (Influent Conc.: 890 mg/L, T: ±20 $^{0}$C, pH: 4.60, Nano-ZnO-Magnetite concentration: 3g/L, UV power: 300 W).

Optimum irradiation time was selected as 30 min because photooxidation equilibrium was reached within 30 min for maximum yields in all OMW parameters. Considering the economical needs, shortening the time of pollutant photodegradation is a necessary goal in this century. The maximum yields should be obtained as short as photodegradation yields.

### *6.4.3 Effects of pH on the of Removal OMW throughout Photodegradation under UV Light*

It is well understood that the adsorption capacity of Nano-ZnO-Magnetite concentration on photocatalyst is a key factor for the degradation efficiency in the photocatalytic oxidation process. Generally, it is observed that the efficiency of decomposition of organics over the photocatalyst is more pronounced if large number of target molecules is adsorbed on the catalyst surface, which either depends on the acidic/basic nature of the surface of the catalyst or surface modifications through change in pH of the system (Hur et al., 2006).

The variations in removals of COD, phenol, TS, total nitrogen and total phosphorous using 3 g/L Nano-ZnO-Magnetite concentrations under acidic (pH 4),

neutral (pH 7) and alkaline (pH 10) pH's at a temperature of ±20 $^0$C after 30 min irradiation time with an UV lamp with a power of 300 W were given in Figures 6.33, 6.34, 6.35, 6.36 and 6.37, respectively.

From Figure 6.33, it is evident that the maximum removal of COD was observed at pH 4 at a temperature of 20 $^0$C after 30 min irradiation time at a 3 g/L concentration of nano-ZnO-Magnetite concentration which this pH is the original pH level of OMW. When the initial pH was increased from 4 to 7 and 10, the COD removal efficiencies decreased from 80% to 78% and 69%. The maximum removal of COD was 80% at pH 4.60 at a temperature of 20 $^0$C after 30 min irradiation time at a 3 g/L concentration of nano-ZnO-Magnetite with an UV lamp with a power of 300 W. In the beginning of the photooxidation, liquid phase compounds responsible for COD are adsorbed by colliding with the surface of the colloidal nano-ZnO-Magnetite photocatalyst. Covalent bonds are formed between adsorbate particles and the adsorbent surface where multiple activated centers were exist on the surface of nano-composite (Smoczyńsk et al., 2014). The reduction of COD efficiency may results.

A linear relationship between pH variations and COD photodegradation efficiencies was obtained (R =0.90) and this regression is not significant (ANOVA p= 0.23 > α=0.05 and F=4.48).

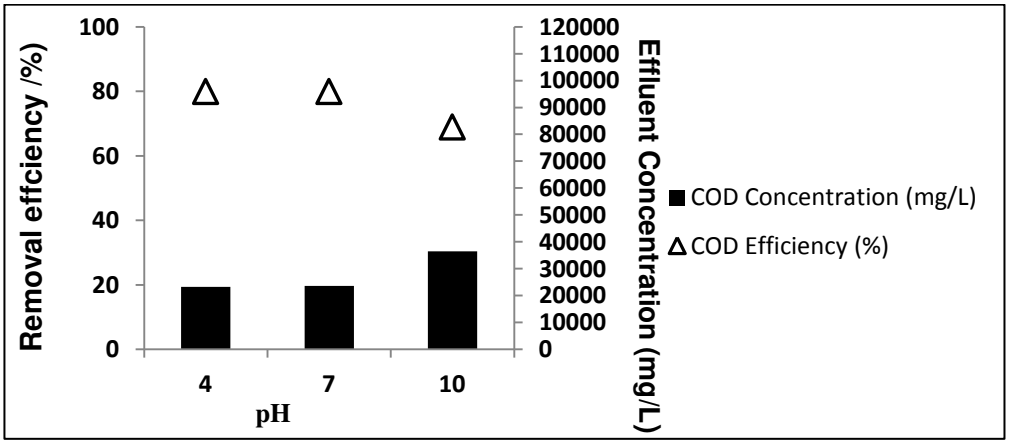


Figure 6.33 The effect of pH on COD yield (Influent Conc.:117000 mg/L, T: ±20 $^0$C, Nano-ZnO-Magnetite conc.: 3g/L, Irradiation time: 30 min, UV power: 30

When the pH of OMW was increased from 4 to 7 and 10, the removal efficiency of phenol increased from 63% to 72% and 75%, respectively, at a temperature of 20 $^{0}$C after 30 min irradiation time at a 3 g/L concentration of nano-ZnO-Magnetite concentration with an UV lamp with a power of 300 W. (Figure 6.34). It is observed that under basic conditions, the amount of phenol degraded is considerably higher as compared to acidic medium. These observations can be ascribed to two phenomenon: (a) Under acidic condition, surface of the nanocomposite is positively charged at both nano ZnO and Magnetite sites that leads to the protonation of active sites and therefore, affects the adsorption of phenol moiety. Moreover, the protonation of phenol occurring under this condition also hindered the adsorption of phenol thereby affecting its removal. (b) The influence of higher pH can be attributed to two processes occurring on the surface of the nanocomposite and phenol. Firstly, the magnetite surface becomes alkaline in nature thus enhancing the adsorption capacity while the nanosized ZnO surface undergoes surface modification resulting in the formation of negatively charged species. Both these features are responsible for cooperative action of simultaneous adsorption followed by photo degradation of phenol on the surface of nano-ZnO-Magnetite nanocomposite. Secondly, phenol undergoes deprotonation under highly alkaline condition that also enhances rate of adsorption on the nano-ZnO-Magnetite nanocomposite throghout photocatalysis (Meshram et al., 2011). It is seen that maximum phenol removal happens on pH 10. The reason can be explained with the fact that tannin, lignin and other polymeric substances may transform into phenol metabolites and degraded with photocatalytic oxidation as reported by Ugurlu and Karaoglu, (2011).

A linear relationship between pH variations and phenol photodegradation efficiencies was obtained ($R = 0.96$) and this regression is not significant (ANOVA $p = 0.23 > \alpha = 0.05$ and $F = 12$).

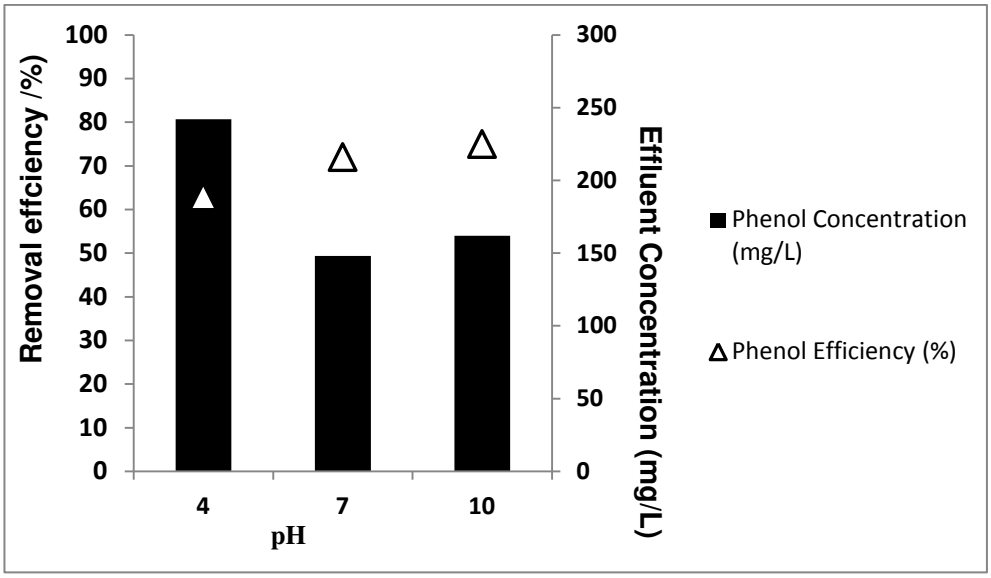


Figure 6.34 The effect of pH on phenol yield (Influent Conc.:660 mg/L, T: ±20 $^{0}$C, Nano-ZnO-Magnetite conc.: 3g/L, Irradiation time: 30 min, UV power: 300 W).

The effect of pH variation (4, 7 and 10) on the TS efficiency was investigated as shown in Figure 6.35. The efficiency of the TS was found to decrease from 70% to 57% and to 52% with increasing the pH from 4 to 7 and to 10, respectively, at a temperature of 20 $^{0}$C after 30 min irradiation time at a 3 g/L concentration of nano-ZnO-Magnetite with an UV lamp with a power of 300 W. The maximum removal efficiency was obtained as 70% at a pH of 4. Pinotti and Zaritzky, (2001) reported that when the pH value was more than pH 5 it leads to precipitate the pollutants in the OMW. This shows that the stabilization of suspended solid in acidic condition.

A linear relationship between pH variations and TS photodegradation efficiencies was obtained (R =0.97) and this regression is not significant (ANOVA p=0.12 > $\alpha$=0.05 and F=15.18).

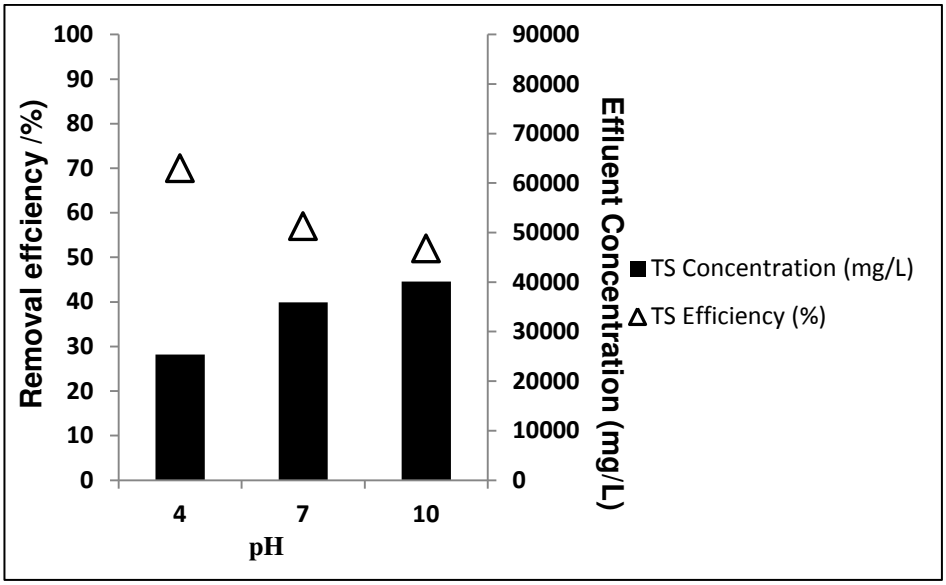


Figure 6.35 The effect of pH on TS yield (Influent Conc.:84250 mg/L, T: ±20 $^0$C, Nano-ZnO-Magnetite conc.: 3g/L, Irradiation time: 30 min, UV power: 300 W).

Figure 6.36 shows the photodagradation efficiencies of total nitrogen at increasing pH of 4, 7 and 10. The total nitrogen yields were found as 79 %, 83% and 97%, respectively, at a temperature of 20 $^0$C after 30 min irradiation time at a 3 g/L concentration of nano-ZnO-Magnetite with an UV lamp with a power of 300 W. When the pH of OMW increased from 4 to 7 and to 10, the yield of total nitrogen increased from 79% to 83%, and to 97%.

The dissociative equilibrium of ammonia in water is in accordance with Equation 6.19 (Huang et al., 2008):

$$NH_4^+ + H_2O \rightarrow NH_3 + H_3O^+ \qquad pKa=9.246 \qquad (6.19)$$

Ammonium is in equilibrium with ammonia at a pKa of 9.25. Accordingly at pH=10.0, $NH_3$ is 85% of total nitrogen (on molar basis) and at pH=12.0, $NH_3$ is over 99% of total nitrogen (on a molar basis). Thus, the decrease of total nitrogen observed in the OMW was from the removal of aqueous ammonia that was oxidized by OH· or potentially through volatilization. It is suspected that at the high pH level (10.0) some of the aqueous ammonia was removed through volatilization as ammonia is typically found in the gas form at high pH levels (Idelovitch and Michail,

1981). The decrease in total nitrogen removal was attributed to an increase in aqueous ammonia removal as reported by Huang et al. (2008). Vohra et al. (2010) have reported 2 mg/L of $NO_3^-$ formation when $NH_4^+$-$NH_3$ undergoes a $TiO_2$ assisted photocatalytic degradation at pH 12.0 (although no $NO_2^-$ was formed). Zhu et al. (2005) have observed the production of $NO_2^-$ (but not $NO_3^-$) after six hours of ammonia treatment with UV irradiation at pH=10.2. Zhu et al. (2005) have suggested that UV irradiation with photocatalyst on ammonia decreased the nitrogen products, such as $NH_2OH$ and $N_2$. The results from this present research suggest that total nitrogen was removed in the system due the conversion of ammonia to other inorganic compounds via formation of $NO_2^-$ or $NO_3^-$. Alkaline pH improved the degradation of total nitrogen, where at pH=12.0 the highest removal (59.5% under UV) was observed by John Bergese (2013).

A linear relationship between pH variations and total nitrogen photodegradation efficiencies was obtained (R =0.86) and this regression is not significant (ANOVA $p=0.26 > \alpha=0.05$ and F=3).

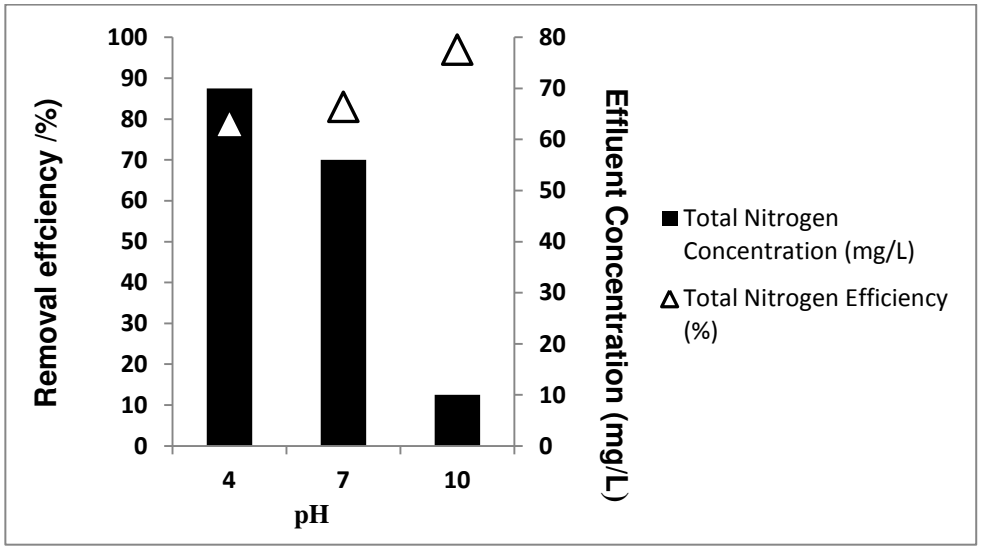


Figure 6.36 The effect of pH on total nitrogen yield (Influent Conc.:330 mg/L, T: ±20 $^0$C, Nano-ZnO-Magnetite conc.: 3g/L, Irradiation time: 30 min, UV power: 300 W).

Figure 6.37 illustrates the removal of total phosphorous with different pH (4, 7 and 10) at a temperature of 20 $^0$C after 30 min irradiation time at a 3 g/L

concentration of nano-ZnO-Magnetite with an UV lamp with a power of 300 W. The maximum removal of total phosphorous was observed at pH 4 with a yield of 85 %. When the pH of OMW was increased from 4 to 7 and 10, the removal efficiency of total phosphorous decreased from 85% to 51% and 37%, respectively. When the pH of OMW was increased, the removal efficiency of total phosphorous decreased. Some negative, positive, and neutral functional groups in the OMW can coexist on the magnetite surface. At pH < pHzero, the $FeOH^{2+}$ groups predominate over the FeO– groups, i.e., although the surface has a net positive charge, some FeO– groups are still present. At the pHzero, the number of $FeOH^{2+}$ groups equals the number of FeO– groups as the pH increases, the number of FeO– groups increases (Wang et al., 2010). Therefore, at a pH higher than pHzero, the Nano-ZnO-Magnetite composite surface is negatively charged, whereas at a lower pH, the surface is positively charged. In fact, this result is expected since the photodegradation efficiency decreased with further increase in solution pH.

A linear relationship between pH variations and total phosphorous photodegradation efficiencies was obtained (R =0.97) and this regression is significant (ANOVA p=0.08 < α=0.05 and F=17.28).

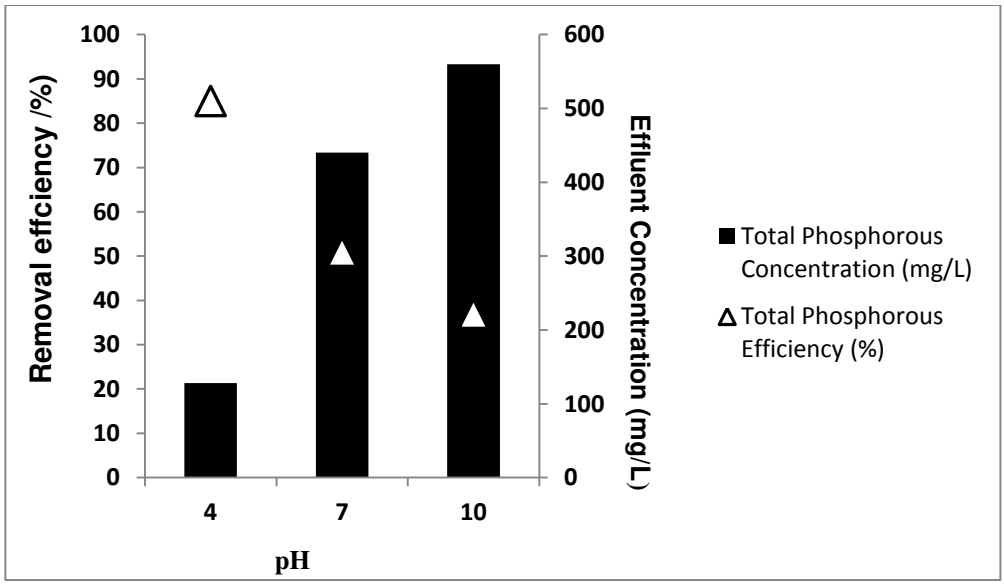


Figure 6.37 The effect of pH on total phosphorous yield (Influent Conc.:890 mg/L, T: ±20 $^0$C, Nano-ZnO-Magnetite conc.: 3g/L, Irradiation time: 30 min, UV power: 300 W).

Considering the above experiments, the maximum removal efficiency was found as 80% for COD, 70% for TS and 85% for total phosphorous, respectively. However, the maximum removal efficiency was found as 75% for phenol and 97% for total nitrogen at pH 10, respectively. But, for phenol and total phosphorous parameters, the removal efficiencies was not considerable at lower pH 4 (63% for phenol and 79% for total phosphorous) than that pH 10. Therefore, optimum pH was selected as 4 because economical needs are necessary for the goal of this research.

## 6.5 Photocatalytic Degradation Processes Under Sunlight

### *6.5.1 Determination of Optimum Nano-ZnO-Magnetite Concentration under Sunlight*

Effects of 0.5 g/L, 1.5 g/L, 3 g/L, 7 g/L and 10 g/L Nano-ZnO-Magnetite concentrations on the removals of COD, phenol, total solids, total nitrogen and total phosphorous in the OMW with constant sunlight time (24 h) at a original pH of OMW (pH: 4.60) with a sunlight with a power of 80 W were given in Figures 6.38, 6.39, 6.40, 6.41 and 6.42, respectively.

Upon exposure to sunlight irradiation, ZnO can be photoexcited to generate negative electrons ($e^-_{CB}$) in the conduction band and positive holes ($h^+_{VB}$) in the valence band. The photoinduced electron–hole pairs are able to either recombine or be captured by other molecules, such as water or oxygen, forming reactive oxygen species (ROS) such as hydroxyl radical ($^{\bullet}OH$) and superoxide radical anion ($^{\bullet}O^{-2}$). The $h^+_{VB}$ reacts with water to produce hydroxyl radicals ($^{\bullet}OH$), whilst the $e^-_{CB}$ reacts with $O_2$ to form superoxide radical anions ($^{\bullet}O^{-2}$) and hydrogen peroxide ($H_2O_2$). The latter also can generate hydroxyl radicals ($^{\bullet}OH$). These ROS can destroy the structure of various organic pollutants, leading to the formation of non-toxic carbon dioxide and water (Pirkanniemi et al., 2002).

Figure 6.38 shows the photodegradation efficiencies of COD at increasing Nano-ZnO-Magnetite concentrations (0.5 g/L, 1.5 g/L and 3 g/L) with constant sunlight

time (24 h) and constant power of 80 W at an original pH of OMW (pH: 4.60) according to the Nano-ZnO-Magnetite concentrations given above. The photodegradation yields were 64%, 67% and 75%, respectively. Further increase of -ZnO-Magnetite concentration to 7 and 10 g/L did not increase the COD yields. For maximum removal efficiencies the optimum nano-ZnO-Magnetite concentration was found as 3 g/L (Figure 6.37).

A linear relationship between Nano-ZnO-Magnetite composite concentrations and COD photodegradation efficiencies was obtained up to a Nano-ZnO-Magnetite composite concentration of 7 g/L (R =0.82) while this regression is not significant (ANOVA p=0.11 > α=0.05 and F=6.11).

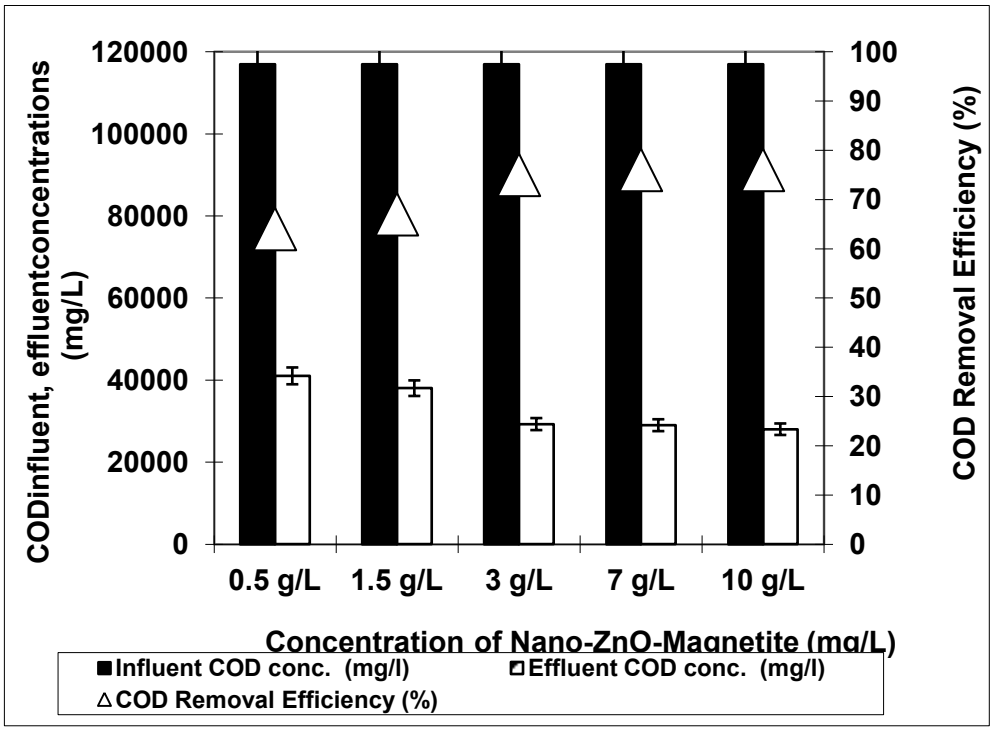


Figure 6.38 The effect of Nano-ZnO-Magnetite concentration on COD yield (Influent Conc.: 11700 mg/L, pH: 4.60, Sunlight irradiation time: 24 h, sunlight power: 80 W).

Figure 6.39 shows the degradation efficiency of phenol with increasing of Nano-ZnO-Magnetite concentrations of 0.5 g/L, 1.5 g/L, 3 g/L, 7 g/L and 10 g/L with constant sunlight time (24 h) and a constant power of 80 W at an original pH of OMW (pH: 4.60). When the concentration of Nano-ZnO-Magnetite increased from

0.5 g/L to 1.5 g/L, 1.5 g/L to 3 g/L from 3 g/L to 7 g/L, from 7 g/L to 10 g/L, the removal efficiency of phenol increased from 34% to 42%, from 42% to 48%, from 48% to 56% and increased from 56% to 61%, respectively. At 10 g/L nano-ZnO-Magnetite concentration, the maximum removal efficiency of COD was achieved as 61%. Parsedhi and Patil (2008) investigated the sunligth oxidation of 75 mg/L phenol and found 100% phenol photo-degradation using 2.5 g/L of ZnO at a sunlight for 8 h. In our study, the phenol yields under sunligth are low compared to the study performed by Parsedhi and Patil (2008). In our study 317 mg/L of phenol was treated with 3 g/L Nano-ZnO-Magnetite concentration. In our study, as the amount of Nano-ZnO-Magnetite photocatalyst increases, the photo degradation efficiency did not increase markedly. This may be due to the fact that as the quantity of ZnO increased; the number of phenol molecules adsorbed was increased resulting in with limited active holes in the nanoparticle due to closed holes. On the other hand, the sunligt power is low. These two items probably decreases the photooxidation yield. Similar results are reported by Anandan et al., (2006). In their study excess ZnO particles showed a small effect on the pollutant yields due to screening effect of solution and scattering of sunlight.

A linear relationship between Nano-ZnO-Magnetite composite concentrations and phenol photodegradation efficiencies was obtained up to a Nano-ZnO-Magnetite composite concentration of 10 g/L ($R = 0.96$) and this regression is significant (ANOVA $p=0.02 < \alpha=0.05$ and $F=37.66$).

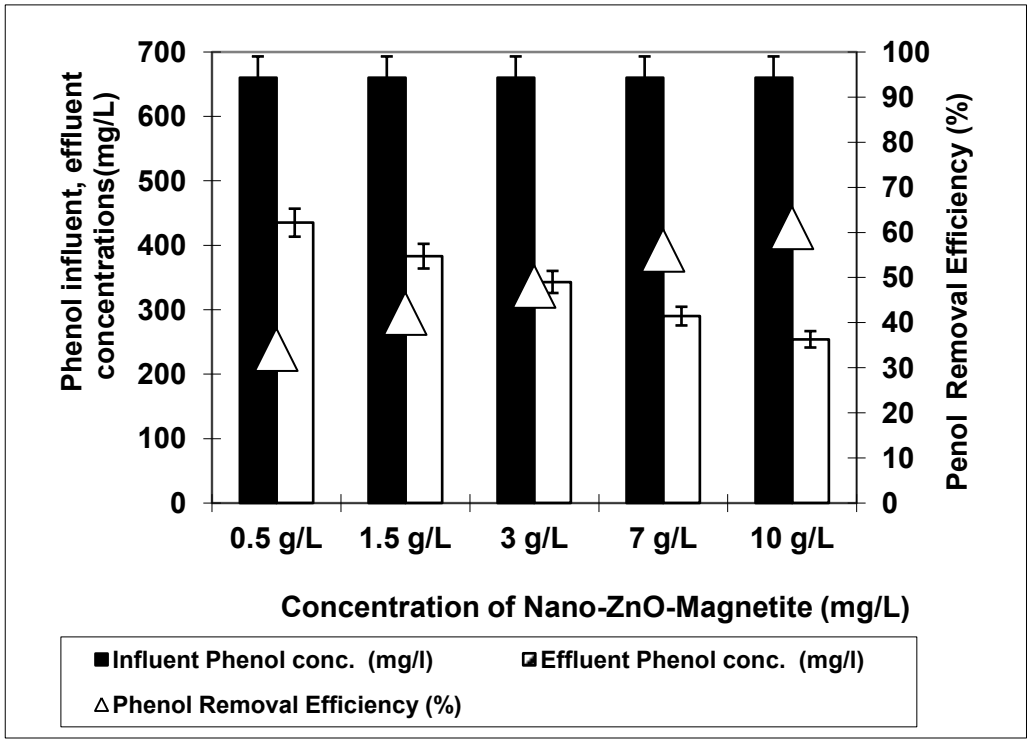


Figure 6.39 The effect of Nano-ZnO-Magnetite concentration on phenol yield (Influent Conc.: 660 mg/L, pH: 4.60, Sunlight irradiation time: 24 h, sunlight power: 80 W).

TS removal efficiencies were found as 59 %, 48%, 38%, 34% and 27% for 0.5 g/L, 1.5 g/L, 3 g/L, 7 g/L and 10 g/L Nano-ZnO-Magnetite nanocomposite, respectively, with constant sunlight time (24 h) and a constant power of 80 W at an original pH of OMW (pH: 4.60) (Figure 6.40). For maximum removal efficiency of TS, the optimum Nano-ZnO-Magnetite composite concentration was found to be 0.5 g/L. This phenomenon can be explained by the turbidity effect of Nano-ZnO-Magnetite composite. Excess Nano-ZnO-Magnetite composite would affect the penetration of sunlight through the suspensions due to the light scattering effects

A linear relationship between Nano-ZnO-Magnetite composite concentrations and TS photodegradation efficiencies was obtained ($R = 0.92$) this regression is significant (ANOVA $p=0.01 < \alpha=0.05$ and $F=15.49$).

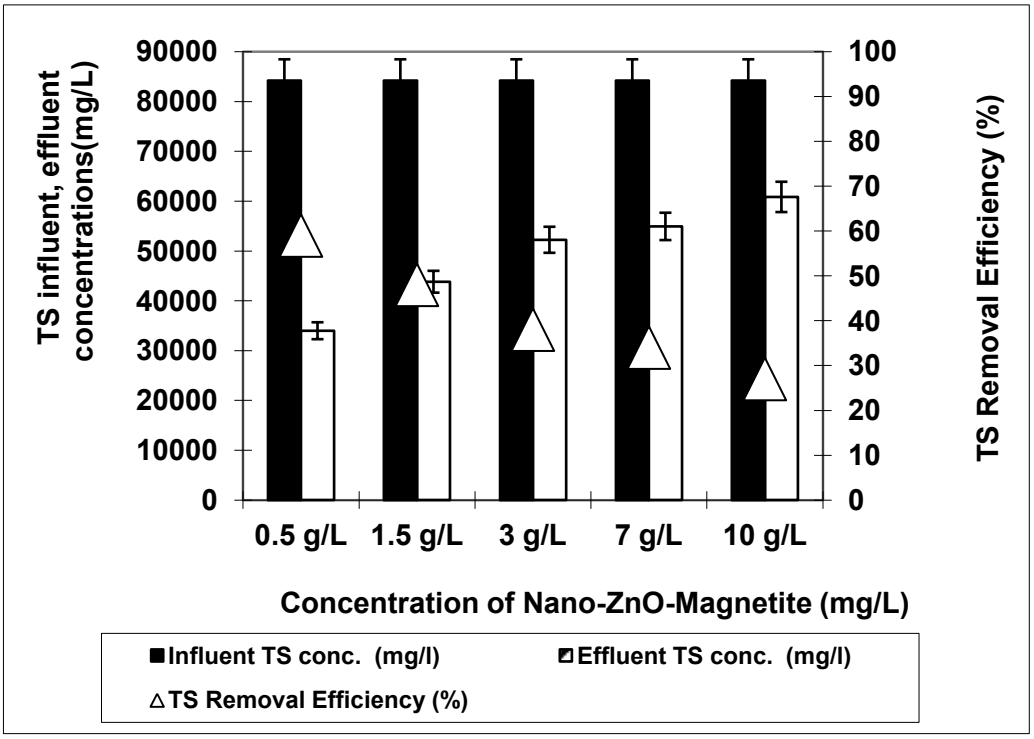


Figure 6.40 The effect of Nano-ZnO-Magnetite concentration on TS yield (Influent Conc.: 84250 mg/L, pH: 4.60, Sunlight irradiation time: 24 h, sunlight power: 80 W).

Figure 6.41 shows the removal efficiency of total nitrogen. It was found that total nitrogen efficiency decreased with increasing Nano-ZnO-Magnetite concentration. The total nitrogen yield decreased from 69% to 62%, to 60%, to 39%, and to 33% with increasing of Nano-ZnO-Magnetite concentration from 0.5 g/L to 1.5 g/L, to 3 g/L, to 7 g/L and to 10 g/L with constant sunlight time (24 h) and a constant power of 80 W at an original pH of OMW (pH: 4.60). The optimum Nano-ZnO-Magnetite concentration can be considered as 0.5 g/L for the maximum removal efficiency of total nitrogen (69%). The use of excessive amounts of catalyst may reduce the amount of sunlight being transferred into the medium due to the turbidity offered by the catalyst particles (Gogate and Pandit, 2004). However, the maximum total nitrogen removal was achieved as 97% at 0.5 g/L Nano-ZnO-Magnetite concentration under UV light (Figure 6.41).

A linear relationship between Nano-ZnO-Magnetite composite concentrations and total nitrogen photodegradation efficiencies was obtained up to a Nano-ZnO-Magnetite composite concentration of 10 g/L (R =0.98) this regression is significant

(ANOVA p=0.0008 < α=0.05 and F=111.22).

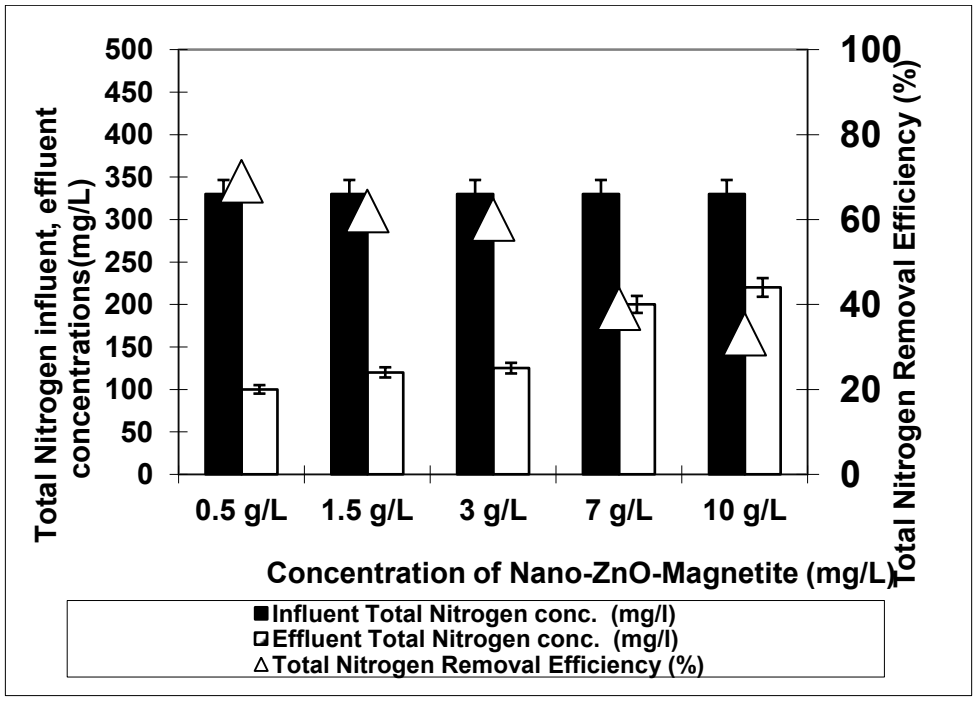


Figure 6.41 The effect of Nano-ZnO-Magnetite concentration on total nitrogen yield (Influent Conc.: 330 mg/L, pH: 4.60, Sunlight irradiation time: 24 h, sunlight power: 80 W).

Effect of nano-ZnO-Magnetite concentrations of 0.5 g/L, 1.5 g/L, 3 g/L, 7 g/L and 10 g/L on the removal of total phosphororus in the OMW were illustrated in Figure 6.42 with constant sunlight time (24 h) and a constant power of 80 W at an original pH of OMW (pH: 4.60). As the Nano-ZnO-Magnetite concentration increased from 0.5 g/L up to 1.5 g/L, to 3 g/L, and to 7 g/L, the phosphorous removals increased gradually from 47% to 61%, to 65%, to 72%, respectively. The number of available adsorption and catalytic sites on the catalyst surface increases with increasing in catalyst concentration, resulting in the observed enhancement in photocatalytic degradation efficiency. At 10 g/L nano-ZnO-Magnetite concentration, the removal efficiency of total phosphorous remains constant.

A linear relationship between Nano-ZnO-Magnetite composite concentrations and total phosphorous photodegradation efficiencies was obtained up to a Nano-ZnO-Magnetite composite concentration of 7 g/L (R =0.84) while this regression is not significant (ANOVA p=0.12 > α=0.05 and F=7.54).

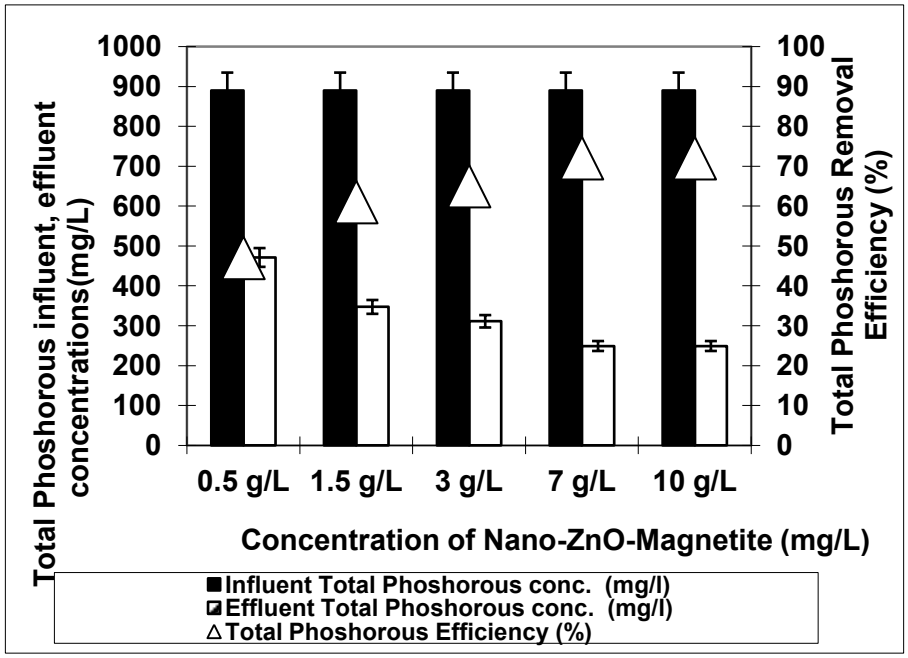


Figure 6.42 The effect of Nano-ZnO-Magnetite concentration on total phosphorus yield (Influent Conc.: 890 mg/L, pH: 4.60, Sunlight irradiation time: 24 h, sunlight power: 80 W).

Considering all the removal efficiencies for studied parameters in the OMW, an optimum nanocomposite concentration was chosen for maximum yields. Since the concentration of Nano-ZnO-Magnetite should be optimized, the cost of the photocatalyst should be as low as. The optimum Nano-ZnO-Magnetite composite concentration was selected as 3 g/L for the maximum removals of all pollutant parameters.

### *6.5.2 Determination of Optimum Irradiation Time of Sunlight*

Figures 6.43, 6.44, 6.45, 6.46 and 6.47 illustrate the effect of the sunlight irradiation time on the removal of COD, phenol, TS, total nitrogen and total phosphorous, respectively. As aforementioned in the upper section, the optimum Nano-ZnO-Magnetite composite concentration was found as 3 g/L. Therefore, the effects of irradiation times of sunlight on the COD, phenol, TS, total nitrogen and total phosphorous removal efficiencies were investigated at four different sunlight irradiation times (3 h., 8 h., 15 h. and 24 h.) at a pH of 4.60 at constant 3 g/L Nano-ZnO-Magnetite composite concentration with a sunlight with a power of 80 W.

Figure 6.43 shows the removal efficiency of COD. It was found that COD efficiency increased with increasing sunlight irradiation time. The COD yield increased from 54% to 65% and to 76% with increasing of sunlight irradiation times from 3 h to 8 h and to 15 h, then, the removal efficiency at 76% for COD after 24 h at a pH of 4.60 at constant 3 g/L Nano-ZnO-Magnetite composite concentration under sunlight with a power of 80 W (Figure 6.43). The optimum sunlight irradiation time can be considered as 15 h for the maximum removal efficiency of COD (76%).

A linear relationship between irradiation times and COD photodegradation efficiencies was obtained up to a irradiation time of 15 h (R =0.89) while this regression is not significant (ANOVA p=0.16 > α=0.05 and F=8.33).

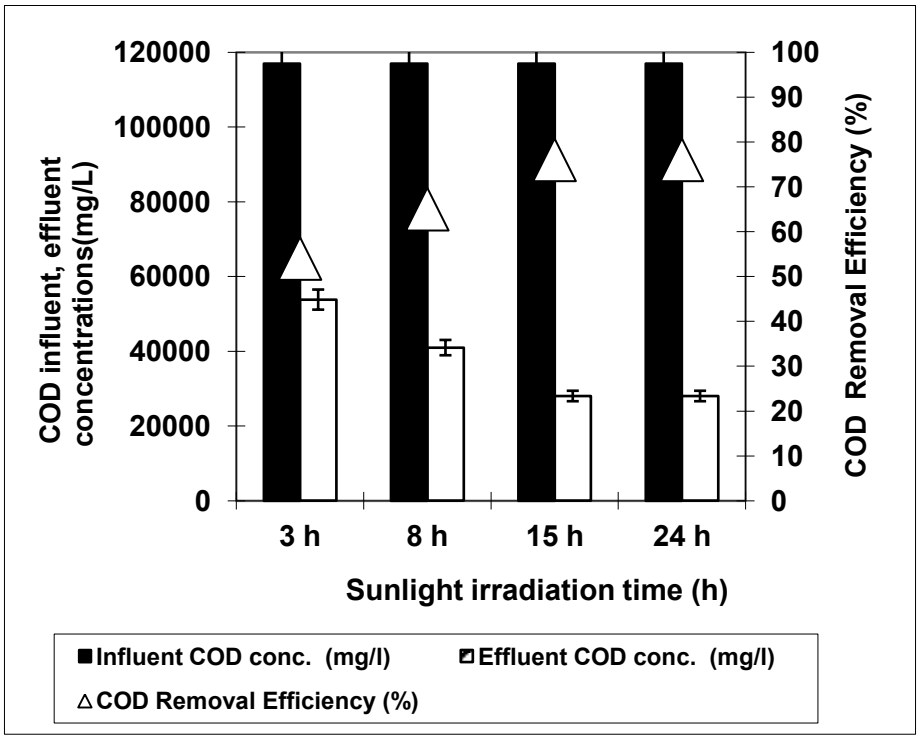


Figure 6.43 The effect of sunlight irradiation times on COD yield (Influent Conc.: 117000 mg/L, pH: 4.60, Nano-ZnO-Magnetite concentration: 3 g/L, Sunlight power: 80 W).

Phenol removal efficiencies were found as 32 %, 40%, 54% and 56 % for 3 h, 8 h, 15 h and 24 h sunlight irradiation times, respectively, at constant 3 g/L Nano-ZnO-Magnetite composite concentration at a original pH of OMW (pH: 4.60) with a sunlight power of 80 W (Figure 6.44). For maximum phenol removal efficiency

(54%), the optimum sunlight irradiation time was 15 h. In our study, in the photooxidation experiment phenol removal efficiency did not ncreased makedly with increasing sunlight irradiation time. This could be attributed to the split of multiphenolic substances to phenols. According to Roig et al. (2006), in the first phase of phenol photooxidation, aromatic intermediates are formed with increase of the total phenol concentration.

A linear relationship between irradiation times and phenol photodegradation efficiencies was obtained up to a irradiation time of 24 h (R =0.94) and this regression is not significant (ANOVA p=0.13 > α=0.05 and F=15.36).

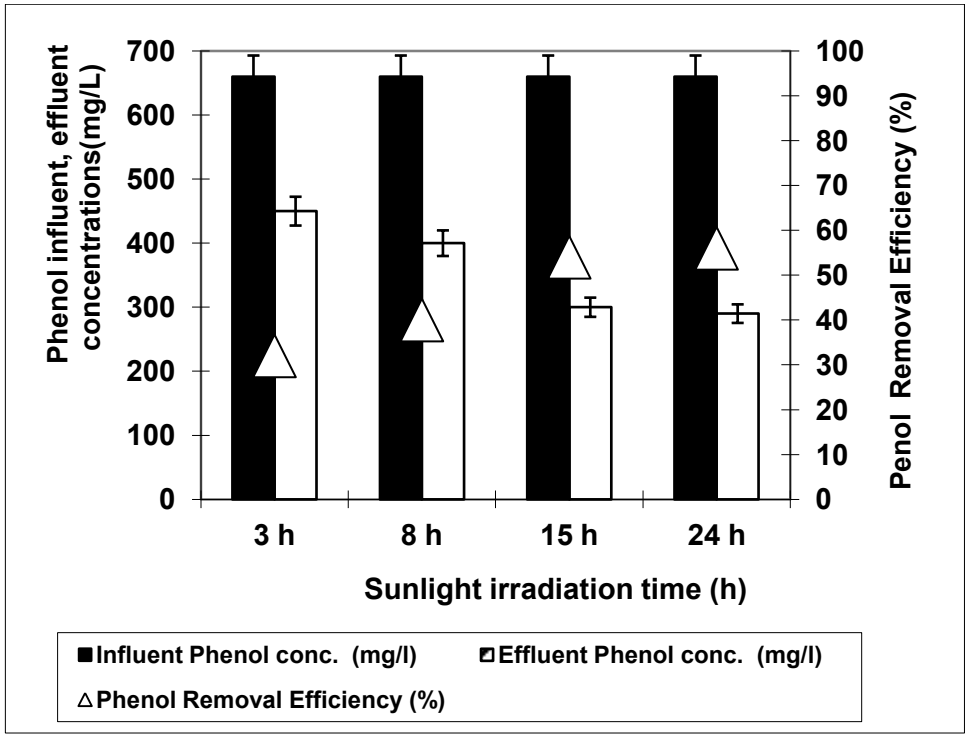


Figure 6.44 The effect of sunlight irradiation times on phenol yield (Influent Conc.: 660 mg/L, pH: 4.60, Nano-ZnO-Magnetite concentration: 3 g/L, Sunlight power: 80 W).

Low TS removal efficiency (34%) was observed with sunlight irradiatİon at an original pH of OMW (pH: 4.60) at 3g/L Nano-ZnO-Magnetite with a sunlight at apower of 80 W as shown in Figure 6.45. After 3 h sunlight irradiaiton times the TS yield reached 26% with the initial TS concentration of 84250 mg/L at an original pH of OMW (pH: 4.60) at 3g/L nano-ZnO-Magnetite with 80 W sunlight. This TS

yield increased to 30%, 32% and 34% with increasing sunlight irradiation times to 8 h, to 15 h and to 24 h, respectively. Long sunlight irradiation times slightly affect the removal efficiency of TS. For maximum yield of TS, the optimum sunlight irradiation time was found to be 15 h (32%).

A linear relationship between irradiation times and TS photodegradation efficiencies was not obtained up to an irradiation time of 15 h (R =0.95) and this regression is significant (ANOVA p=0.06 > α=0.05 and F=19.95).

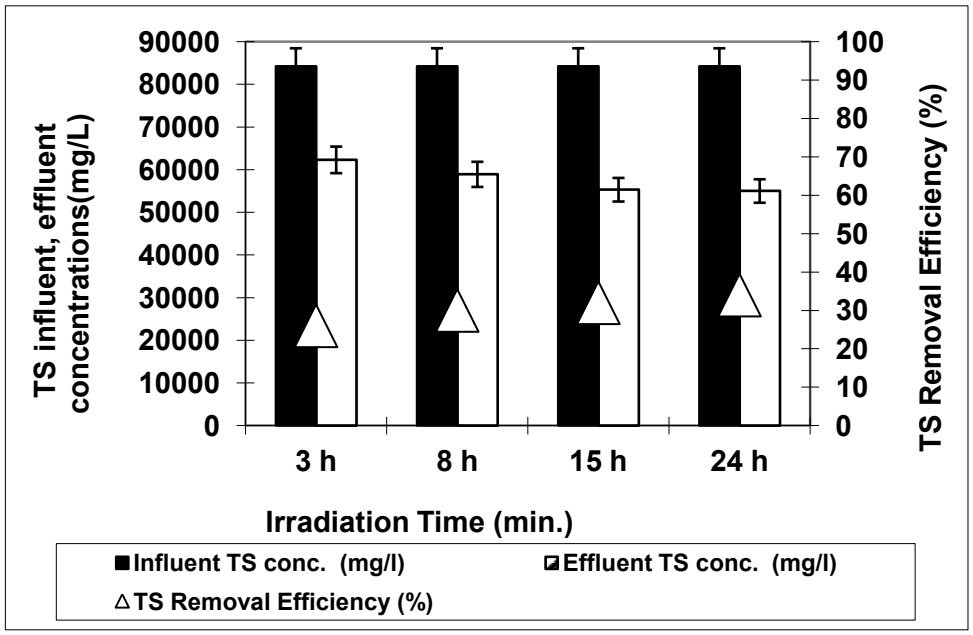


Figure 6.45 The effect of sunlight irradiation times on TS yield (Influent Conc.: 84250 mg/L, pH: 4.60, Nano-ZnO-Magnetite concentration: 3 g/L, Sunlight power: 80 W).

Figure 6.46 shows the nitrogen removal efficiency with different sunlight irradiation times at a pH of 4.60, at 3g/L Nano-ZnO-Magnetite with sunlight at a power of 80 W. After 3 h sunlight irradiation time, the removal efficiency of total nitrogen was 28%. Increasing the sunlight irradiation time from 3 h to 8 h, to 15 h, to 24 h increased the total nitrogen efficiencies from 35%, to 38%, and to 39%. For maximum yield of total nitrogen, the optimum sunlight irradiation time was found to be 15 h.

A linear relationship between irradiation times and total nitrogen photodegradation efficiencies was not obtained up to an irradiation time of 24 h (R =0.89) and this regression is not significant (ANOVA p=0.17 > α=0.05 and F=7.15).

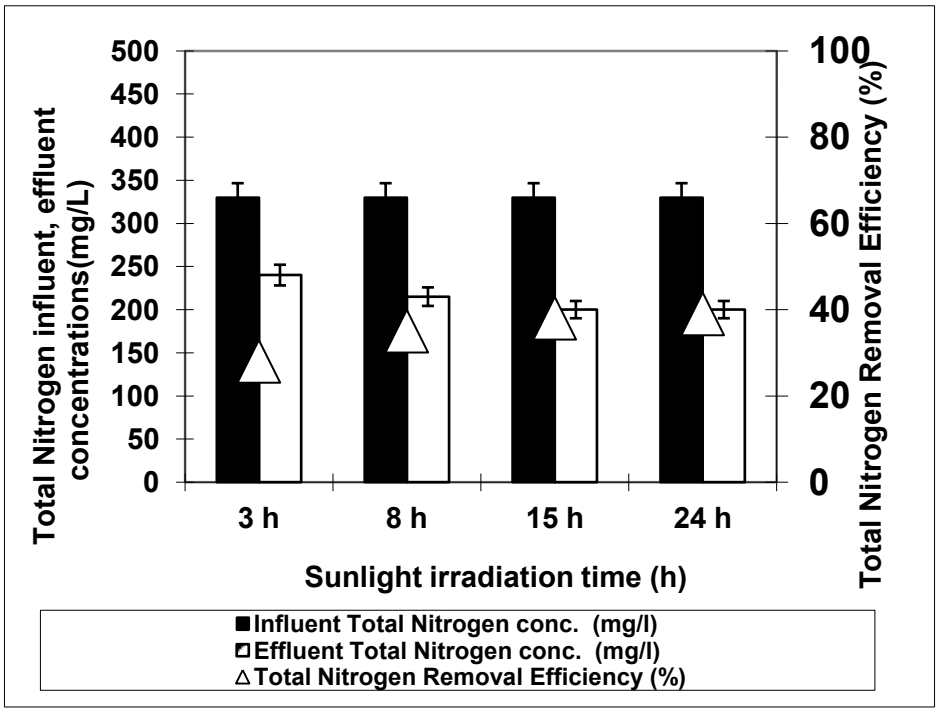


Figure 6.46 The effect of sunlight irradiation times on total nitrogen yield (Influent Conc.: 330 mg/L, pH: 4.60, Nano-ZnO-Magnetite concentration: 3 g/L, Sunlight power: 80 W).

Figure 6.47 shows the removal efficiency of total phosphorous. It was found that total phosphorous efficiency increased with increasing sunlight irradiation time. The total phosphorous yield increased from 62% to 65%, to 68% and to 72% with increasing of sunlight irradiation times from 3 h to 8 h, to 15 h and to 24 h at a pH of 4.60, at 3g/L nano-ZnO-Magnetite with 80 W sunlight power. The optimum sunlight irradiation time can be considered as 24 h for the maximum removal efficiency of total phosphorus (72%). The photogenerated reactive oxygen species

A linear relationship between irradiation times and total phosphorous photodegradation efficiencies was obtained up to a irradiation time of 24 h (R =0.99) and this regression is significant (ANOVA p=0.002 < α=0.05 and F=448.66).

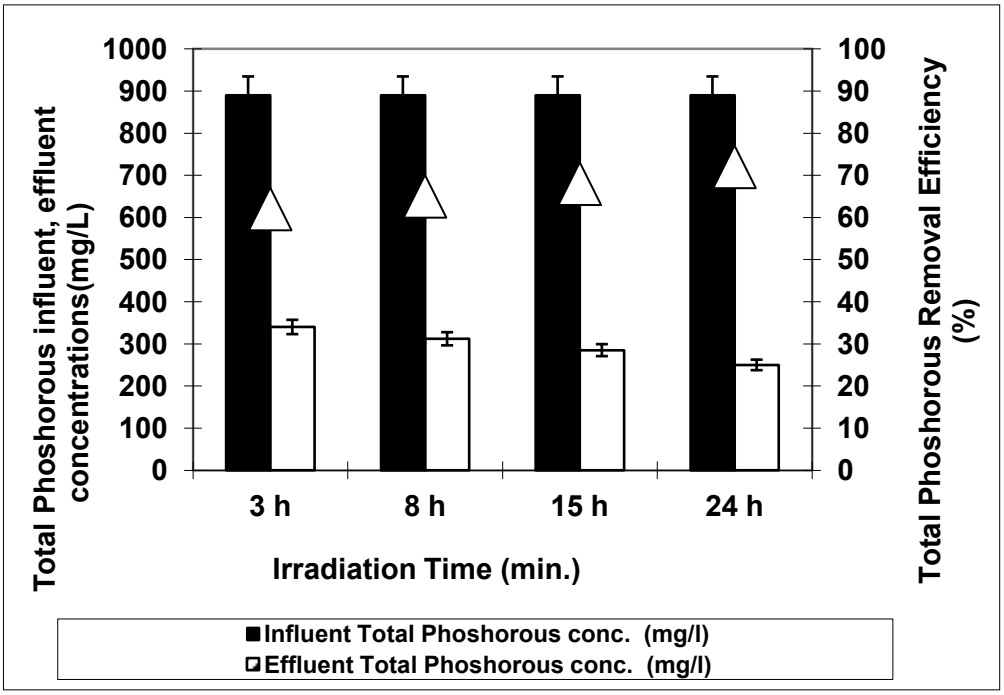


Figure 6.47 The effect of sunlight irradiation times on total phosphorous yield (Influent Conc.: 890 mg/L, pH: 4.60, Nano-ZnO-Magnetite concentration: 3 g/L, Sunlight power: 80 W).

Optimum sunlight irradiation time was selected as 15 h because the removal efficiency equilibrium was reached within 15 h for maximum yields in all pollutant parameters studied in the OMW.

### *6.5.3 Effects of pH on the of Removal OMW throughout Photodegradation under Sunlight*

The variations in removals of COD, phenol, TS, total nitrogen and total phosphorous using 3 g/L Nano-ZnO-Magnetite concentrations under acidic (pH 4), neutral (pH 7) and alkaline (pH 10) pH's after 15 h irradiation time with sunlight with a power of 80 W were given in Figures 6.48, 6.49, 6.40, 6.51 and 6.52, respectively.

From Figure 6.48, it is evident that the maximum removal of COD by photo degradation under sunlight was observed at a 3 g/L concentration of Nano-ZnO-Magnetite concentration after 15 h irradiation time with sunlight at a power of 80 W. As the initial pH was increased from 4 to 7 and 10, the COD removal efficiencies

decreased from 76% to 64% and 58%. The maximum removal of COD was 76% at pH 4.60 under sunlight irradiation.

A linear relationship between pH variations and COD photodegradation efficiencies was not obtained (R =0.98) and this regression is significant (ANOVA p=0.09 > α=0.05 and F=27).

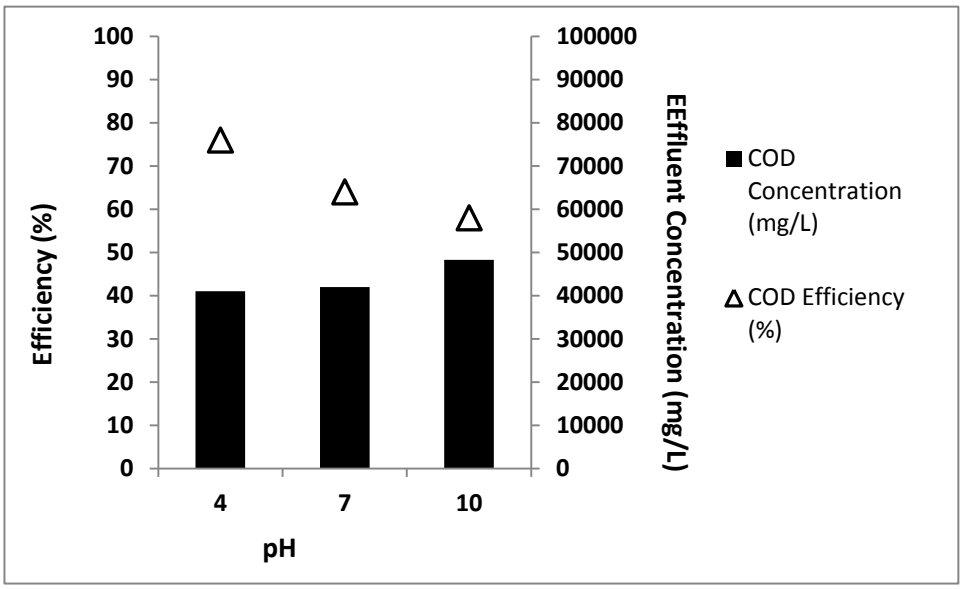


Figure 6.48 The effect of pH on COD yield (Influent Conc.: 117000 mg/L, Nano-ZnO-Magnetite concentration: 3 g/L, Sunlight irradiation time: 15 h, Sunlight power: 80 W).

From Figure 6.49, it can be clearly seen that the removal of phenol was affected sligtly from the pH changes significantly. The yields of phenol increased from 56% to 61% and to 64% with increasing of pH from 4 to 7 and 10, respectively, at a 3 g/L concentration of Nano-ZnO-Magnetite concentration after 15 h irradiation time with sunlight with a power of 80 W. The maximum phenol yield under sunlight was found as 64% at pH=10.

A linear relationship between pH variations and phenol photodegradation efficiencies was not obtained (R =0.98) and this regression is significant (ANOVA p=0.10 > α=0.05 and F=48).

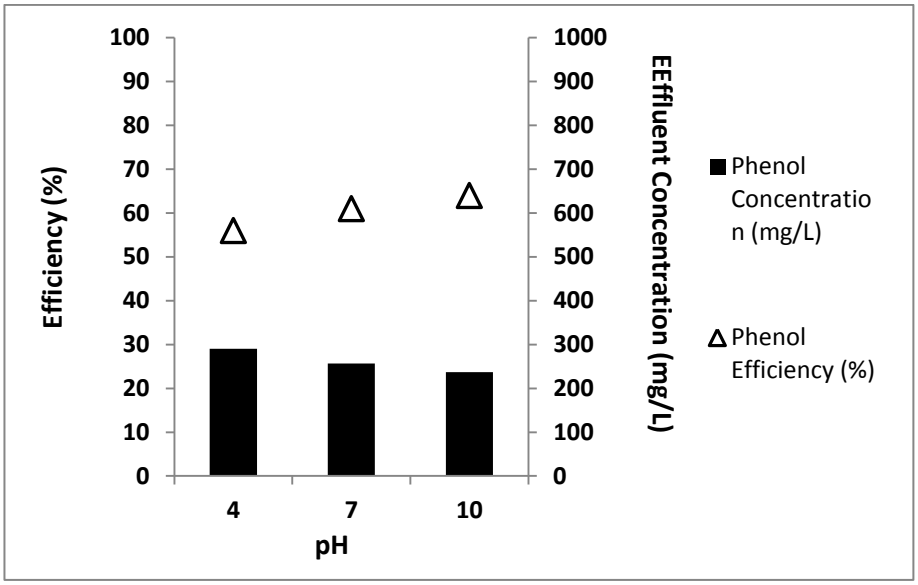


Figure 6.49 The effect of pH on phenol yield (Influent Conc.: 660 mg/L, Nano-ZnO-Magnetite concentration: 3 g/L, Sunlight irradiation time: 15 h, Sunlight power: 80 W).

Figure 6.50 illustrates the removal of TS with different pHs (4, 7 and 10), at a 3 g/L concentration of Nano-ZnO-Magnetite concentration after 15 h irradiation time with 80 W sunlight power. The maximum removal of TS was observed at pH 4 with a yield of 34%. When the pH of OMW was increased from 4 to 7 and 10, the removal efficiency of TS decreased from 34% to 28% and 25%, respectively.

A linear relationship between pH variations and TS photodegradation efficiencies was obtained (R =0.98) and this regression is not significant (ANOVA p=0.08 > $\alpha$=0.05 and F=27).

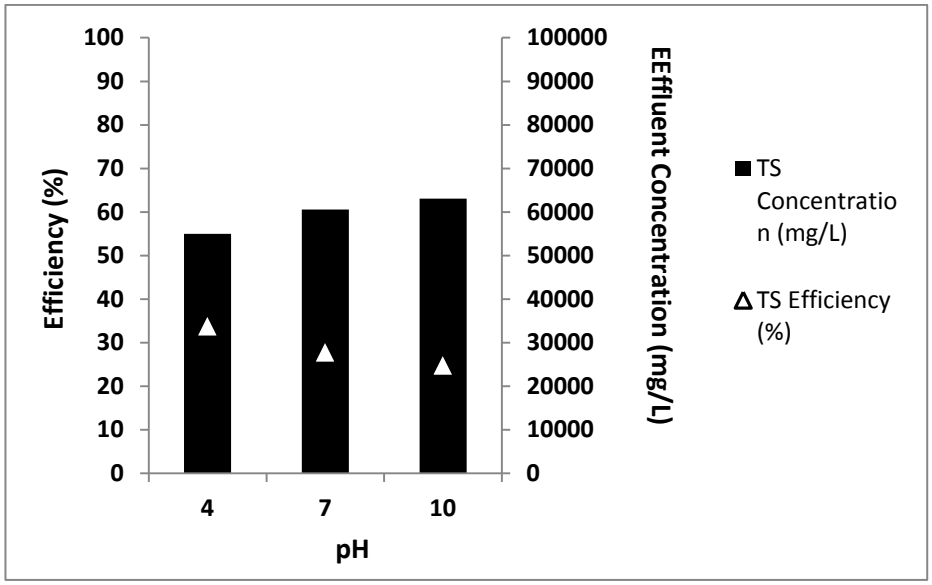


Figure 6.50 The effect of pH on TS yield (Influent Conc.: 84250 mg/L, Nano-ZnO-Magnetite concentration: 3 g/L, Sunlight irradiation time: 15 h, Sunlight power: 80 W). (örneğin çıktı alındığında bu grafik figure 53 olmuş ve sonrasında 6.51. ile devam etmiş.

Figure 6.51 shows the photodegradation efficiencies of total nitrogen at increasing pH of 4, 7 and 10. The total nitrogen yields were found as 28 %, 30% and 39%, respectively, at a 3 g/L concentration of Nano-ZnO-Magnetite concentration after 15 h irradiation time with sunlight with a power of 80 W.

A linear relationship between pH variations and total nitrogen photodegradation efficiencies was obtained (R =0.94) and this regression is not significant (ANOVA $p=0.37 > \alpha=0.05$ and F=7.40).

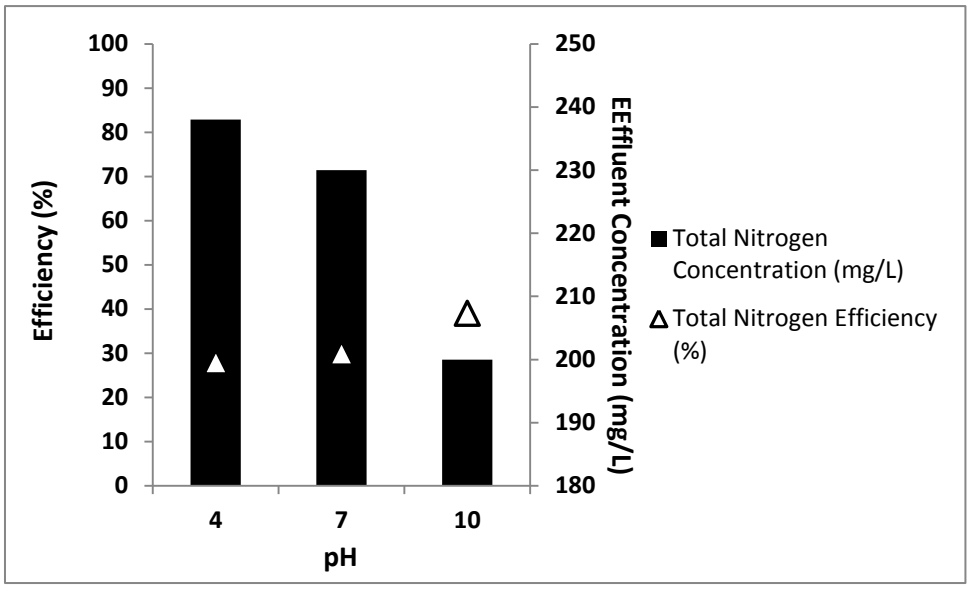


Figure 6.51 The effect of pH on total nitrogen yield (Influent Conc.: 330 mg/L, Nano-ZnO-Magnetite concentration: 3 g/L, Sunlight irradiation time: 15 h, Sunlight power: 80 W).

Figure 6.52 illustrates the removal of total phosphorous with different pHs (4, 7 and 10) at a 3 g/L concentration of Nano-ZnO-Magnetite concentration after 15 h irradiation time with sunlight with a power of 80 W. The maximum removal of total phosphorous was observed at pH 4 with a yield of 72 %. When the pH of OMW was increased from 4 to 7 and 10, the removal efficiency of total phosphorous decreased from 72% to 60% and 45%, respectively. When the pH of OMW was increased, the removal efficiency of total phosphorous decreased.

A linear relationship between pH variations and total phosphorous photodegradation efficiencies was obtained ($R = 0.99$) and this regression is significant (ANOVA $p=0.02 < \alpha=0.05$ and $F=243$).

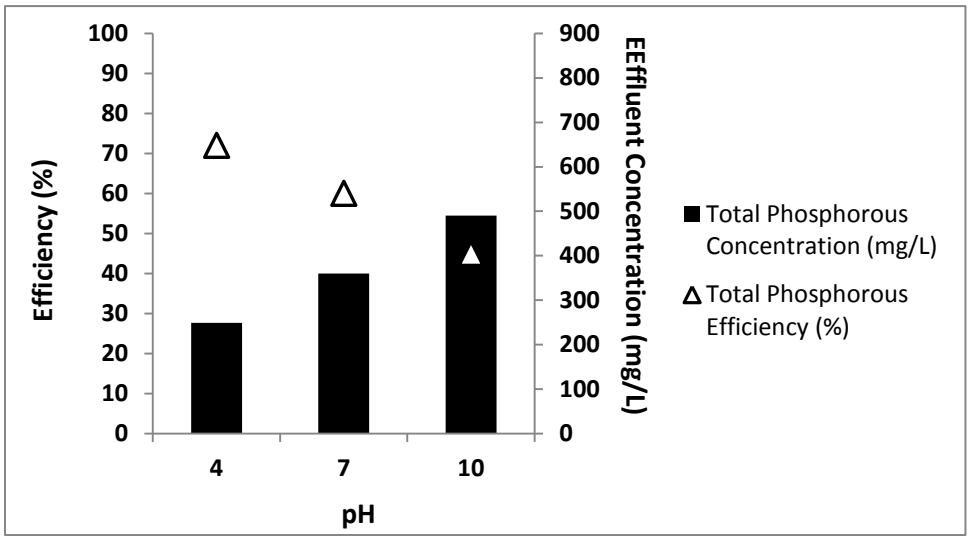


Figure 6.52 The effect of pH on total phosphorous yield (Influent Conc.: 890 mg/L, Nano-ZnO-Magnetite concentration: 3 g/L, Sunlight irradiation time: 15 h, Sunlight power: 80 W).

## 6.6 Kinetic Investigation of Photocatalytic Degradation of COD with using Nano-Zno-Magnetite Nanocomposite

In this study, zero-order kinetic, first-order kinetic and second-order kinetic models were investigated to detect the removal kinetics of COD and phenol on the surface of Nano-Zno-Magnetite nanocomposite throughout photodegradation under UV.

### *6.6.1 Zero-Order Kinetics*

Zero-order kinetics is always an artifact of the conditions under which the reaction is carried out. For this reason, reactions that follow zero-order kinetics are often referred to as pseudo-zero-order reactions. Clearly, a zero-order process cannot continue after a reactant has been exhausted. Just before this point is reached, the reaction will revert to another rate law instead of falling directly to zero as depicted at the upper left (Chemwiki, n.d.).

This situation commonly occurs when the COD or phenol removal reactions are catalyzed by attachment to a solid surface of Nano-Zno-Magnetite nanocomposite.

General equation of Zero-order reactions is shown below (6.20):

$$[A] = -kt + [A] \tag{6.20}$$

is in the form y = mx+b where slope = m = -k and the y-intecercept = b = $[A]^0$

where $A^0$ is the influent concentration of OMW (mg/L) and A is the effluent concentration of OMW (mg/L) at any time t (min), respectively and $k_0$ is the constant of pseudo-zero-order reaction ($min^{-1}$).

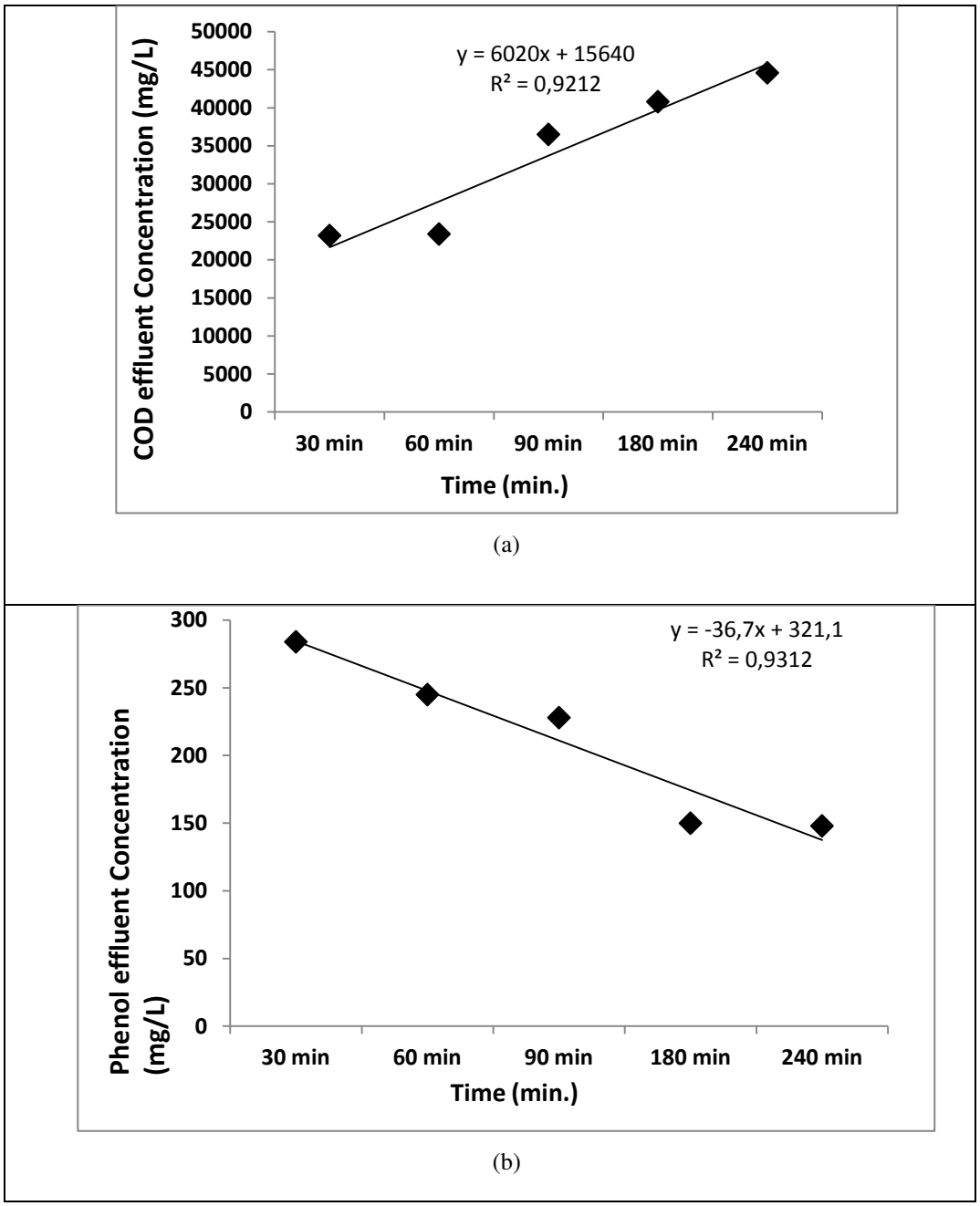


Figure 6.53 Pseudo-zero-order reaction of COD and phenol.

The $R^2$ values for Pseudo-zero-order reaction was found to be 0.9212 for COD and 0.9312 for phenol, respectively, performed with Nano-ZnO-Magnetite. Pseudo-zero-order reaction's the zero order rate kinetic constant is $k_0$. The $k_0$ values evaluated from Pseudo-zero-order reaction plots were found to be 6020 $min^{-1}$ for COD and 36.7 $min^{-1}$ for phenol, respectively.

### *6.6.2 First-Order Kinetics*

A first-order reaction is a reaction that proceeds at a rate that depends linearly on only one reactant concentration.

Differential rate laws are generally used to describe what is occurring on a molecular level during a reaction, whereas integrated rate laws are used for determining the reaction order and the value of the rate constant from experimental measurements Chemwiki (n.d.).

The equation describing first-order kinetics is given below:

$$\ln[A] - \ln[A]^{o} = -k_1 t \tag{6.21}$$

where $A^0$ is the influent concentration of OMW (mg/L) and A is the effluent concentration of OMW (mg/L) at any time t (min), respectively and $k_1$ is the constant of pseudo-firs-order reaction ($min^{-1}$).

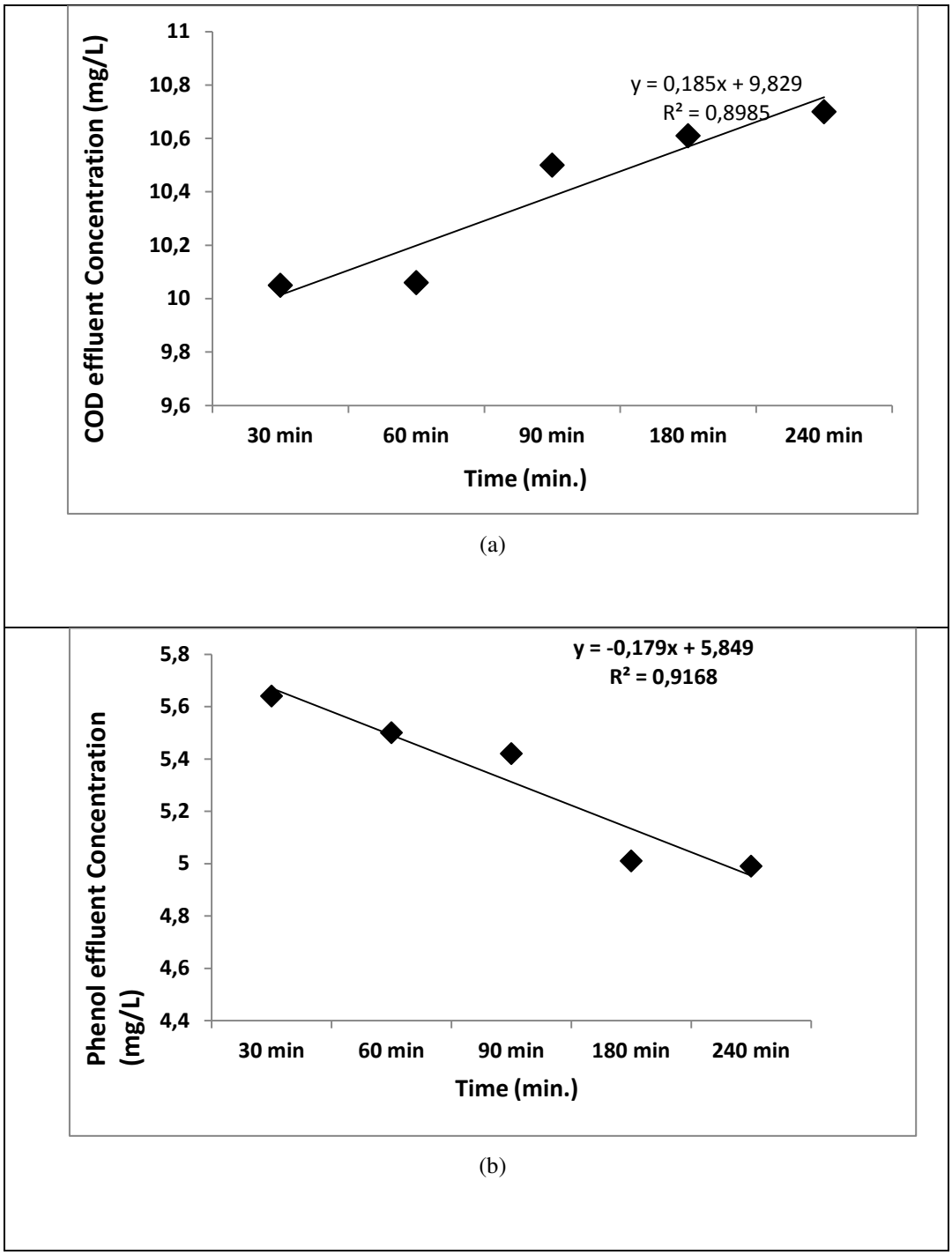


Figure 6.54 Pseudo-first-order reaction of COD and phenol.

The $R^2$ values for Pseudo-first-order reaction was found to be 0.8985for COD and 0.9168 for phenol, respectively, performed with Nano-ZnO-Magnetite. Pseudo-first-order reaction's the first order rate kinetic constant is $k_1$. The $k_1$ values evaluated from Pseudo- first -order reaction plots were found to be 0.185 $min^{-1}$ for COD and 0.179 $min^{-1}$ for phenol, respectively.

### *6.6.3 Second-Order Kinetics*

In a second-order reaction, the sum of the exponents in the rate law is equal to two. The two most common forms of second-order reactions will be discussed in detail in this section (Chemwiki n.d.).

The equation describing first-order kinetics is given below:

$$1/ [A]t=kt + 1/[A] \quad (6.22)$$

where $A^0$ is the influent concentration of OMW (mg/L) and A is the effluent concentration of OMW (mg/L) at any time t (min), respectively and $k_2$ is the constant of pseudo-second-order reaction ($min^{-1}$).

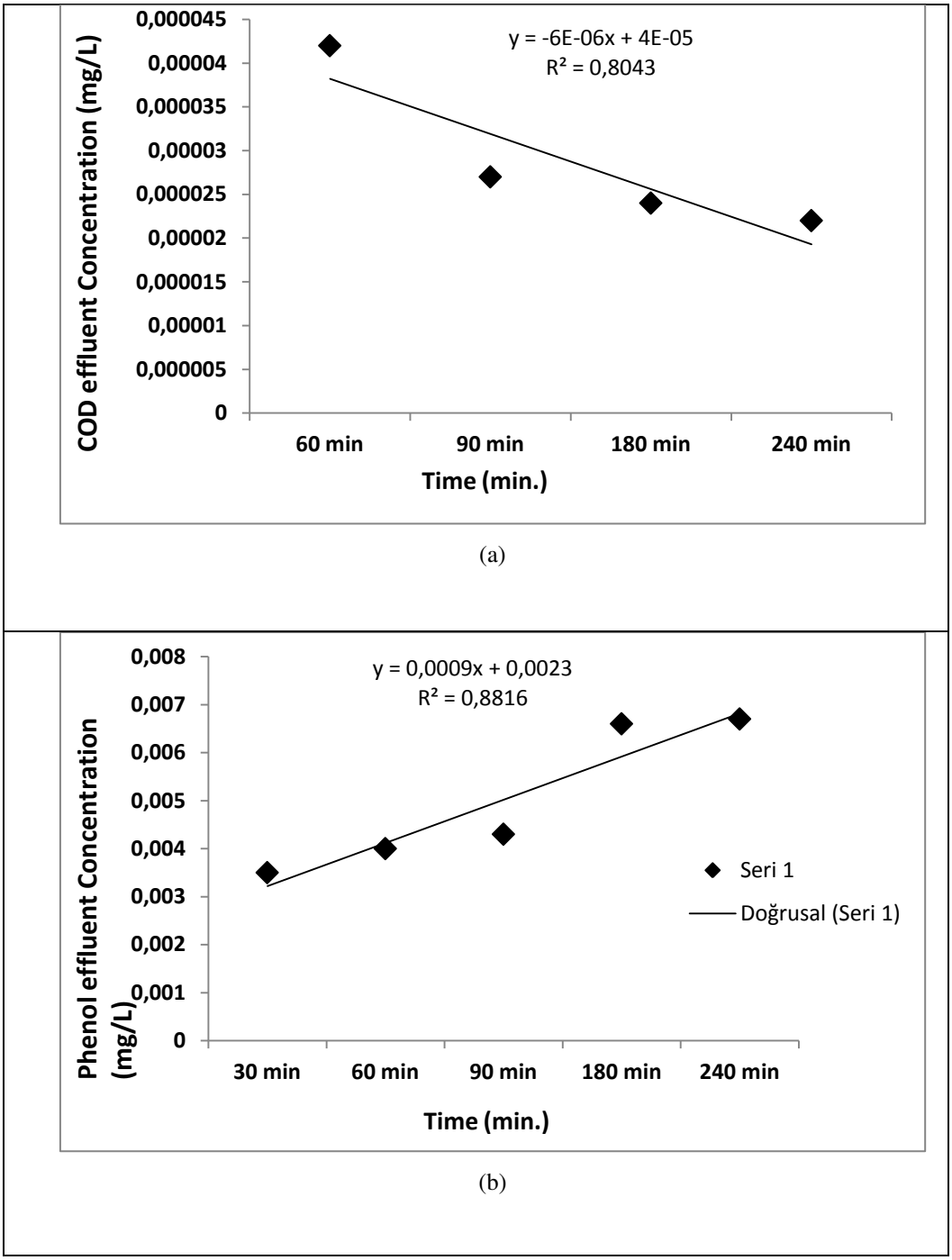


Figure 6.55 Pseudo-second-order reaction of COD and phenol.

The $R^2$ values for Pseudo-second-order reaction was found to be 0.8043 for COD and 0.8816 for phenol, respectively, performed with Nano-ZnO-Magnetite. Pseudo-second-order reaction's the second order rate kinetic constant is $k_2$. The $k_2$ values evaluated from Pseudo-second-order reaction plots were found to be 6E-06 $min^{-1}$ for COD and 0.0009 $min^{-1}$ for phenol, respectively.

Among the photocatalytic reaction kinetics used it was found that first-order kinetic is suitable for the removal of COD ($R^2$: 0.8985, $k_1$: 0.185 $min^{-1}$) and phenol ($R^2$: 0.9168, $k_1$: 0.179 $min^{-1}$) throughout photooxidation in the OMW with meaningfull photocatalytic rate constants.

## 6.7 Identification of Phenolic Compounds in the OMW by HPLC

Calibration graphs were plotted for the three polyphenols (caffeic acid, tyrosol and hydroxytyrosol) illustrated in Figure 6.56, 6.57 and 6.58, respectively. They will be used for making measurements on HPLC analysis. For each of a phenolic compound has been studied four different concentrations (1 mg/L, 10 mg/L, 20 mg/L and 50 mg/L) for drawing calibration graphs. $R^2$ values of calibration graphs of caffeic acid, tyrosol and hydroxytyrosol was found as 0.99, 0.99 and 0.99, respectively (Figure 6.56, 6.57 and 6.58).

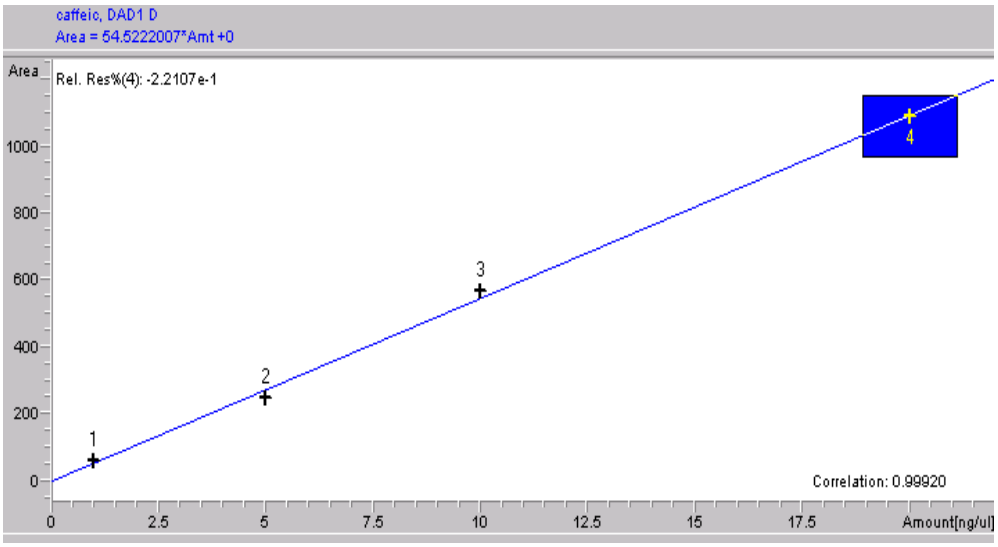


Figure 6.56 Calibration graph of caffeic acid.

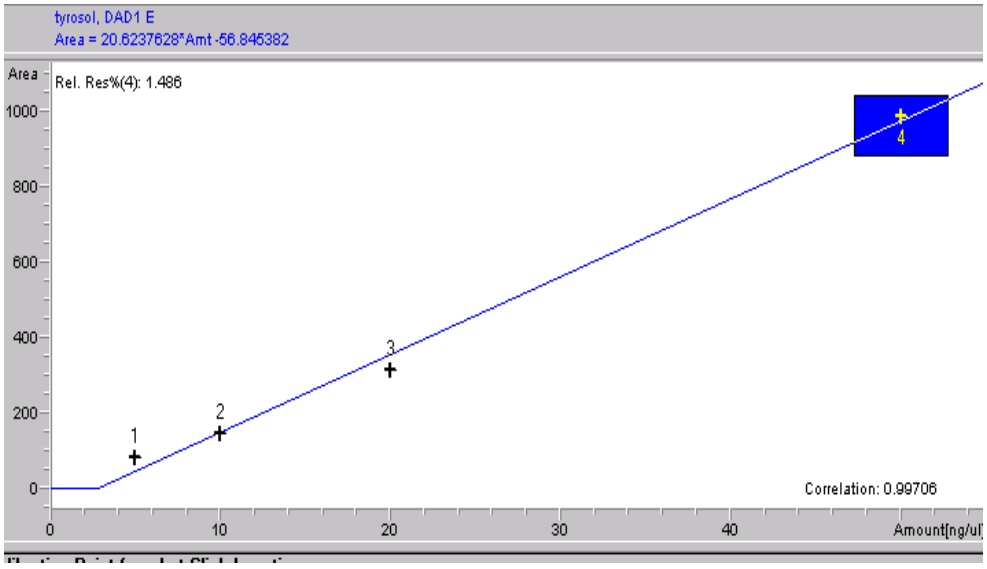


Figure 6.57 Calibration graph of tyrosol

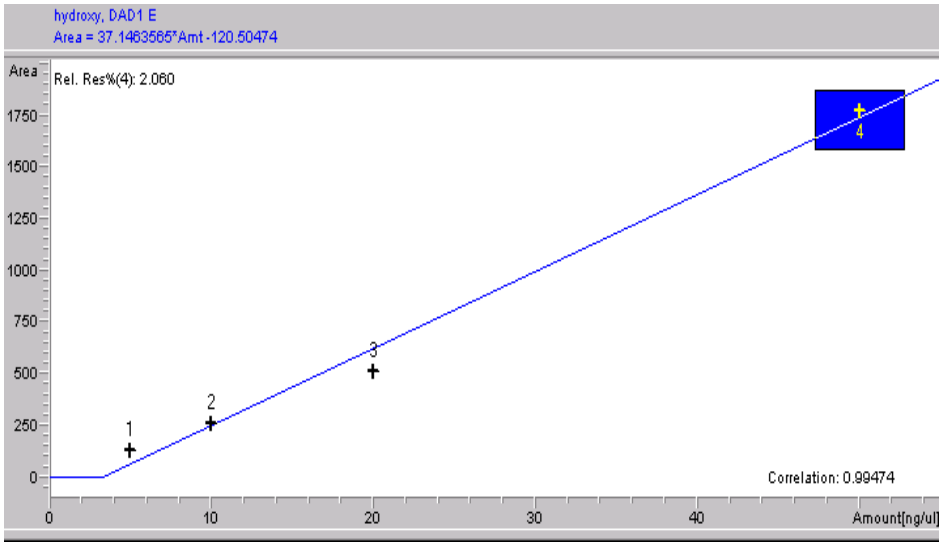


Figure 6.58 Calibration graph of hydroxytyrosol.

### *6.7.1 Measurement of the Concentration of Phenolic Compounds by HPLC in Raw OMW*

The concentrations of the phenolic compounds identified in the raw sample of OMW were determined quantitatively. HPLC technique was used to identify and quantify the caffeic acid, tyrosol and hydroxytyrosol phenolic compounds contained in the raw OMW. For this purpose, a standards mixture solution of phenolic compounds was analysed. Sample concentrations were calculated, based on peak

areas compared to those of each of the external standards. The phenolic compounds were identified by their retention times in comparison with external standards (Fki et al., 2005). As a result of this analysis, tyrosol and hydroxytyrosol were measured at λ = 280 nm and caffeic acid was measured at λ = 320 nm. Figure 6.59 and 6.60 shows the concentration of caffeic acid, tyrosol and hydroxytyrosol phenolic compounds, respectively, containing in raw OMW.

Figure 6.59 shows that 7.07 mg/L concentration of caffeic acid has been found in raw OMW as a result of HPLC measurements. Hajjouj et al., (2007) have found a close result to our study. They studied that the analysis of the amount of polyphenols in the olive mill wastewater and the amount of caffeic acid were found as 5.7 mg/L. In another study was performed by Mulinacci et al. (2001) and similar results are reported. 4 mg/L concentration of caffeic acid was found in OMW.

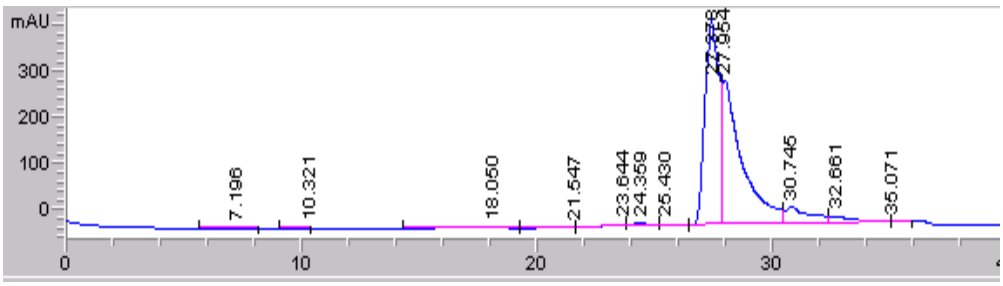


| RetTime [min] | Type | Area [mAU*s] | Amt/Area | Amount [nq/ul] | Grp | Name |
|---|---|---|---|---|---|---|
| 24.359 | VV | 406.34161 | 1.74038e-2 | 7.07187 | | caffeic |

Figure 6.59 The concentration of caffeic acid found in raw OMW.

According to the results of chromatograms in HPLC analysis, 112.6 mg/L concentration of hydroxytyrosol and 172.7 mg/L concentration of tyrosol was identified in raw OMW illustrated in Figure 6.60. In a study investigated by Akardere (2012), polyphenols were analyzed in the olive oil mill effluents. 115.9 mg/L and 50.3 mg/L concentration of hydroxytyrosol and tyrosol were found, respectively, and these data are consistent with our results.

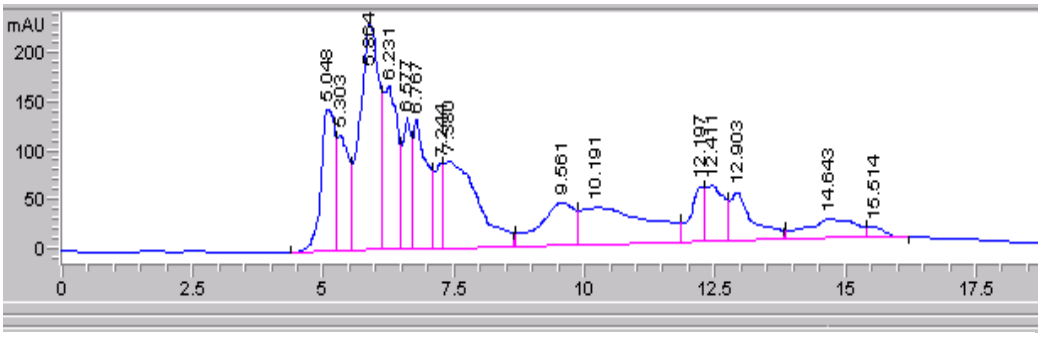


| RetTime [min] | Type | Area [mAU*s] | Amt/Area | Amount [ng/ul] | Grp | Name |
|---|---|---|---|---|---|---|
| 7.380 | VB | 4064.94434 | 2.77186e-2 | 112.67455 | | hydroxy |
| 10.191 | VV | 3505.01660 | 4.92855e-2 | 172.74657 | | tyrsol |
| Totals : | | | | 285.42112 | | |

Figure 6.60 The concentration of tyrosol and hydroxytyrosol found in raw OMW.

The results showed that hydroxytyorosl and tyrosol were most abundant phenolic compounds in OMW (Figure 6.60). Hydroxytyrosol and caffeic acid show a powerful antioxidant activities (Cofrades et al., 2011; Obied et al., 2007). Hydroxytyrosol inhibits human LDL oxidation, inhibits platelet aggregation and exhibits anti-inflammatory and anticancer properties (Bouallagui et al., 2011; Obied et al., 2007). The caffeic acid also was found in OMW samples, but at very low concentrations (Figure 6.59). Obied et al., (2008) reported that caffeic acid shows a higher antioxidant activity than hydroxytyrosol. Tyrosol showed similar concentrations with hydroxtytrosol in the OMW (Figure 6.60). Samuel et al. (2008) is reported to be effective in preserving cellular anti-oxidant defenses.

### *6.7.2 Measurement of the Concentration of Phenolic Compounds by HPLC in Treated OMW with Nano-ZnO-Magnetite under UV Irradiation*

By using 3 g/L Nano-ZnO-Magnetite nanocomposite with 30 min irradiation time at pH 4 and a temperature of ±20 $^{0}$C with an UV power of 300 W during photooxidation, the concentration of caffeic acid decreased from 7.07 mg/L to 1.47 mg/L (4,00184e$^{-1}$) (Figure 6.61) and the caffeic acid yields were recorded as 80% (Table 6.6). Baransi et al. (2012), investigates the adsorption of the phenolic compounds caffeic acid on PAC (powdered activated carbon) and $TiO_2$, as well as

their degradation via direct photocatalysis. 90% removal of caffeic acid was obtained within 0.5 h of UV exposure time at PAC concentration of 0.45 g/L while in our study, 80% removal of caffeic acid efficiency was found with 30 min UV irradiation time at a 3 g/L Nano-ZnO-Magnetite nanocomposite concentration.

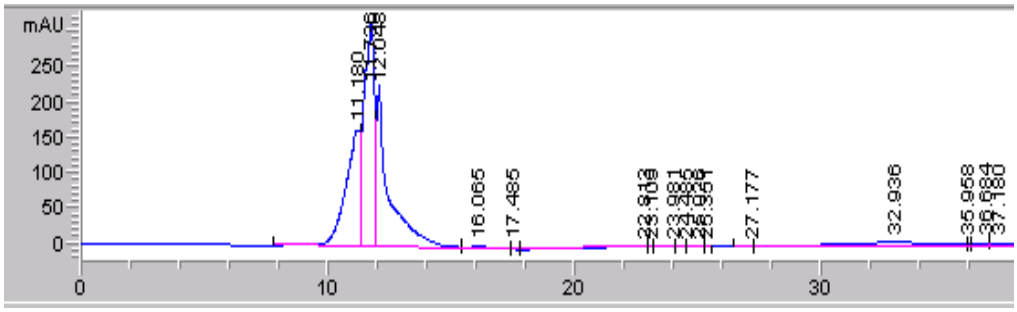


| RetTime [min] | Type | Area [mAU*s] | Amt/Area | Amount [ng/ul] | Grp | Name |
|---|---|---|---|---|---|---|
| 24.485 | VV | 22.99409 | 1.74038e-2 | 4.00184e-1 | | caffeic |

Figure 6.61 The concentration of caffeic acid found in treated OMW with UV photooxidation (Nano-ZnO-Magnetite concentration: 3 g/L, T: ±20 0C, pH: 4.60, UV irradiation time: 30 min, UV power: 300 W).

And also, the removal efficiencies of tyrosol and hydroxytyrosol were obtained as 80% and 51%, respectively. Their concentrations decreased from 172.7 mg/L to 34.8 mg/L for tyrosol and from 112.6 mg/L to 55.2 mg/L for hydroxytyrosol, respectively, after treatment with 3 g/L Nano-ZnO-Magnetite nanocomposite under 300 W UV irradiation after 30 min irradiation time (Figure 6.62, Table 6.6).

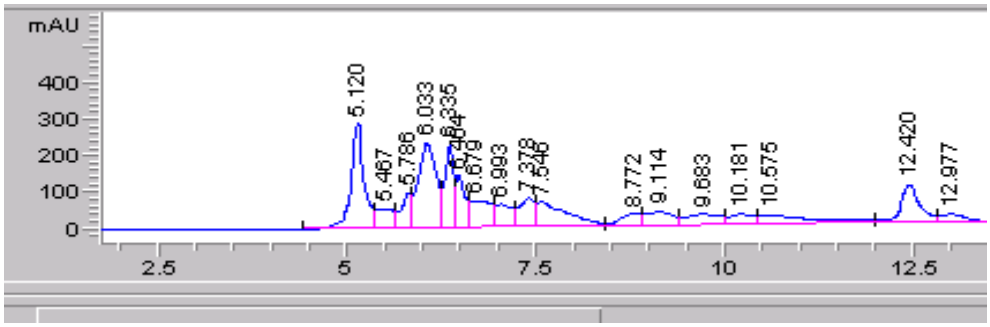


| RetTime [min] | Type | Area [mAU*s] | Amt/Area | Amount [ng/ul] | Grp | Name |
|---|---|---|---|---|---|---|
| 7.546 | VV | 1930.11353 | 2.86013e-2 | 55.20375 | | hydroxy |
| 10.181 | VV | 661.75018 | 5.26512e-2 | 34.84192 | | tyrsol |
| Totals : | | | | 90.04567 | | |

Figure 6.62 The concentration of tyrosol and hydroxytyrosol found in treated OMW with UV photooxidation.

Table 6.6 Removal Efficiencies of polyphenols (caffeic acid, tyrosol and hydroxytyrosol) in OMW.

| **Polyphenols** | **Raw OMW (mg/L)** | **Treatment of OMW with UV photooxidation (mg/L)** | **Removal Efficiency (%)** |
|---|---|---|---|
| **Caffeic acid** | 7.07 | 1.47 | 80 |
| **Tyrosol** | 172.7 | 34.8 | 80 |
| **Hydorxytyrosol** | 112.6 | 55.2 | 51 |

## 6.8 UV Absorption Spectra of OMW

The UV–visible spectra of the OMW were recorded on a spectro photometer in the wave lentgs changing from 190 nm to 1100 nm. UV absorption spectra of raw OMW and treated OMW with UV light were illustrated in Figures 6.63 and 74, respectively. The maximum absorbances were recorded at between 2600 and 4000 at wavelentgs between 180 nm and 380 nm in raw omw. When OMW were irradiated under UV light with 3 g/L Nano-ZnO-Magnetite nanocomposite, spectral changes were observed (Figure 6.64). The maximum absorbances decreased close to zero after UV treatment. The reason of this

can be explained by the production of polyphenols namely caffeic acid, tyrosol and hydroxytyrosol after photodegradation of OMW.

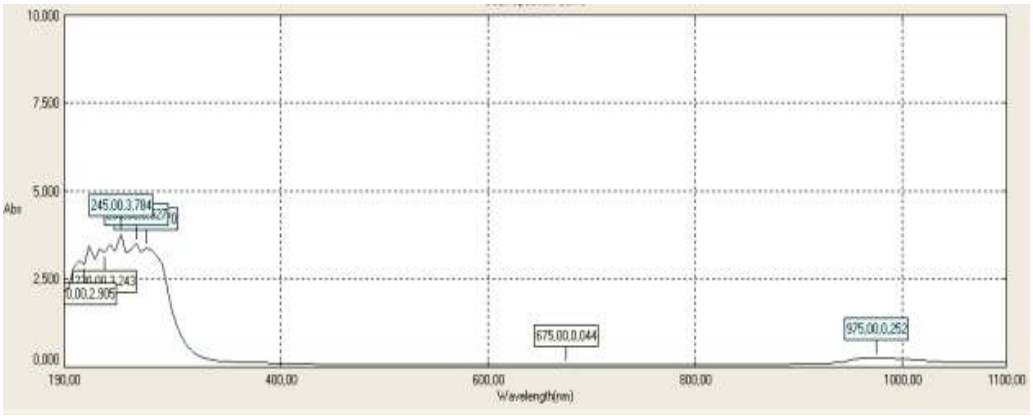


Figure 6.63 Change in UV absorption spectra in the raw OMW.

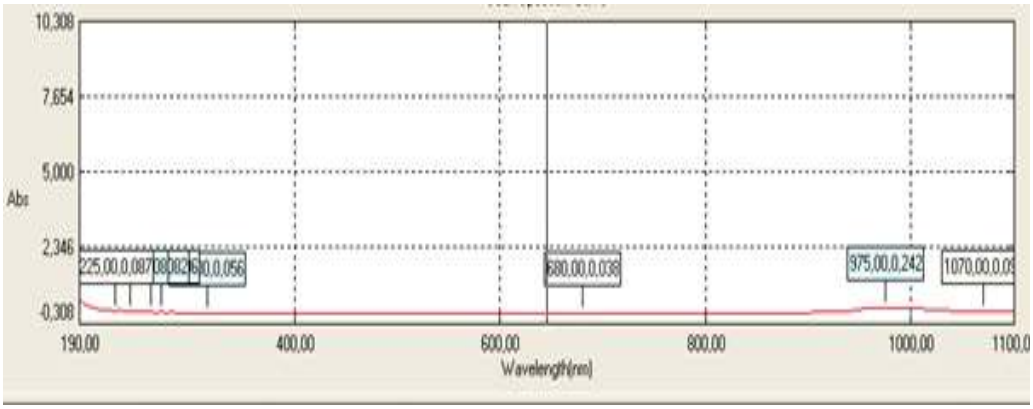


Figure 6.64 Change in UV absorption spectra in the treated OMW under UV irradiation (Nano-ZnO-Magnetite concentration: 3 g/L, pH: 4.60, UV irradiation time: 24 h, UV power: 300 W).

## 6.9 Determination of Inert Chemical Oxygen Demand (COD) Fractions of Olive Mill Wastewater

In this study, in order to determine inert fractions of olive mill wastewaters batch experimental studies were carried out. This analysis is important for modelling, design and operation of olive mill wastewater treatment systems and determination of discharge limits. Experimental study conducted on three parallel batch reactors operated with wastewater sample for 41 days until the COD and glucose levels were stabilized and a plateau was observed with unchanged COD concentrations during consecutive 7 days.

Figure 6.65 shows the total inert COD and soluble inert COD fractions of raw OMW. Total inert COD and dissolved inert COD of OMW tests were performed. As a result after the inert COD of glucose reached close to zero, the total inert COD of raw OMW was found as 8765 mg/L. The soluble inert COD of raw OMW was found as 3674 mg/L, respectively.

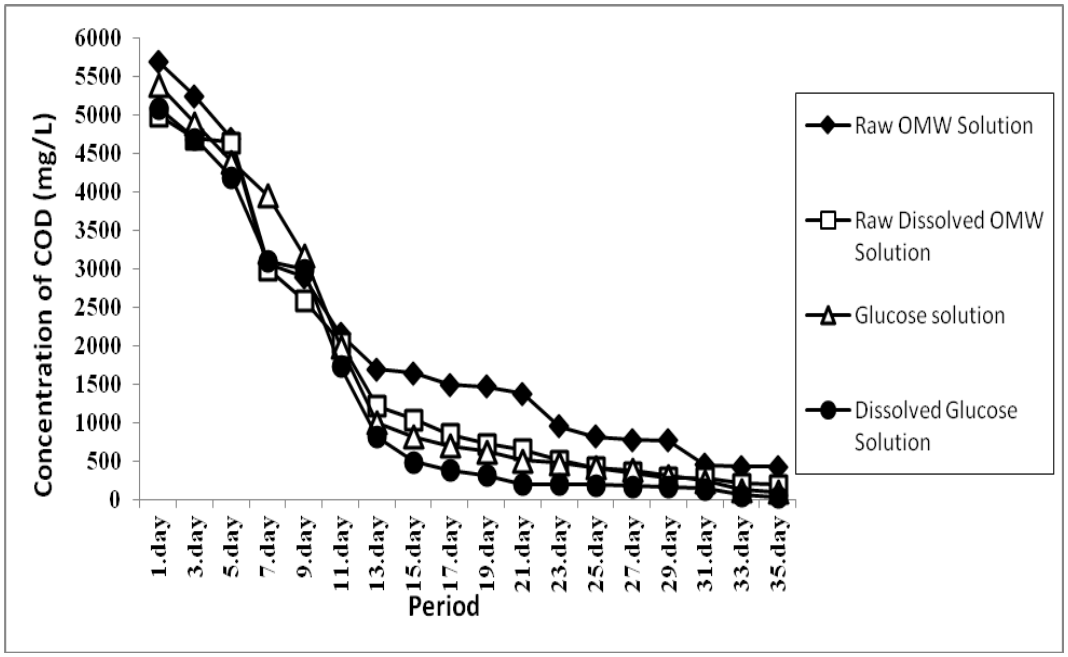


Figure 6.65 Total inert COD and soluble inert COD of raw OMW (T: ±20 0C, pH: 4.60).

Figure 6.66 illustrated the total inert COD and soluble inert COD fractions of treated OMW at a original pH at a temperature of 20 $^{0}$C after 30 min irradiation time at a 3 g/L concentration of nano-ZnO-Magnetite with an UV lamp with a power of 300 W. After treatment with 300 W UV, the total inert COD and soluble inert COD concentrations of OMW obtained as 694 mg/L and 395 mg/L, respectively.

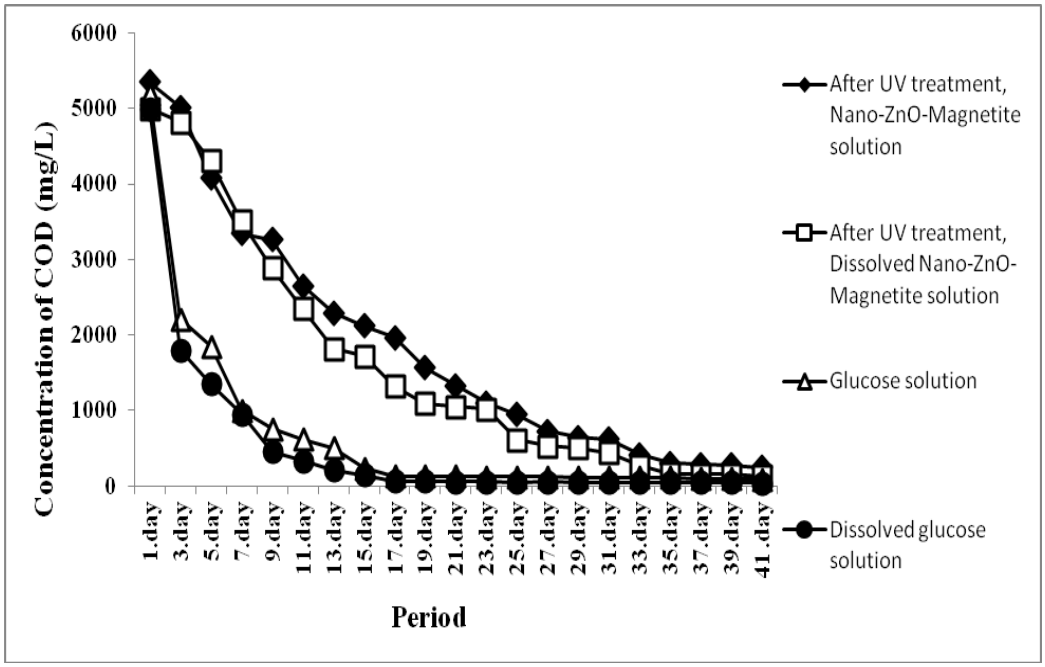


Figure 6.66 Total inert COD and dissolved inert COD of treated with UV irradiation of OMW (T: ±20 0C, Nano-ZnO-Magnetite conc.: 3g/L, Irradiation time: 30 min, UV power: 300 W, pH: 4.60).

The resulting total inert COD and soluble inert COD of OMW removal efficiency via photocatalytic treatment was found to be 92% and 89%, respectively as shown in Table 6.7.

Table 6.7. Removal Efficiencies of total inert COD and soluble inert COD of OMW.

| Parameter | Raw OMW (mg/L) | Treatment of OMW with UV (mg/L) | Removal Efficiency (%) |
|---|---|---|---|
| **Total Inert COD** | 8765 | 694 | 92 |
| **Soluble Inert COD** | 3674 | 395 | 89 |

## 6.10 Determination of Recovery of Nano-ZnO-Magnetite

The main handicap in applying photocatalytic processes for the reclamation of industrial effluents relies in the cost of the catalyst. In this sense, the difficulty in recovering the catalyst poses the main technical-economical drawback. To solve this

problem, a novel photocatalyst with ferromagnetic properties such as magnetite for ease of recovery and high effectiveness in the treatment of OMW was developed Magnetic separation provides a very convenient approach for removing and recycling magnetic particles (such as magnetite) by applying external magnetic fields. The incorporation of magnetic components into ZnO nanoparticle-based catalysts may, therefore, enhance the separation and recovery of nanosized Nano-ZnO-Magnetite (Ye et al., 2010). The evolution of COD, phenol and TS degradation rates were determined.

From Table 6.8 it can be clearly seen that the utilization of Nano-ZnO-Magnetite composite first, second, third, fourth and fifth times, the removal efficiency of COD decreased from 80% to 75%, to 70%, to 64% and to 52%, respectively. Likewise, the removal efficiency of phenol was decreased from 75% to 68%, to 62%, to 54% and to 48%. The TS removal efficiency also decreased from 70% to 63%, to 59%, to 57% and to 56%, respectively, after first, second, third, fourth and fifth times utilisation of the same Nano-ZnO-Magnetite composite . Although in this study very high recovery yields were not obtained this partly reduce the cost spending for nanocomposite.

Table 6.8 Recovery of Nano-ZnO-Magnetite (T: ±20 – 30 $^{0}$C, Nano-ZnO-Magnetite Concentration: 3 g/L, UV irradiation time:24 h, UV power: 300 W, pH: 4.60).

| **Parameters** | **First Treatment** | **Second Treatment** | **Third Treatment** | **Forth Treatment** | **Fifth Treatment** |
|---|---|---|---|---|---|
| **COD** | 80% | 75% | 70% | 64% | 52% |
| **Phenol** | 75% | 68% | 62% | 54% | 48% |
| **TS** | 70% | 63% | 59% | 57% | 56% |

## 6.11 Cost Analysis

Cost analysis for 1 liter treatment of OMW under UV light was shown in Table 6.9. Considering all the removal efficiencies for studied parameters in the OMW, the optimum Nano-ZnO-Magnetite composite concentration was found as 3 g/L for the maximum removals of all pollutant parameters in the OMW via photocatalysis. Electricity, UV lamp and Nano-ZnO-Magnetite composite was used for treatment of OMW. All the comsumptions were calculated and are given in Table 6.7. Total cost of treatment OMW was obtained as 505.33 TL for treat 1 liter of OMW. 500 TL was spent for 20 UV lamps, while the chemical cost and nanocomposite cost were only 5.33 TL for 1 liter OMW treatment.

Table 6.9 Cost Analyis of treatment OMW under UV light

| **Cost Analysis** | **Treatment of OMW under UV light** |
|---|---|
| **UV** | **1 UV lamp:** 25 TL<br>**20 UV lamp:** 20 * 25 = 500 TL |
| **Electricity consumption** | **24 hour UV irradiaition:** 1.12 TL |
| **Chemicals** | **Magnetite ($Fe_3O_4$)(1 kg):** 12.99 €<br>**Zinc acetate monohydrate (500 g):** 78.40 €<br>**N,N-dimethylformamide (DMF) (1 lt):** 152 € |
| **Cost analysis for treatment of 1 liter OMW:**<br>3 g Nano-ZnO-Magnetite was used for treatment of 1 liter OMW under UV light. 10 g magnetite, 2 g Zinc acetate monohydrate and 250 mL N,N-dimethylformamide (DMF) was used for prepare 3 g Nano-ZnO-Magnetite. | **For 3 g Nano-ZnO-Magnetite:**<br>**10 g magnetite**: 0.1299 € (0.3935 TL)<br>**2 g Zinc acetate monohydrate:** 0.3136 € (0.95 TL)<br>**250 mL N,N-dimethylformamide (DMF):** 31.25 € (2.87 TL) |
| **Total cost for treatment of 1 liter OMW** | 500 TL + 1.12 TL + 0.3935 TL + 0.95 TL + 2.87 TL = **505.33 TL** |
| The cost of chemicals is calculated according to market prices. Electricity costs are calculated according to the consumer price industrial units. Recent euro exchange rate was used to convert the Euro currency Turkey (1€ = 3.03 TL). | |

## 6.12 A Summary for Statistical ANOVA Test Results

The sensitive operating parameters in adsorption process are listed below;

- TS and total phosphorous parameters are sensitive in determination of optimum Nano-ZnO-Magnetite concentration.
- TS and total phosphorous are sensitive in determination of optimum adsorption time.
- Phenol and total phosphorous are sensitive in determination of optimum pH.

The sensitive operating parameters in photocatalytic process under UV light are listed below;

- All pollutants (COD, phenol, TS, total nitrogen and total phosphrous parameters) are sensitive in determination of optimum Nano-ZnO-Magnetite concentration and optimum irradiation time.
- Total nitrogen and total phosphorous parameters are sensitive in determination optimum pH.

The sensitive operating parameters in photocatalytic process under sun light are listed below;

- Phenol, TS and total nitrogen are sensitive in determination of optimum Nano-ZnO-Magnetite concentration.
- Total phosphorous is sensitive in determination of optimum sunlight irradiation time.
- Total phosphorous is sensitive in determination of optimum pH.

# CHAPTER SEVEN
# CONCLUSION

This work aimed to study olive mill wastewater treatment process based on adsorption and photocatalytic oxidation using Nano-ZnO-Magnetite. UV and sunlight was used for energy source and the removal efficiencies of pollutant parameters were compared under different operational conditions.

Five pollutants removal efficiencies (COD, phenol, TS, total nitrogen and total phosphorous), polyphenols (caffeic acid, tyrosol and hydroxytyrosol), nanocomposite concentration, time and pH were investigated for two treatment processes and adsorption process. Table 7.1 shows the comparison of removal efficiencies.

Table 7.1 The comparison of removal efficiencies.

| **Treatment Processes OPTIMUM** | **Maximum Removal Efficiencies (%)** | | | | |
|---|---|---|---|---|---|
| | **COD** | **Phenol** | **TS** | **Total Nitrogen** | **Total Phosphorous** |
| **Adsorption** (3 g/L Nano-ZnO-Magnetite and 180 min adsorption time) | 12% pH: 4 | 9% pH:4 | 10% pH:4 | 7% pH:10 | 10% pH:10 |
| **Photocatalytic treatment under UV light** (3 g/L Nano-ZnO-Magnetite and 30 min irradiation time) | 80% pH: 4 | 75% pH:10 | 70% pH:4 | 97% pH:10 | 85% pH:4 |
| **Photocatalytic treatment under sun light** (3 g/L Nano-ZnO-Magnetite and 24 h irradiation time) | 76% pH: 4 | 64% pH:10 | 34% pH:4 | 39% pH:10 | 72% pH:4 |

Table 7.1 shows that;

The adsorption processes are not suitable for treatment of OMW with using Nano-ZnO-Magnetite. The removal efficiencies of COD, phenol, TS, total nitrogen and total phosphorous are too low.

The removal efficiencies of COD (80%-76%), phenol (75%-64%) and total phosphorous (85%-72%) from the UV studies are **slightly** higher from the sunlight studies.

The removal efficiencies of TS (70%-34%) and total nitrogen (97%-39%) from the UV studies are **strongly** higher from the sunlight studies.

For maximum removal efficiencies of COD, TS, total phosphorous and total nitrogen pollutant parameters of OMW, the optimum irradiation time was selected as 30 min for UV and 15 h for sunlight. Much lower time was spent for photocatalytic studies under UV light (30 min) compared to sunlight irradiation time (15 h).

For maximum removals of COD, TS and total nitrogen the optimum pH was found at pH: 4 .60 which this is the pH of the original pH value of OMW. This decrease the cost of the chemical utilized in both photocatalytic studies (under UV light and sunlight).

In this study by using Nano-ZnO-Magnetite nanocomposite through advanced treatment with UV photooxidation, The removal efficiencies of caffeic acid, tyrosol and hydroxytyrosol were found as 80%, 80% and 51%, respectively. UV photoxidation process was suitable for removal of polyphenolic compounds.

In this study, recovery of nano-ZnO- Magnetitewith five treatment sequential steps was investigated. The removal efficiencies of COD, phenol and TS was only decreased from 80% to 75%, from 75% to 68% and from 70% to 63%, respectively, for second treatment recovery cycle. After five treatment cycle, the removal

efficiencies of COD, phenol and TS was decreased to 52%, from 48% to 56%, respectively. According to resuls, the recovery and reuse of photocatalyst minimizes the operating costs of the treatment process.

Cost analysis was made for removal of OMW under UV light. Total cost of treatment OMW was obtained as 505.33 TL, while 500 TL was spent for 20 UV lamps. Only 5.33 TL was spent for treatment of 1 liter OMW.

Nano-ZnO-Magnetite can be re-used in the treatment processes. This decrease the cost of treatment.

**Recommendations for future studies**

Some of the recommendations for future studies are listed below:

- Nano-ZnO-Magnetite have been recommended to be efficient photocatalysts for the degradation of various toxic, organic pollutants such as COD, phenol, TS, total nitrogen and total phosphorous in OMW.
- The investigations also suggest that the coexistence of photocatalyst and lights exposure is necessary for photocatalytic degradation of OMW.
- Various operating parameters such as irradiation time of UV light, pH of the OMW, concentration of catalyst Nano-ZnO-Magnetite and type of catalysts have a considerable effect on degradation efficiency of pollutants in OMW.
- Optimization of the photodegradation parameters is essential from the viewpoint of efficient design and the application of photocatalytic oxidation processes to sustainable OMW treatment process.

## REFERENCES


Abbruzzetti, S., Carcellli, M., Pelagatti, P., Rominga, D., & Viappiani, C. (2001). Acid-induced unfolding of myoglobin triggered by a laser pH jump method. *Chemical Physics Letters*, *34*, 387.

Abu Al-Rub, F., El-Naas, M.H., Ashour, I., & Al-Marzouqi, M. (2006). Biosorption of copper on Chlorella vulgaris from single, binary and ternary metal aqueous solutions. *Process Biochemistry, 41,* 457–464

Akardere, E. (2012). *Investigation of phenol-degrading enzyme activities in bioremediation of olive mill wastewater.* Master Thesis, .Ankara University, Ankara.

Aktaş, E., Imre, S., & Ersoy, L.( 2001). Characterization and lime treatment of olive oil mill wastewater. *Water Research*, *35* (9), 2336-2340.

Al-Malah, K., Azzam, M., & Abu-Lail, N. I. (2000). Olive mills effluent (OME) wastewater posttreatmentusing activated clay. *Separation and Purification Technology*, *20*, 225.

Ambrus, Z., Balázs, N., Alapi, T., Wittmann, G., Sipos, P., Dombi, A., & Mogyorósi, K. (2008). Synthesis, structure and photocatalytic properties of Fe(III)-doped $TiO_2$ prepared from $TiCl_3$. *Applied Catalysis B: Environmental, 81,* 27–37.

Anandan, S., Vinu, A., Venkatachalam, N., Arabindoo, B., & Murugesan, V. (2006). Photo catalytic activity of ZnO impregnated Hb and mechanical mix of ZnO/Hb in the degradation of monocrotophos in aqueous solution. *Journal of Molecular Catalysis A: Chemical, 256*, 312–320.

Azzam, M.O.J., Al-Malah, K.I., & Abu-Lail, N.I. (2004). Dynamic post treatment response of olive mill effluent wastewater using activated carbon. *Journal of Environmental Science and Health, A 39*, 269–280.

Ba-Abbad, M.M., Kadhum, A.A.H., Mohamad, A.B., Takriff, M.S., & Sopian, K. (2013). Visible light photocatalytic activity of $Fe^{3+}$-doped ZnO nanoparticle prepared via sol–gel technique. *Chemosphere, 91,* 1604–1611.

Badawya, M.I., Goharya, F.El., Ghalyb, M.Y., & Alia, M.E.M. (2009). Enhancement of olive mill wastewater biodegradation by homogeneous and heterogeneous photocatalytic oxidation. *Journal of Hazardous Materia*ls, *169,* (1–3), 673–679.

Balasubramanian, G., Dionysiou, D.D., Suidan, M.T., Baudin, I., & Laine, J.-M. (2004). Evaluating the activities of immobilized $TiO_2$ powder films for the photocatalytic degradation of organic contaminants in water. *Applied Catalysis, B: Environmental, 47*, 73-84.

Balistrieri L.S., & Murray J.W. (1981). The surface chemistry of goethite (aFeOOH) in major ion seawater. *American Journal of Science*, 788–806.

Banat, F.A., Al-Bashir B., Al-Asheh S., & Hayajneh O. (2000). Adsorption of Phenol by Bentonite. *Environmental Pollution*, *107*, 390-398.

Bedard, K., & Krause, K.H. (2007). The NOX family of ROS-generating NADPH oxidases: physiology and pathophysiology. *Physiological Reviews*, *87*, 245.

Beltran, F.J., Garcia-Araya, J.F., Frades, J., Alvarez, P., & Gimeno O. (1999). Effects of single and combined ozonation with $H_2O_2$ or UV radiation the chemical degradation and biodegradability of debittering table olive industrial wastewaters. *Water Research, 33*, 723-732.

Benitez, F.J, Beltran-Heredia, J., Torregrosa, J., & Acero, J.L. (1999). Treatment of olive mill wastewaters by ozonation, aerobic degradation and the combination of both treatments. *Journal of Chemical Technology and Biotechnology*, *74*, 639–646.

Bergese J. (2013). *Kinetics and benefits of employing uv light for the treatment of aqueous ammonia in wastewater.* Master Thesis, University Halifax, Nova Scotia.

Bideau, M., Claudel, B., Dubien, C., Faure, L., & Kazouan, H. (1995). On the"immobilization" of titanium dioxide in the photocatalytic oxidation of spent waters. *Journal of Photochemistry & Photobiology, A: Chemistry*, *91*, 137-144.

Bouallagui, Z., Bouaziz, M., Lassoued, S., Engasser, J. M., Ghoul, M., & Sayadi, S. (2011). Hydroxytyrosol Acyl Esters: Biosynthesis and Activities. *Applied Biochemistry and Biotechnology, 163* (5), 592–599.

Cang Sun, R., Fang, J.M., & Tomkinson, J. (2000). Delignication of rye straw using hydrogen peroxide. *Industrial Crops and Products*, *12,* 71–83.

Chemwiki (n.d.-a). *First order kinetics*. Retrived, July 18, 2015 from, http://chemwiki.ucdavis.edu/Physical_Chemistry/Kinetics/Reaction_Rates/Second-Order_Reactions).

Chemwiki (n.d.-b). *Second order kinetics.* Retrived, July 18, 2015 from, (http://chemwiki.ucdavis.edu/Physical_Chemistry/Kinetics/Reaction_Rates/Second-Order_Reactions).

Chemwiki (n.d.-c). Zero order kinetics. Retrived, July 18, 2015 from, http://chemwiki.ucdavis.edu/Physical_Chemistry/Kinetics/Reaction_Rates/Zero-Order_Reactions).

Chen, C.C. (2006). Degradation pathways of ethyl violet by photocatalytic reaction with ZnO dispersions. *Journal of Molecular Catalysis*. *A: Chem*stry, *264*, 82.

Chen, G.H, Lei, L.C., & Yue, P.L. (1999). Wet oxidation of highconcentration reactive dyes. *Industrial and Engineering Chemistry Research*, *38,* 1837–1843.

Chen, X. (2005). *Synthesis and investigation of novel nanomaterials for ımproved photocatalysis.* PhD. Thesis, Case Western Reserve University.

Chen, Z., & Gao, L. (2008). A new route toward ZnO hollow spheres by a base-erosion mechanism. *Crystal Growth & Design, 8*, 460–464.

Clifford, A.B., & Luis, S. (1979). Hydrophobic and coulombic interactions in the micellar binding of phenols and phenoxide ions. *The Journal of Physical Chemistry*, 680–683.

Cofrades, S., Salcedo Sandoval, L., Delgado-Pando, G., López-López, I., Ruiz-Capillas, C., & Jiménez-Colmenero, F. (2011). Antioxidant activity of hydroxytyrosol in frankfurters enriched with n-3 polyunsaturated fatty acids. *Food Chemistry, 129* (2), 429–436.

Comparelli, R., Fanizza, E., Curri, M. L., Cozzoli, P. D., Mascolo, G., & Agostiano A. (2005). UV-induced photocatalytic degradation of azo dyesby organic capped ZnOnanocrystals immobilized onto substrates. *Applied Catalysis B: Environmental, 62*, 144–149.

Contescu, A., Vass, M., Contescu, C., Putyera, K., & Schwarz, J.A. (1998). Acid buffering capacity of basic carbons revealed by their continuous pK distribution. *Carbon, 36,* 247–258.

Cox, L., Celis, R., Hermosin, M. C., Becker, A., & Cornejo, J. (1997). Porosity and herbicide leaching in soils amended with olive-mill waste water. *Agriculture, Ecosystems & Environment, 65*,151.

Daneshvar, N., Aber, S., Seyed Dorraji, M. S., Khataee, A. R., & Rasoulifard, M.H. (2008). Preparation and Investigation of photocatalyticproperties of ZnO nanocrystals: Effect of operational parametersand kinetic study. *International Journal of Chemical and Biomolecular Engineering, 1*, 24-29.

Daneshvar, N., Salari, D., & Khataee, A.R. (2004). Photocatalytic degradation of azo dye acid red 14 in water on ZnO as an alternative catalyst to $TiO_2$. *Journal of Photochemistry and Photobiology, 162*, 317.

Dhananjeyan, M. R., Kiwi, J., & Thampi, K. R. (2000). $Fe_2O_3$ immobilizedon derivatized polymer filmfor mineralization of pollutants. *Chemical Communications,* 1443.

Dindar, S. & Icli, J. (2001). Unusual photoreactivity of zinc oxideirradiated by concentrated sunlight. *Journal of Photochemistry and Photobiology A: Chemistry, 140*, 263.

Dolinina, E.S. & Parfenyuk, E.V. (2014). The effects of surface chemistry of mesoporous silica materials and solution pH on kinetics of molsidomine adsorption, *Journal of Solid State Chemistry*, *209*, 105–112.

Eba F., Gueu S., Mvongbote A., Ondo J., Yao B., Nlo J., & Kouya Biboutou R. (2010). Evaluation of the absorption capacity of the natural clay from Bikougou (Gabon) to remove Mn (II) from aqueous solution. *International Journal of Engineering Science and Technology*, *2,* (10), 5001-5016.

Ekama, G.A., Dold, P.L., & Marais, G.V. (1986). Procedures for determining influent COD fractions and the maximum specific growth-rate of heterotrophs in activated sludge systems. *Water Science and Technology*, *18,* 91-114.

El-Hajjouji H., Barje F., Pinelli E., Baily J.R., Richard C., Winterton P. et al., (2008). Photochemical UV/TiO2 treatment of olive mill wastewater (OMW). *Bioresource Technology*, *99*, 7264-7269.

Emmanuel Aluyor, O. & Olalekan Badmus, A. M. (2008). COD removal from industrial wastewater using activated carbon prepared from animal horns. *African Journal of Biotechnology, 7* (21), 3887-3891.

Fiorentino, A., Gentili, A., Isidori, M., Lavorgna, M., Parrella, A., & Temussi, F., (2004). Olive oil mill wastewater treatment using a chemical and biological approach, *Journal of Agricultural and Food Chemistry, 51*, 5151.

Fouad, O. A., Ismail, A. A., Zaki, Z. I., & Mohamed, R. M. (2006). Zinc oxidethin films prepared by thermal evaporation deposition and itsphotocatalytic activity. *Applied Catalysis B: Environmental, 62*, 144–149.

Fujishima, A. & Honda, K. (1972). Electrochemical photolysis of waterat a semiconductor electrode. *Nature, 238.5358*, 37-38.

Galiatsatou, P., Metaxas, M., Arapoglou, D., & Kasselouri-Rigopoulou, V. (2002) Treatment of olive mill waste water with activated carbons from agricultural by-products, *Waste Management, 22*, 803.

Galindo, C., Jacques, P., & Kalt, A. J. (2000). Photochemical and photocatalytic degradation of an indigoid dye: A case study of acid blue 74 (AB74). *Photochemistry and Photobiology, 130,* 35.

Ginos, A., Manios, T., & Mantzavinos, D. (2006). Treatment of olive mill effluents by coagulation–flocculation–$H_2O_2$ oxidation and effect on phytotoxicity. *Journal of Hazardous Materials, B133*, 135-142.

Gogate, P.R., & Pandit, A.B. (2004a). A review of imperative technologies for wastewater treatment I: oxidation technologies at ambient conditions. *Advances in Environmental Research, 8*, 501-551.

Gouvea, C. A. K., Wypych, F., Moraes, S. G., Duran, N., Nagata, N., & Peralta-Zamora, P. (2000). Semiconductor-assisted photocatalytic degradationof reactive dyes in aqueous solution. *Chemosphere*, *40*, 433–440.

Greenwood N. N., & Earnshaw, A. (1997). Pd on amine-terminated ferrite nanoparticles: a complete magnetically recoverable facile catalyst for hydrogenation reactions. *Chemistry of the Elements* (2nd Ed.). Butterworth-Heinemann, ISBN 0080379419.

Griffiths, P. & de Hasseth, J.A. (2007). *Fourier transform infrared spectrometry.* (2nd Ed.). Wiley-Blackwell, ISBN 0-471-19404-2.

Guin D., Baruwati B., & Manorama S.V., (2007). Pd on amine-terminated ferrite nanoparticles: a complete magnetically recoverable facile catalyst for hydrogenation reaction, *Organic Letters*, *9*,1419–1421.

Hajjouji H. E., Pinelli E., Guiresse M., Merlina G., Revel J.C., & Hafidi M. (2007). *Assessment of the genotoxicity of olive mill waste water (OMWW) with the Vicia faba micronucleus test,* doi:10.1016/j.mrgentox.

Han, R., Zou, W., Zhang, Z., Shi, J., & Yang, J. (2006). Removal of Copper(II) and Lead(II) from aqueous solution by manganese oxide coated sand i. characterization and kinetic study. *Journal of Hazardous Materials, B137*, 384.

Hanno zur, L. (2013). *X-Ray diffraction how it works what it can and what it cannot tell us.* Msc. Thesis, University of South Carolina.

Hasanpour, A ., Niyaifar, M ., & Asan, M . (2012). Synthesis and Characterization of $Fe_3O_4$ & ZnO Nanocomposites by Sol- Gel Method. *Proceedings of the 4th International Conference on Nanostructures.* (ICNS4) 12-14 March, Kish Island, I.R. Iran.

Hoffman, M. R., Martin, S. T., Choi, W., & Bahnernann,D. W. (1995). Environmental Applications of Semiconductor Photocatalysis. *Chemical Reviews, 95,* 69-96.

Hong, R.Y., Zhang, S.Z., Di, G.Q., Li, H.Z., Zheng, Y., Ding, J., & Wei, D.G. (2008). Preparation, characterization and application of $Fe_3O_4$/ZnO core/shell magnetic nanoparticles. *Materials Research Bulletin, 43,* 2457–2468.

Hu, H., Shao, M.W., Zhang, W., Lu, L., Wang, H., & Wang, S., *J.* (2007). Observation of electron-antineutrino disappearance at Daya Bay. *The Journal of Physical Chemistry C, 111,* 3467–3470.

Hua, M., Zhang, S.J., Pan, B.C., Zhang, W.M., Lu, L., & Zhang, Q.X. (2011). Heavy metal removal from water/wastewater by nanosized metal oxides: A review. *Journal of Hazardous Materials, 211*, *317*, 31.

Huang, L., Li, L., Dong, W., Liu, Y., & Hou, H. (2008). Removal of ammonia by OH radical in aqueous phase. *Environmental Science & Technology, 42* (21), 8070-8075.

Hur, S.G., Kim, T.W., Hwang, S.J., Hwang, S.H., Yang, J.H., & Choy, J.H. (2006). Heterostructured nanohybrid of zinc oxide–montmorillonite clay. *The Journal of Physical Chemistry A, B, 110,* 1599–1604.

Idelovitch, E., & Michail, M. (1981). Nitrogen removal by free ammonia stripping from high pH ponds. *Journal (Water Pollution Control Federation), 53(9*), 1391-1401.

İnan, H., Dimoglo, A., Şimşek, H., & Karpuzcu, M. (2004). Olive oil mill wastewater treatment by means of electro-coagulation. *Separation and Purification Technology, 36*, 23-31.

Ines, F., Noureddine, A., & Sami, S. (2005). The use of polyphenolic extract, purified hydroxytyrosol and 3,4-dihydroxyphenyl acetic acid from olive mill wastewater for the stabilization of refined oils: a potential alternative to synthetic antioxidants, *Food Chemistry, 93* (2), 197–204.

Juan-Ding, X., Ling-Guang, Q., Xin, J., Yu-Jun, Z., Sheng, Y., & Xia J.(2013). Magnetic porous carbons with high adsorption capacity synthesized by a microwave-enhanced high temperature ionothermal method from a Fe-based metal-organic framework. *Carbon, 59,* 372-382.

Kamat, P. V. (1993). Photochemistry on nonreactive and reactive(semiconductor) surfaces. *Chemical Reviews, 93*, 267.

Kandavelu, V., Kastien, H., & Thampi, *K.R.* (2004). Photocatalytic degradation of isothiazolin-3-ones in water and emulsion paints containing nanocrystalline TiO 2 and ZnO catalysts. *Applied Catalysis B: Environmental, 48,* 101.

Katie, B., Yael, D., & Isam, S. (2012) Synergetic effect between photocatalytic degradation and adsorption processes on the removal of phenol compounds from olive mill wastewater, *Water Research 46*, 789-798.

Kestioglou K, Yonar T., & Azbar N. (2005). Feasibility of physicochemical treatment and advanced oxidation processes (AOPs) as a means of pretreatment of olive mill effluent (OME). *Process Biochemistry, 40,* 2409–2416.

Khodja, A. A., Sheili, T., Pihichowski, J. F., & Boule P. (2001). Photocatalytic degradation of 2-phenylphenol on $TiO_2$ and ZnO inaqueous suspentions. *Journal of Photochemistry and Photobiology A, 141,* 231–239.

KirilMert, B., Yonar, T., YaliliKilic, M., & Kestioğlu, K. (2010). Pre-treatment studies on olive oil mill effluent using physicochemical, Fenton and Fenton-like oxidations processes, *Journal of Hazardous Materials*, *174*, 122-128.

Kobayakawa, K., Sato, C., Sato, Y., & Fujishima, A., (1998). Continuous-flow photoreactor packed with titanium dioxide immobilized on large silica gel beads to decomposeoxalic acid in excess water. *Journal of Photochemistry & Photobiology, A: Chemistry, 118*, 65-69.

Komilis, D.P., Karatzas, E., & Halvadakis, C.P. (2005). The effect of olive mill wastewater on seed germination after various pretreatment techniques. *Journal of Environmental Management*, *74*, 339–348.

Kononova, M.M. & Alexandrova, I.V. (1973). Formation of humic acids during plant residue humication and their nature. *Geoderma, 9,* 157–164.

Langmuir, I. (1918). *Journal of the American Chemical Society, 40,* 1361.

Lathasree, S., NageswaraRao, A., SivaSankar, B., Sadasivam, V., & Rengaraj, K. (2004). Heterogeneous photocatalyticmineralisation of phenols in aqueous solutions. *Journal of Molecular Catalysis, Chemical, 223*(12), 101–105.

Lech, S., Kamilla, T.M., Marta, K., & Bogusław, P. (2014). Phosphorus and COD removal from chemically and electrochemically coagulated wastewater. *Environment Protection Engineering, 40* (3), 63-73.

Lev., D. (2001). *Photocatalytic degradation of organic contaminants: Novel catalysts and processes.* Ph.D. Dissertation Mendeleev Institute.

Liu, X.W., Fang, Z., Zhang, X.J., Zhang, W., Wei, X.W., & Geng, B.Y. (2009). Preparation and characterization of $Fe_3O_4$/CdS nanocomposites and their use as recyclable photocatalyst. *Crystal Growth & Design, 9,* 197–202.

Luo, H.B., Li, F., Lv, H., Zeng, Y.M., Zhang, K., & Huang, B. (2012). Adsorption control performance of phosphorus removal from agricultural non-point source pollution by nano-aperture lanthanum-modified active alumina, *Advance Journal of Food Science and Technology, 4(6),* 337-343.

Ma, P., Xiao, C., Li, L., Shi, H. & Zhu, M. (2008). Facile preparation of ferromagnetic alginate-g-poly(vinyl alcohol) microparticles. *European Polymer Journal, 44*, 3886–3889 .

Manoj, A. L., Shaji, V., & Santhosh, S. (2012). Nair Photocatalytic Water Treatment by Titanium Dioxide: Recent Updates, *Catalysts 2*, 572-601.

Manouchehr, N., Mehriana, A., Reza, L., & Mohammad, H. R. (2014). The optimum conditions for synthesis of $Fe_3O_4$/ZnO core/shell magnetic nanoparticles for photodegradation of phenol, *Journal of Environmental Health Science & Engineering 12*, 21.

Mantzavinos, D., & Kalogerakis, N. (2005). Treatment of olive mill effluents. Part I: organic matter degradation by chemical and biological processes—an overview. *Environment International, 31*, 289–295.

Marco, S. L., & José, A. (2009). Peres Removal of COD from olive mill wastewater by Fenton's reagent: Kinetic study. *Journal of Hazardous Materials 168*, 1253–1259.

Marques, P.A.S.S., Rosa, M.F., Mendes, F., Collares, P.M., Blanco, J., & Malato, S. (1996). Wastewater detoxification of organic and inorganic toxic compounds with solar collectors, *Desalination, 108,* 213-220.

Meyssami, B., & Kasaeian, A.B. (2005). Use of coagulants in treatment of olive oil wastewater model solutions by induced air flotation. *Bioresource Technology*, *96*, 303-307.

Mikulec, F.V., Kuno, M., Bennati, M., Hall, D.A., Griffin, R.G., & Bawendi, M.G. (2000). *Journal of the American Chemical Society, 122*, 2532–2540.

Mingjie, M., Weijie, G., Zhengpeng, Y., Shanxiu, H., & Guanyu, W. (2015). Preparation and photocatalytic activity of $TiO_2$/Fine char for removal of rhodamine B, *Journal of Nanomaterials Article ID 538275*, 5.

Mulinnacci, N., Romani, A., Galardi, C., Pinelli, P., Giaccherini, C., & Vincieri, F. F., (2001). Polyphenolic content in olive oil wastewaters and related olive samples, *Journal of Agricultural and Food Chemistry, 4*9, 3509-3514.

Murti, S. D. S., Yang, H., Choi, K. H., Korai, Y., & Mochida, I. (2003). Influences of nitrogen species on the hydrodesulfurization reactivity of a gas oil over sulfide catalysts of variable activity. *Applied Catalysis, 252,* 331.

Nassar, N.N. (2012a). Iron oxide nanoadsorbents for removal of various pollutants from wastewater: an overview. *A. Bhatnagar (Ed.), Application of Adsorbents for Water Pollution Control, Bentham Science Publishers.*

Niaounakisand, M., & Halvadakis C. P. (2004). *Olive-mill waste management – literature review and patent survey.* Waste Management Series (2nd Ed.), Amsterdam, The Netherlands: Elsevier.

Niaounakisand, M. & Halvadakis C. P. (2006). *Olive processing waste management literature review and patent survey.* Waste Management Series (2nd Ed.), Amsterdam, The Netherlands: Elsevier.

Nieto, L. M., Hodaifa, G., Rodr´ıguez, S., Gim´enez J. A., & Ochando, J. (2011). Degradation of organic matter in olive-oil mill wastewater through homogeneous Fenton-like reaction. *Chemical Engineering Journal, 173*, (2), 503–510.

Obied, H. K., Bedgood, D. R., Jr., Prenzler, P. D., & Robards, K. (2007). Bioscreening of Australian olive mill waste extracts: Biophenol content, antioxidant, antimicrobial and molluscicidal activities. *Food and Chemical Toxicology, 45,* 1238–1248.

Ohko, Y., Tatsuma, T., & Fujishima, A. (2001). Characterization of $TiO_2$ Photocatalysis in the gas phase as a photoelectrochemical system:Behavior of salt-modified system. *The Journal of Physical Chemistry, 10016,* 105.

Oppenlander T, (2003). *Photochemical purification of water and air.* Weinheim: Wiley-VCH.

Özgür, Ü., Alivov, Y. I., Liu, C., Teke, A., Reshchikov, M. A., Doğan, S., et al. (2005). *Journal of Applied Physics, 98*, *041301.*

Oztekin R., & Sponza, D.T. (2013). Treatment of wastewaters fromthe olive mill industry by sonication. *Journal of Chemical Technology and Biotechnology, 88,* 212-225.

Panasuik O. (2010). *Phosphorus removal and recovery from wastewater using magnetite.* Royal Institute of Technology, M.Sc. Thesis Stockholm.

Pankhurst, Q.A., Thanh, N.T.K., Jones, S.K., & Dobson, J. (2009). Progress in applications of magnetic nanoparticles in biomedicine. *Journal of Physics D: Applied Physics*, *42* (224001), 15.

Pardeshi, S.K., & Patil, A.B. (2008). A simple route for photocatalytic degradation of phenol in aqueous zinc oxide suspension using solar energy. *Solar Energy, 82,* 700–705.

Paredes, C., Cegarra, J., Roig, A., Sanchez-Monedero, M.A., & Bernal, M.P.. (1999). Characterization ofolive mill wastewater (alpechin) and its sludge for agricultural purposes. *Bioresource Technology. 67*, 111.

Peral, J., Domenech, X., & Ollis, D. F. (1997). Heterogeneous photocatalysisfor purification, decontamination and deodorization of air. *Journal of Chemical Technology and Biotechnology, 70*, 117.

Pinotti, A., & Zaritzky. N. (2001). Effect of aluminum sulfate and cationic polyelectrolytes on the destabilization of emulsified wastes. *Waste Management, 21,* 535–542.

Pirkanniemi, K. & Sillanpää, M. (2002). Heterogeneous water phase catalysis as an environmental application: a review. *Chemosphere 48*, 1047–1060.

Poole Jr, C. P. F., & Owens, J. (2003). *Introduction to nanotechnology*, & Sons Inc., Hoboken, New Jersey: John Wiley.

Pozzo, R.L., Baltanas, M.A., & Cassano, A.E., (1997). Supported titanium oxide as photocatalyst in water decontamination: state of the art. *Catalysis Today, 39,* 219-231.

Radovic, L.R. (1999). Surface chemistry of activated carbon materials: state of the art and implications for adsorption, in: *J.A. Schwarz, C.I. Contescu (Eds.),*

Surfaces of Nanoparticles and Porous Materials, NewYork: Marcel Dekker, 529–565.

Rinaldi, M., Rana, G., & Introna, M., (2003). Olive-mill wastewater spreading in southern Italy: effects on a durum wheat crop. *Field Crops Research, 84,* 319.

Rizzo, L., Lofrano, G., Grassi, M., & Belgiorno, V. (2008). Pre-treatment of olive mill wastewater by chitosan coagulation and advanced oxidation processes. *Separation and Purification Technology, 63,* 648–653.

Roig, A., Cayuela, M.L., & Sanchez-Monedero, M.A. (2006). An overview on olive mill wastes and their valorisation methods. *Waste Management 26,* 960–969.

Roostaei N. & Tezel F. H. (2004). Removal of phenol from aqueous solutions by adsorption. *Journal of Environmental Management, 70,* 157-164.

Sakthivel, S., Neppolian, B., Shankar, M. V., Arabindoo, B., Palanichamy, A., & Murugesan, V. (2003). Solar photocatalytic degradation of azodye: comparison of photocatalytic efficiency of ZnO and $TiO_2$. *Solar Energy Materials and Solar Cells, 77,* 65–82.

Sakthivel, S., Shankar, M.V., Palanichamy, M., Arabindoo, B., & Murugesan,V., (2002). Photocatalytic decomposition of leather dye Comparative study of $TiO_2$ supported onalumina and glass beads. *Journal of Photochemistry & Photobiology, A: Chemistry, 148,* 153-159.

Samuel, S. M., Thirunavukkarasu, M., Penumathsa, S. V., Paul, D., & Maulik, N. J. (2008). Akt/$FOXO_3$a/SIRT1-mediated cardioprotection by tyrosol against ischemic stress in rat in vivo model of myocardial infarction: switching gears toward survival and longevity. *Journal of Agricultural and Food Chemistry, 56,* 9692–9698.

Satish, M., Rohan, L., Shailesh, G., Shachi, N., Shirish, S., & Rajeev, C. (2011). Continuous flow photocatalytic reactor using ZnO–bentonite nanocomposite for degradation of phenol, *Chemical Engineering Journal, 172,* 1008– 1015.

Serpone, N., Maruthamuthu, P., Pichat, P., Pelizzetti, E., & Hidaka, H. (2001). Exploiting the interparticle electron-transfer process in thephotocatalyzed oxidation of phenol, 2-chlorophenol andpentachlorophenol—chemical evidence for electron and holetransfer between coupled semiconductors. *Journal of Photochemistry and Photobiology, A: Chemistry, 85,* 247–253.

Sharma, A., Rao, P., Mathur, R. P., & Ameta, S. C. (1995). Photocatalyticreactions of xylidineponceau on semiconducting zinc oxidepowder. *Journal of Photochemistry and Photobiology, A: Chemistry, 86*, 197–200.

Sierra, J., Martn, E., Montserrat, G., Cruaras, R. & Garau, M. A. (2001). Characterisation and evolution of a soil affected by olive oil mill wastewater disposal. *Science of the Total Environment, 279*(1–3*),* 207.

Teja, A. S. & Koh, P.Y. (2009). Synthesis, properties, and applications of magnetic iron oxide nanoparticles. *Progress in Crystal Growth and Characterization of Materials, 55* (1-2), 22–45.

Turchi, C. S. & Ollis, D. F. (1990). Photocatalytic degradation oforganic water contaminants: Mechanisms involving hydroxylradical attack. *Journal of Catalysis*, *122*, 178.

Ugurlu, M., & Karaoglu, M.H. (2011). $TiO_2$ supported on sepiolite: Preparation, structural and thermal characterization and catalytic behaviour in photocatalytic treatment of phenol and lignin from olive mill wastewater, *Chemical Engineering Journal, 166,* 859–867.

Uğurlu, M., & Kula, İ. (2007). Decolourization and removal of some organic compounds from olive mill wastewater by advanced oxidation processes and lime treatment. *Environmental Science and Pollution Research, 14*(5), 319-325.

Vohra, M. S., Selimuzzaman, S. M., & Al-Suwaiyan, M. S. (2010). $NH_4^+$ -$NH_3$ removal from simulated wastewater using UV-$TiO_2$ photocatalysis: effect of co-pollutants and pH. *Environmental Technology, 31*(6), 641-654.

Wana, J., Hui L., & Kezheng C. (2009). Synthesis and characterization of $Fe_3O_4$@ZnO core–shell structured nanoparticles, *Materials Chemistry and Physics 114*, 30–32.

Wang, C.Y., Böttcher, C., Bahnemanne, D.W., & Dohrmann, J.K. (2003). *Journal of Materials Chemistry*, *13*, 2322–2329.

Wang, R., Xin, J.H., Yang, Y., Liu H., Xu, L., & Hu, J. (2004). The characteristics and photocatalytic activities of silver doped ZnO nanocrystallites. *Applied Surface Science, 227,* 312–317.

Weber Jr, W.J., & Morris, J. C. (1963). Kinetics of adsorption on carbon from solution. *American Society of Civil Engineers, 89, SA2,* 31.

Xiaohui, F., Haijuan, G., Kunal, P., Hong, Z., & Xia, L. (2014). High performance, recoverable $Fe_3O_4$/ZnO nanoparticles for enhanced photocatalytic degradation of phenol. *Chemical Engineering Journal 244,* 327–334.

Xue, S.W., Jun, R., Hai, J.L., Lei, Z., Fei, L., Zhang Q., & Juan X. (2010). Removal of Ni(II) from aqueous solutions by nanoscale magnetite. *Clean – Soil, Air, Water, 38* (12), 1131–1136.

Yang W., Kan A.T., Chen W., & Tomson M.B. (2010). pH-dependent effect of zinc on arsenic adsorption to magnetite nanoparticles. *Water Research ,44,* 5693-5701.

Ye, M., Zhang, Q., & Hu, Y. (2010). Magnetically recoverable core-shell nanocomposites with enhanced photocatalytic activity. *Organic Chemistry, 16,* 6243–6250.

Yeber, M. C., Roderiguez, J., Freer, J., Baeza, J., Duran, N. H., & Mansilla, D. (1999) Advanced oxidation of a pulp mill bleaching wastewater. *Chemosphere 39,* 1679-1688.

Yu, J., Xiang, Q., & Zhou, M. (2009). Preparation, characterization and visible-light-driven photocatalytic activity of Fe-doped titania nanorods and first-principles study for electronic structures. *Applied Catalysis B: Environmental*, *90,* 595–602

Yuan, G., & Keane, M. A. (2003). Liquid phase catalytichydrodechlorination of 2,4dichlorophenol over carbon supportedpalladium: An evaluationof transport limitations. *Chemical Engineering Science, 58*, 257-267.

Zarzycki, J. (1982*). Les verres et l'état vitreux.* Paris: Masson English.

Zhu, X., Castleberry, S. R., Nanny, M. A., & Butler, E. C. (2005). Effects of pH and catalyst concentration on photocatalytic oxidation of aqueous ammonia and nitrite in titanium dioxide suspensions. *Environmental Science & Technology, 39*(10), 3784-3791.